T-4758

# OPTIMIZATION OF PRODUCTION METHODS FOR FULLERENE SYNTHESIS BY COMBUSTION



by

Jeffrey Todd Jones

A thesis submitted to the Faculty and Board of Trustees of the Colorado School of Mines in partial fulfillment of the requirements for the degree of Master of Science (Chemical and Petroleum-Refining Engineering).

Golden, Colorado

Date 1/16/96

Signed: ______________________
J. Todd Jones

Approved: ______________________
Dr. J. Thomas McKinnon
Thesis Advisor

Golden, Colorado

Date 1/16/96

______________________
Dr. Robert M. Baldwin
Professor and Head
Department of Chemical and Petroleum
Refining Engineering

## ABSTRACT

Fullerenes are the third stable form of pure carbon known to exist. The importance of carbon in every form of life as well as in an extensive number of commercial chemical applications is well known. Since the initial discovery of fullerenes in 1985, and later, the 1990 breakthrough which made macroscopic quantities available, they have become the focus of thousands of publications as well as the main interest in hundred of patents issued world wide. Fullerenes have many unique properties that will inevitably lead to new products and possibly large scale use in chemical process industries. However, to date there is no economical use or individual application for them. This is largely due to their high cost. Therefore, one major step to bringing their potentials to a reality, is cost reduction.

One of the methods proven to produce fullerenes in abundance is the combustion of aromatic hydrocarbons at low pressures. The main process variables that are of interest are chamber pressure, cold gas velocity and the composition of the reactant gas or equivalence ratio. Using the methods of experimental design, the effects of flame conditions on fullerene yields for low pressure benzene/oxygen/argon premixed flames were systematically studied in an experimental space where optimum conditions to fullerene yields were expected to be found.

Within the experimental space studied, yields and production rates of the fullerenes $C_{60}$ and $C_{70}$ were found to increase towards increasing cold gas velocities and chamber pressures. The equivalence ratio was the most influential variable in that decreases in it exhibited significant increases in the soot yields. Whereas for yields from carbon fed and rates of production, a peak was detected near a value of 2.4. The cold gas velocity also exhibited a similar peak in the yields from carbon fed and rates of production that ranged from 40 to 50 cm/s, increasing as the pressure increased. At values of (P, v, $\phi$) for $C_{60}$ and $C_{70}$ respectively, the highest measured yields from soot were 10.4% and 9.2% at (35, 40, 2.1875), from carbon fed were 0.24% and 0.18% at (27.5, 50, 2.375), highest rates of production were 0.62 g/hr and 0.46 g/hr also at (27.5, 50, 2.375).

# TABLE OF CONTENTS

# LIST OF FIGURES

# LIST OF TABLES

# ACKNOWLEDGMENTS

I would like to thank all of the following persons:

- Dr. J. Thomas McKinnon, for the chance to make a contribution to the field of fullerenes and the guidance, critiques, creative freedom and responsibilities he offered to me during the course of this thesis.
- Dr. Terry Parker for his insight and advice to my work on flame temperature calculations.
- Dr. J. Douglas Way for his thoughts and encouragement in the HPLC analytical work.
- All of my laboratory co-workers: Hiayue Zhang, Dr. Hong Duan, Robert Higgins, Rajiv Srivastiva and Chris Casias for their shared suggestions and technical insight.
- John Jezek from the department of engineering for his extensive help in the fabrication of the burner and other equipment.
- The National Science Foundation for the financial support of this research under Grant CTS - 9215795.

The greatest thanks to my wife Wendy, whose patience and belief in what I wanted to accomplish allowed me an experience that I could have gained nowhere else.

# Chapter 1

# INTRODUCTION

## 1.1 Fullerenes

Fullerenes are the third known pure form of carbon. Unlike the network solids, diamond and graphite, fullerenes are discrete molecules that are spherical, hollow structures comprised of even numbers of carbon atoms and vary only by the number of atoms in their shell. The most spherical and prominent member of the fullerenes is $C_{60}$ or Buckministerfullerene.

The first evidence of its existence was "accidentally" discovered by Kroto et. al. (1) in 1985 while conducting experiments relating to interstellar research. The group named it after the American engineer and philosopher, R. Buckminister Fuller whose geodesic dome structures also resembled the hypothesized configuration of a soccer ball. Soon it became known as a buckyball. Also discovered at the same time was $C_{70}$ and the family now called the fullerenes was born. A model of $C_{60}$ is shown in Figure 1.

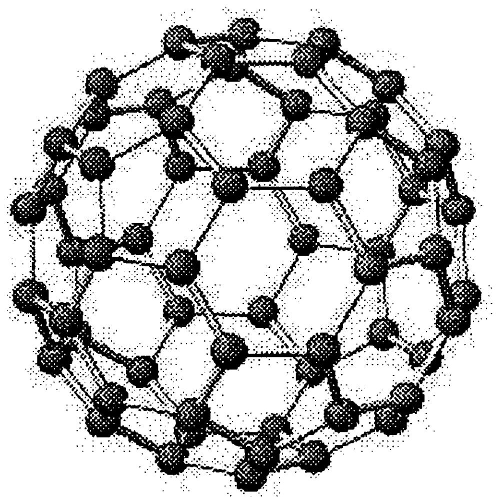

Figure 1 Buckminsterfullerene

The method by which the group created them was through laser vaporization of graphite in an helium atmosphere. Unfortunately the initial discovery produced only trace amounts that were insufficient to confirm the structure. Additional attempts with the original experimental apparatus failed to provide macroscopic quantities. It was not until 1990 when its structure along with some other theoretical and computational predictions were confirmed. Kraetschmer and Huffman (2), through a different method, produced and extracted a large enough quantity and published this method which became known as the graphite vaporization process. This enabled any laboratory to make their own fullerenes with ease and low equipment costs.

At the time of this writing, there have been well over 2700 separate publications concerning the fullerenes (3). In the early stages of research, before the Kraetschmer-Huffman discovery, investigators concentrated on predicting many of its properties through theoretical and computational methods. From then on, with the ability to produce and manipulate them, much of the focus has been directed towards probing its physical, chemical and electronic properties in order to discover their commercial applications.

## 1.2 Applications

Ultimately, there may be many uses for fullerenes, but to date, there is no single practical commercial application using them. However, there have been over 44 granted U.S. patents and many more patent applications all over the world involving fullerenes in some sort of use (4). Some examples of uses suggested by these patents are; optical limiters, toners and developers, conversion to diamond, polymers, superconductors, electrochemical cells, chromatography media, surface coatings and many, many more. MER (Materials and Electrochemical Research) which is a major supplier of fullerenes, conducted a market study in 1993 that compared the value of certain applications against the time required to develop them and reported a fairly linear relationship (5). Ranked in order of increasing value and time of development: 1. Optical devices, 2. Carbides as hardening agents, 3. Chemical sensors, 4. Gas separation, 5. Thermal insulation,

6. Diamonds (thin film and bulk), 7. Batteries, 8. Catalysts, 9. Hydrogen storage medium, 10. Polymers as additives and 11. Medical applications.

Two of the more intriguing uses that deserve expanding upon are medical applications and superconductors. Though the utilization of fullerenes in the biological/medical fields may be many years from reality, one highly intense area of research that found a role for $C_{60}$ is in AIDS inhibition. In 1993 researchers at the University of California, San Francisco and Emory University in Atlanta found that a water soluble derivative of $C_{60}$, a key need for biological systems, had the dimensions and properties that enabled it to block the active sites of two different viruses (6). HIV-1 protease and HIV-2 reverse transcriptase are two viruses that cause AIDS. The scientists add that "The derivative is not a drug candidate itself, but it offers a potential lead for designing anti-HIV agents."

Concerning superconductors, some of the most interesting properties of fullerenes are electronic. These allow it to function in various compounds as an insulator, a conductor, a semiconductor and a superconductor (7). Researchers at AT&T Bell Laboratories were the first to report superconductivity in alkali metal doped $C_{60}$ (8). They were able to attain zero resistance at 18 K for a potassium doped form, $K_3C_{60}$, and up to 29 K for a rubidium form, $Rb_3C_{60}$. The same group has been able to etch thin films of $C_{60}$ much like a photoresist used in the microprocessor industry (9).

If the applications of fullerenes, both proven and potential are to be pursued by the chemical and manufacturing industries, then the value of the benefit must outweigh the additional cost of their use. The ability to produce fullerenes cheaply, around the cents per pound range, is a key obstacle to overcoming this hurdle. Currently, 99.9+ % purity $C_{60}$ and 98.0+ % $C_{70}$ costs \$150.00 and \$ 550.00 per gram respectively (MER quote, 1/5/96).

## 1.3 Thesis Objectives

The focus of this thesis is to investigate and determine the optimal operating conditions to economically produce fullerenes by combustion. In particular, a factorial designed experiment studying the effects of chamber pressure, cold gas velocity and equivalence ratio ($\phi$)[1] on the yields of fullerenes from fuel carbon fed and the soot produced.

[1] Equivalence ratio is a normalized fuel/oxidant ratio, $\phi$ = (actual fuel/oxidant ratio)/(stoichiometric fuel/oxidant ratio).

# Chapter 2

# BACKGROUND AND PREVIOUS WORK

## 2.1 Fullerenes

Though it was not seen until the Kroto discovery, Buckministerfullerene was first speculated to exist by David Jones in 1966 (10) and investigated by other research groups throughout the seventies (11, 12, 13, 14). David Jones, writing under the pen name of Daedalus, was seeking to bridge the density gap between gasses and liquids. He ultimately conceived a hollow, closed spherical molecule composed of carbon atoms that were bonded together hexagonally like chicken wire. Later, in 1982, he wrote that "defects" in the graphitic sheet (pentagons) were needed in order for the sheet to curve (15).

In 1985, Kroto, Curl and Smalley were seeking to answer questions relating to interstellar research that involved long chained cyanopolyynes ($HC_nN$ ($n = 5$-$11$)). These were discovered in the late seventies by radio astronomy and later indicated that they were being blown out of red giant carbon stars (16, 17). Kroto et al. confirmed these stars to be likely sources by simulating the chemistry with laser focused on a pure carbon (graphite) target (1). During these experiments they observed a large presence of two stable pure carbon species that had molecular weights of 720 and 840, which if comprised of only carbon, indicated the formulas $C_{60}$ and $C_{70}$ respectively. Without being aware of the earlier theoretical work on C60 (10-14), the group hypothesized C60 to be a closed cage and to have the truncated icosahedron polyhedral structure as shown in Figure 1 and named the molecule Buckministerfullerene.

Unfortunately, only trace quantities were able to be produced by the laser vaporization technique. This meant that its existence in nature and structure was unable to be established. Subsequent attempts to produce macroscopic quantities by the laser technique failed.

Between the years 1985 to 1989, Homann et al. conducted experiments on flat premixed acetylene and benzene-oxygen flames (18, 19, 20) with a flat disk burner. By sampling the flame gasses at different heights above the burner surface, and analyzing them with an on line mass spectrometer, they observed charge-to-mass ratios that indicated a pure carbon species with molecular weights similar to fullerenes produced with the graphite vaporization process. However, they could not prove that the species was a closed cage structure and that flames could produce recoverable, macroscopic quantities of fullerenes.

In this same time period, other research groups from the fields of physics and chemistry focused on theoretical calculations regarding seemingly endless aspects of fullerenes and large carbon clusters. Some examples of the topics investigated were electronic properties and normal vibrational frequencies (21), ab initio studies of its thermodynamic stability (22), ionization potentials and electron affinities (23), carbon cluster growth kinetics (24) and quantum chemical calculations (25).

While searching for the source of an astronomical absorption feature at 217 nm surrounding carbon stars, Kraetschmer et al. (26) accidentally stumbled upon a method to produce macroscopic quantities of fullerenes. The IR spectrum of the carbon dust produced in their apparatus showed four sharp absorption bands at 1429, 1183, 577 and 528 $cm^{-1}$. The group recognized that the spectrum fit the IR absorption bands for $C_{60}$ that were predicted by theoretical chemists. This led to the first isolation of large quantities of fullerenes (2).

Their method involved electrically arcing two graphite rods together, producing a high temperature carbon vapor which condensed into a fullerene rich soot. This was done in a low pressure, inert helium atmosphere. The fullerenes were then extracted from the surrounding soot with benzene. A general representation of the graphite vaporization process is shown in Figure 2. The large quantities of $C_{60}$ produced enabled testing of the structure by standard analytical methods and its identity was confirmed.

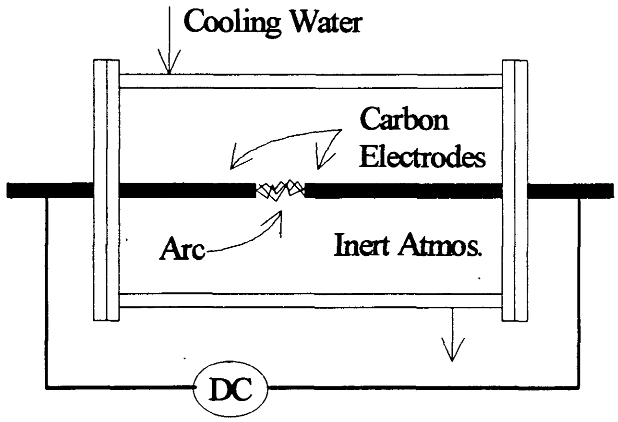


Figure 2. Graphite Vaporization Process

In 1990, Howard et al. (27, 28) reported the discovery that macroscopic quantities of $C_{60}$ and other fullerenes could also be produced in a sooting flame. This process involved combustion at low pressures of premixed benzene-oxygen in the presence of argon. Also noted was that by controlling the selection of flame conditions, the combustion process could vary the production of $C_{70}$ to $C_{60}$ over a wider range than graphite vaporization. The molar $C_{70}/C_{60}$ ratio was limited to 0.02 to 0.18 for graphite vaporization, whereas the combustion technique produced $C_{70}/C_{60}$ molar ratios in the range of 0.26 to 5.7. A further contrast from graphite vaporization was that with combustion, oxygen and hydrogen are present, whereas these elements cannot be present in graphite vaporization. It requires a completely inert atmosphere.

Shortly after that discovery, McKinnon investigated the thermodynamic limits to fullerene production by hydrocarbon pyrolysis and combustion (29). The equilibrium calculations concluded that $C_{60}$ yields are favored by high carbon-to-hydrogen ratios, low oxygen concentrations and low pressures. Also stated was that high yields exist in a temperature window of 2200 to 2600 K. Further studies on combustion synthesis that addressed the economics of production, indicated that the cost of fullerenes could be as low as \$6/kg compared to \$90/kg for graphite vaporization (30). These values are based on yields from carbon fed of 5% and 20% for combustion and graphite vaporization respectively.

An examination of the combustion synthesis technique by Howard et al. (31) investigated the effects of pressure, gas velocity, molar C/O ratio and the molar fraction and type of diluent in the feed gas on the yields of fullerenes and $C_{70}/C_{60}$ molar ratio. The ranges of their variables were the following: pressure, 12 to 100 torr; velocity, 14.4 to 50.3 cm/s; C/O ratio, 0.717 to 1.072; molar fraction of argon, 0.0 to 0.39. The samples were taken from the chamber surface deposits and a flame sampling probe.

Their results showed that fullerenes are produced in sooting flames but not under the heaviest sooting conditions. The largest conversion of carbon to soot was about 12% but the largest yields and production rates of fullerenes were observed when 2-3% of carbon was converted to soot. The largest yield of $C_{60}+C_{70}$ as a percentage of soot was 20% at a pressure of 37.5 torr, C/O ratio of 0.959 and 25% helium. The largest $C_{60}+C_{70}$ yield on a basis of carbon fed was about 0.5%. And the largest production rate of $C_{60}+C_{70}$ (g/hr) was observed at a pressure of 69 torr, C/O ratio of 0.989 and 25% helium. The $C_{70}/C_{60}$

molar ratios ranged from 0.26 to 8.8, though they typically varied from 1.5 to 1.8 for the conditions of the largest $C_{60}$ + $C_{70}$ production rates and yields.

## 2.2 Process Comparison

Comparison between the processes used to produce fullerenes, combustion and graphite vaporization, illuminates five main differences: maximum reaction temperatures, the effect of hydrogen and oxygen, the range of the $C_{70}/C_{60}$ ratio, rates of production and presence of modified structures.

In the graphite vaporization process, peak initial temperatures above 6000 K are reached (32). At this temperature the carbon is completely sublimed to the atomic level. Whereas in the combustion process, peak initial temperatures are around 2300 K (31, 33). At flame temperatures in this range, the feed molecules do not completely atomize, but instead break down into smaller species (33).

A striking difference exists between the processes concerning the composition and nature of the feed. For graphite vaporization, the feed is only solid carbon, whereas for combustion, oxygen and hydrogen present in considerable quantities. In the graphite vaporization process, the presence of oxygen and hydrogen causes a severe reduction in fullerene yields (34). This results in the need for purging the reactor with an inert, usually helium, as a start up procedure. However, for combustion, oxygen and hydrogen are present at the beginning of the reaction and during the formation of fullerenes in the flame.

Perhaps the most important difference is the $C_{70}/C_{60}$ ratios. The graphite vaporization process yields a $C_{70}/C_{60}$ molar ratio that varies between 0.02 to 0.18. Obviously preferring the production of $C_{60}$ over $C_{70}$. In combustion the ratio is much higher and covers a larger range. Values of 0.26 to 8.8 have been reported (31), with the ability to control it by the selection of flame conditions. Due to the price of $C_{70}$ and the higher fullerenes, combustion should prove to be a more economical method of production.

Concerning fullerene production, the maximum yields of $C_{60}$ and $C_{70}$ as a percentage of soot are comparable for the two processes. However, the yield from the condition with the largest rate of production for combustion is considerably larger than that of graphite vaporization at its largest rate of production (31). It should be noted that for the investigation, the system was not designed for fullerene research. Process scale up is also a main concern in the production of any material. A combustion process is much more amenable to scale up than a vaporization process since graphite vaporization is stuck with an unreducable cost of electricity. But since there is no direct electrical input for combustion, a larger burner with the ability for kilograms per minute of feed throughput could produce grams per minute of fullerenes without significant additional operating costs.

The ability to produce fullerenes with modified structures is an ability that combustion has over graphite vaporization. Structures such as $C_{60}O$, $C_{70}O$, $C_{60}H_2$, $C_{60}H_4$, $C_{70}H_2$, $C_{60}CH_4$ and $C_{60}(CH_4)_2$ were identified by Anacleto et al. (35, 36). These derivatives are not present in the soots of the graphite vaporization process. It has also been hypothesized that by doping the flame with compounds such as ferrocene, a fullerene with an iron atom enclosed within the cage could be obtained (30). Some of the suggested uses of fullerenes, such as catalysts and batteries, indicate that the enclosure of a metal atom within the cage could modify its properties to favor these applications.

To summarize briefly, a combustion route for synthesis of fullerenes holds three key advantages over the conventional method of graphite vaporization. First, the ability to control the $C_{70}/C_{60}$ composition of the product by a more than 30-fold range by adjustment of flame conditions. This could lead to a more economical method of producing the more valuable, larger fullerenes. Second, scale up of a combustion process is much easier and involves a comparatively insignificant increase in operational costs. Lastly, the possibility for production of modified fullerene structures that may have properties desirable for uses not yet even thought of.

## 2.3 Flames

The burner design and flame type that was used for this work is involved frequently in the field of combustion research. Therefore, a brief discussion about its significance and applications seems appropriate. The key aspects of the type of system used is that it is a premixed laminar flame stabilized on a cooled surface. A description of the design of the burner and other related equipment is covered in Chapter 3.

Flame types may be classified as either premixed or diffusion depending on the degree of mixing of the reactants before entering the reaction zone. The transition between these types of flames is dependent upon the ratio of the burners dimensions to the diffusion limited mixing length. The premixed characterization of this flame describes that the fuel and oxidizer have been completely mixed before they reach the burner exit. A diffusion flame could be described as the other end of the spectrum. If only fuel passes through the burner, it must mix with the surrounding oxidizer by diffusion in order to burn. An example of these would be the difference between opening and closing the air inlet ports on an ordinary laboratory Bunsen burner.

The flow character of the flame is another means of classification. In laminar flames, diffusion and thermal conduction are what dominate the transport mechanism. Whereas in turbulent flow, transport is sometimes dominated by macroscopic eddy motion within the flame. The laminar nature of this flame helps to minimize the backmixing of reaction intermediates so that the results be mostly due to a one-dimensional flow of the reactants to products along the axial path of the flame. Therefore, a premixed laminar flame can be imagined as a differentially thin sheet, separating the unburned from the burned gasses and propagating normally through them at a characteristic velocity.

The chemical composition at different locations or residence times within the flame can vary greatly. Consequently, a strong utility of premixed laminar flames in combustion research is the ability to sample the flames composition at different residence times with a sampling probe. Measurements of this type can lead to significant understanding of the flames chemistry and the reaction intermediates that lead to products. Though no measurements of this type were performed in this study, it will be used in future work with this system to investigate fullerene growth mechanisms.

# Chapter 3

# APPARATUS AND PROCEDURE

## 3.1 Apparatus

For the synthesis of fullerenes under the prescribed conditions, a chamber that was able to be operated at low pressures, and withstand high temperatures was priority. The system had to include the following, flow control for the reactants, a burner with two separate flame regions, a housing for the burner, a section for product collection and means for pressure control. The remainder of this section is subdivided into these five main areas:

3.1.1 Burner and Chamber

3.1.2 Reactants Metering

3.1.3 Product Collection

3.1.4 Chamber Pressure Control

3.1.5 Temperature Measurements

### 3.1.1 Burner and Chamber

The burner was constructed of high purity copper except for the base which was made of brass. It is shown in Figure 3. Due to the requirement of a constant cold gas temperature, heat extraction from the burner surface was needed and facilitated by the high thermal conductivity of the copper. This also allowed for a smaller radial temperature gradient across the surface directly under the flame. The upper surface has two separate regions for reactant feed to the flame, an inner "core" and outer "shield." The core region held the flame which was responsible for the fullerene production and whose feed characteristics were manipulated in this study. The shield region held a flame

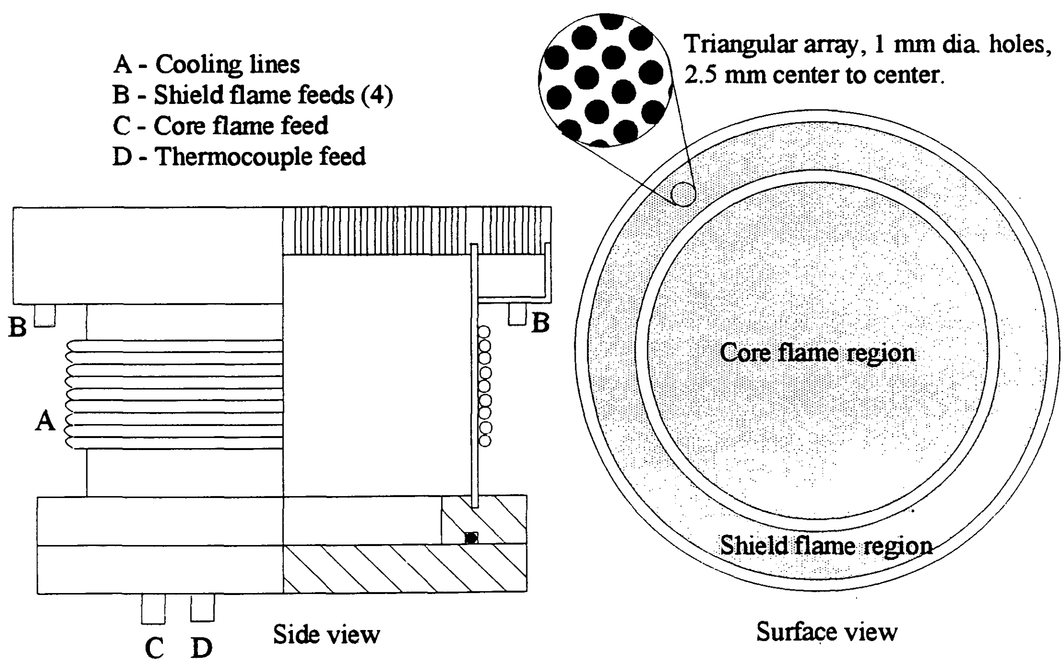


Figure 3. Burner

which served the purpose of "thermally insulating" the core flame allowing it to approximate an adiabatic one-dimensional system. The burner's overall diameter is 5-1/2 inches with over 2100 holes in the surface which is 1/2 inch thick. The inner core region has a diameter of approximately 3-3/4 inches, which around 75 % of the holes lie within. The burners height from base to surface is about 3-1/2 inches.

The feeds to the burner include reactants for the core and shield flames and the coolant. The cooling fluid used was a standard automotive anti-freeze/coolant that was diluted approximately 1:1 and was pumped through nine wraps of 1/8 inch o.d. copper tubing around its body. There was also a 1/16 inch dia. type K thermocouple fed through the base and stuck into an incompletely drilled hole, located approximately in the center of the core flame region.

The burner was housed in a stainless steel cross identical to a Nor-Cal part # 4C-600V. It is equipped with 6 inch Conflat flanged fittings at the end of each arm. The chamber with the burner inside it is shown in Figure 4. The burner is mounted inside on a 1 inch diameter polished brass rod which passes through the bottom flange enabling the burner height to be adjusted as needed for ignition and flame temperature measurements. The rod is held by a stainless steel Ultra-torr fitting which is welded to the center of the bottom flange. The feeds for the flame, burner coolant and thermocouple pass through Swagelok fittings which have been tapped into the bottom flange.

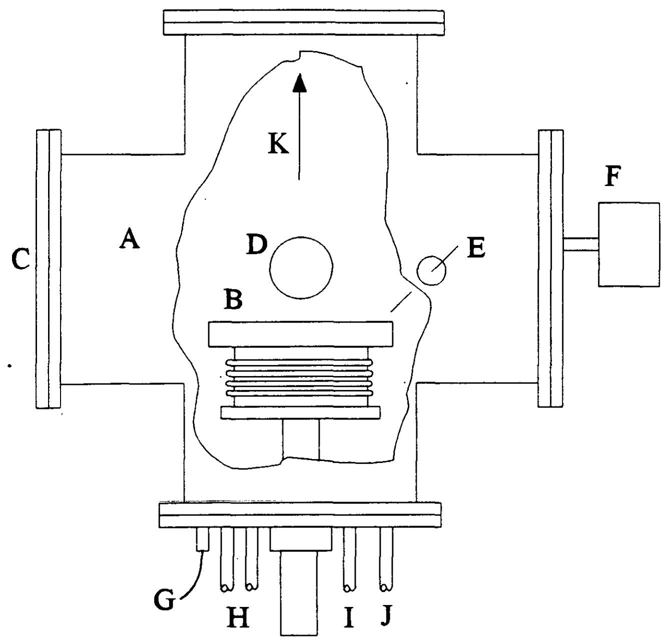


A - stainless steel chamber
B - burner
C - quartz window
D - thermocouple/optical port
E - spark igniter
F - pressure transduecer
G - burner thermocouple wire
H - coolant inlet/outlet lines
I - core flame feed
J - shield flame feed
K - product flow to collection

Figure 4. Chamber with Burner and Feeds

Additional fittings were welded to the sides of the chamber. Two ports are located across from each other, at the center of the chamber to be used for future optical measurements of the flame. However, they currently serve the purpose of a thermocouple access for flame temperature measurements. These ports are 1-1/2 inch Conflat half nipples. Thermocouples and temperature measurements will be discussed in section 3.1.5. Ignition of the flame is accomplished by striking a spark to the surface of the burner from a 1/8 inch dia. steel rod. The rod which is epoxied into a 1/2 dia. tube is sealed by an Ultra-torr fitting mounted on the side of the chamber. A hand held tesla coil is used to create the spark.

To assist in viewing of the flame during the experiment, a 1/2 inch thick quartz window, 6 inches in diameter, is mounted into a flange that bolts to one of the side arms of the chamber. This also facilitates measuring the distance between the burner surface and thermocouple junction. Quartz was chosen due to its ability to withstand high thermal gradients. The thickness of the window was dictated by the vacuum conditions of the experiments. On the side opposite the large window, a blank flange with an Ultra-torr fitting mounted onto it holds the pressure transducer responsible for monitoring the system during the experiment. A 13 inch long Conflat nipple (not shown in Figure 4) is mounted to the top of the chamber. This is used for product collection and will be described in section 3.1.3.

### 3.1.2 Reactants Metering

The feeds to the burner are metered to meet experimental conditions and then sent to the burner premixed. The gasses that were used in the experiments were oxygen, argon and ethylene. Oxygen and argon used were of 99.999 % purity, the ethylene used was of CP grade. Precise flow control was achieved by choked flow through an orifice. By controlling the upstream pressure, a constant mass flow rate can be insured provided that the ratio of the downstream to upstream pressure is less than 0.53. A schematic of the flow control system is shown in Figure 5. The calibration curves for the orifices used are shown in Appendix A. The gas metering system consisted of four of the units shown in

Figure 5, two streams fed the shield flame with oxygen and ethylene, the other two fed the core flame with oxygen and argon.

The gas metering unit consists of the following pieces: Whitey needle valve part # SS-22RS4, used to control the upstream pressure; Omega pressure transducer part # 236PC-100GV, measured upstream pressure in psig up to 100 psi; a three-way valve used to divert flow to one of two orifices; two orifices, large and small, for greater extent of flow

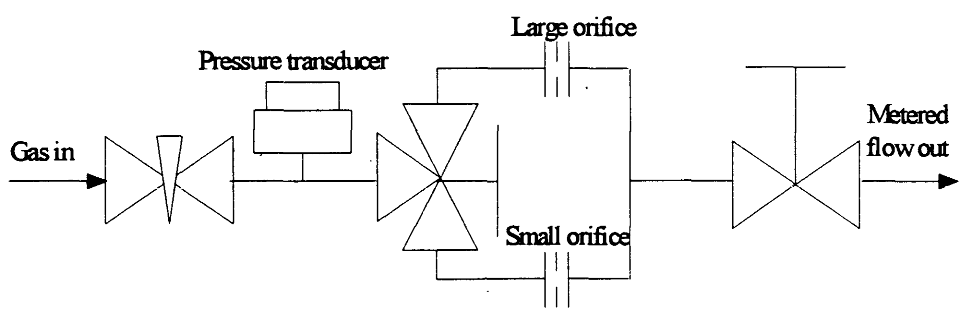


Figure 5. Gas Metering System

rates available; an on/off valve so that the gas flow could be interrupted without disturbing the settings of the needle valve or regulator on the gas cylinder.

The shield flame consisted of only oxygen and ethylene. These gasses were metered and mixed together into one stream and sent directly to the shield flame of the burner. The feed for the core flame was comprised of oxygen, argon and benzene. As with the feed to the shield flame, the oxygen and argon were metered and mixed together, but then sent to be mixed with vaporized benzene. A schematic of the vaporization/mixing unit is shown in Figure 6.

Over the course of the experiments benzene was procured from a couple of different suppliers but the quality was kept at ACS grade. The benzene flow was metered by a HPLC pump, ISCO model # 2350, that delivered the liquid at a rate controllable to the tenth of a milliliter per minute. From the pump the benzene was vaporized in a heated vessel packed with sand and kept at an elevated pressure. The temperature and pressure of this vessel was maintained at 135° C and between 20 to 30 psig. At these conditions the benzene is well above the saturation point and could be considered a superheated vapor. The temperature was controlled by an Omega model # CN76122 control unit, pressure controlled by a needle valve, Nupro model # SS-SS4, located downstream of the

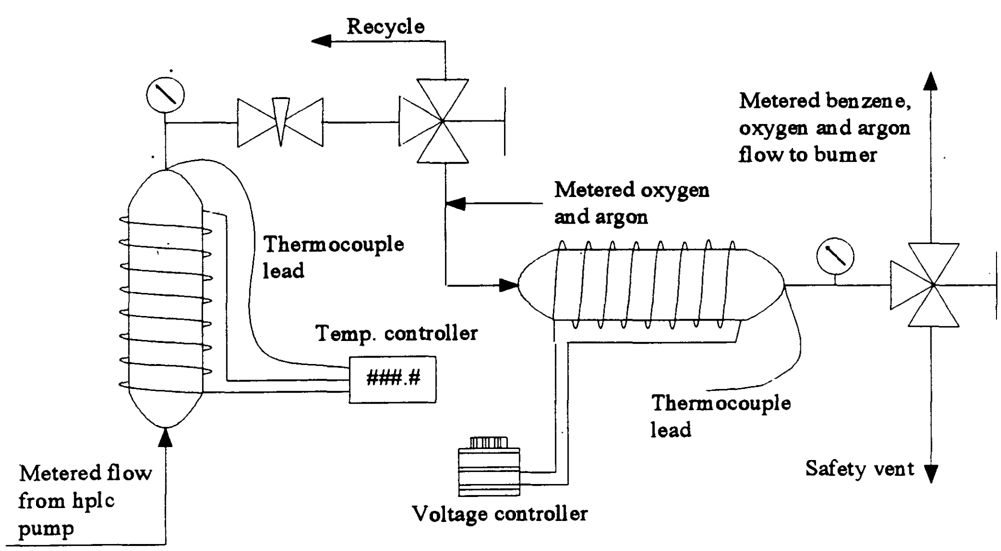


Figure 6. Benzene Vaporization and Mixing

vessel after the pressure gauge. The elevated pressure also guarded against pulses in the benzene flow due to the pump.

After leaving the vaporization vessel, the benzene vapor stream is mixed with the oxygen/argon stream just before entering another heated vessel. This second container is packed with sand to guarantee the complete mixing of the gasses. The heating ensures that no benzene will accumulate by condensation inside it. There is no pressure control on this vessel and at the exit it is usually at sub-atmospheric pressure and cools quickly. However, since the partial pressure of the benzene is below its saturation pressure at room temperature, no benzene is condensed in the line past the second vessel and the core flame feed remains constant and proceeds directly to the burner. On both feed lines to the burner, a sintered metal frit with a nominal pore size of 7 μm used for filtering flow was placed just before the chamber to guard against flashback.

3.1.3 Product Collection

The flame products (soot), were trapped in two main areas, collection plates and a filter. The collection plates were housed in a 13 inch long pipe section that bolted to the top of the main chamber and the filter was placed in-line between the collection plates section and the vacuum pumps. A schematic for the collection system is shown in Figure 7. The plates were constructed of copper and held together by threaded rods with 1/4 piping as spacers, separating the plates by about 1 inch. The rods were then tapped into the top flange so that they could be removed from the top section and the soot scraped off.

The filter used was a store brand automotive air filter obtained from Big A Auto Parts in Golden, part # 94224. Its size is roughly 4.5 inches in diameter by 5.5 inches tall and has approximately 3 square feet of surface area. Each one lasted for one or two runs and cost approximately $10.00 a piece. The tubing that connected the product flow lines from the top of the plate section to the filter housing and to the vacuum pumps was about 2 inches in diameter and used NW40 fittings as connectors.

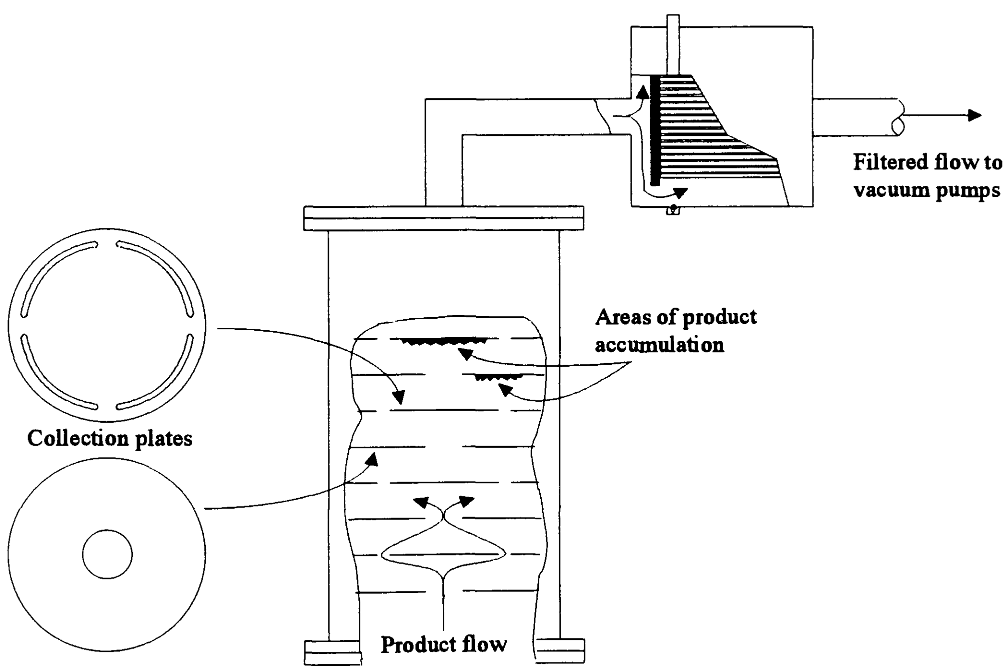


Figure 7. Product Collection Method

### 3.1.4 Chamber Pressure Control

The pressure of the chamber was controlled manually during all experiments. The schematic is shown in Figure 8. Two different valves were used to accomplish this task. A large gate valve designed for vacuum applications was placed just before the vacuum pumps and served the purpose of coarse control of the pressure. Fine control was achieved by bleeding air into the vacuum line with a needle valve just before the gate valve.

Due to the high flow rates passing through the chamber, two large Leybold-Heraeus, model # D60AC vacuum pumps were needed in order to maintain chamber pressure to that of the prescribed experimental conditions. Pressure of the chamber was measured by a Baratron pressure transducer, model # 122AA, with its output converted to units of torr by a Baratron digital readout/power supply, model # PDR-5B. Both units were obtained from MKS Instruments.

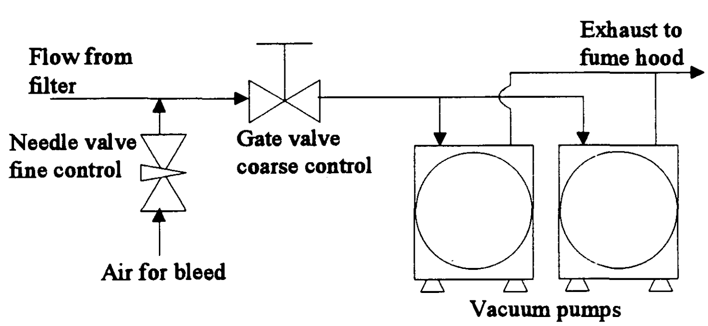


Figure 8. Chamber Pressure Control

### 3.1.5 Temperature Measurements

The flame temperature is an important variable to be considered in the combustion synthesis process. However, it was not able to be directly controlled for this work. A flames peak temperature can be calculated if the assumption of an adiabatic flame is made, and composition of the products are known or can be assumed to some degree of accuracy. Since the product composition of this flame is very large, and the system is far from adiabatic, an attempt to obtain some estimate of the flames peak temperature in this reactor needed to be measured directly.

This was accomplished by thermocouple measurements in two places, a type K thermocouple embedded into the bottom surface of the burner plate and a type B thermocouple that entered the chamber from the side as discussed in section 3.1.1. The hardware used for data acquisition was the following: a Gateway 2000 486DX PC, a data acquisition board, model # AT-MIO-16L-9 and signal conditioning board model # SC2070 from National Instruments. The software used was LabVIEW version 3.1.1 also from National Instruments.

Since the software enabled the acquisition and recording of temperature, the burners thermocouple could be used to measure the temperature of the surface as a function of time. Therefore, after a steady state temperature is reached, shutting off the flame and recording the decrease in the surface temperature allows for calculation of the rate of heat extraction from the flame by the cooled burner surface.

The thermocouple used for measuring the flame temperature had to be carefully planned. Type B is intended for use in high temperature, oxidizing environments. The wire diameter and size of the junction needed to be small enough to not disturb the flames structure, yet not so small that it would sag due to its own weight when hot. It also needed to be movable within the chamber. The temperature of the flame at start up is much higher than the melting point of the wire. Therefore, the thermocouple could not be in the flame region until the flame had stabilized to its lower-temperature sooting conditions. The design of the thermocouple used for flame measurements is shown in Figure 9.

What was finally built was a thermocouple with a wire diameter of 0.01 inches that was exposed about 1 cm from the end of a ceramic tube with a total length of about 8 inches. The tube had an o.d. of 1/16 inch, and two holes of 1/64 inch diameter that the thermocouples wires ran through. The ceramic tube was placed inside a short piece of 1/8 inch o.d. thin wall stainless steel tubing and was sealed by vacuum grease. The short piece of s.s. tubing was then held in place on the side of the chamber by an ultra-torr fitting. A schematic of the entire system is shown in Figure 10.

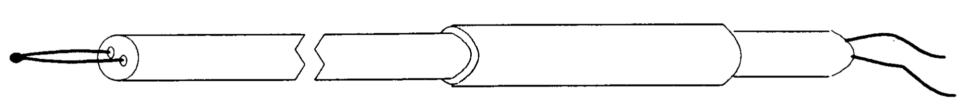

Figure 9. Thermocouple for Flame Measurements

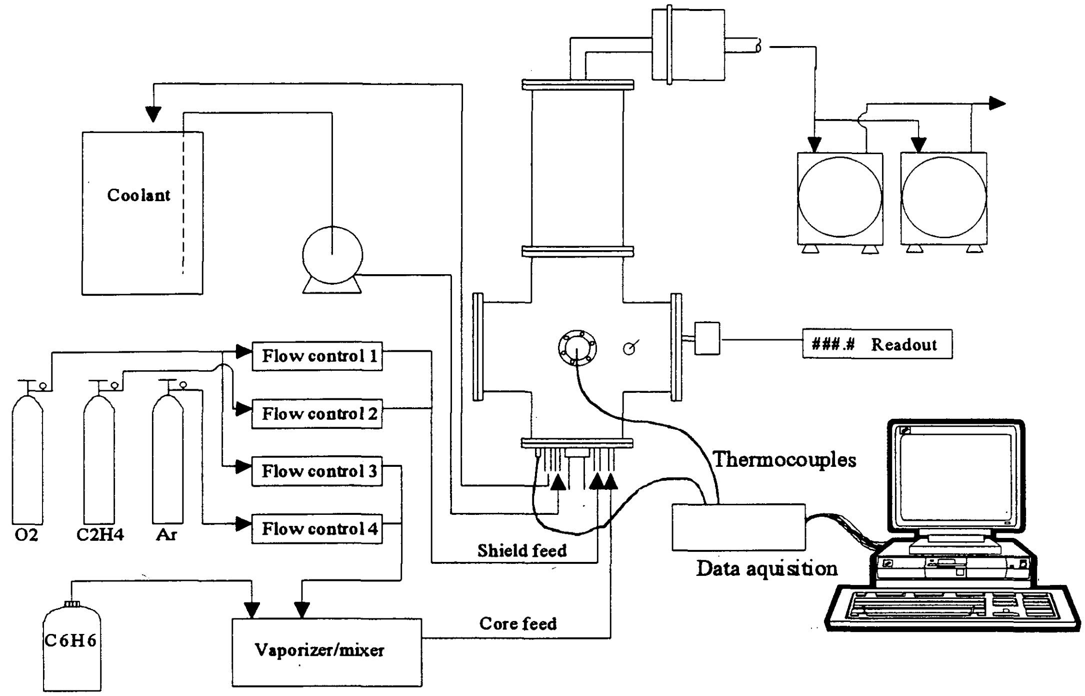


Figure 10. System

## 3.2 Experimental Procedure

The objective of this work was to investigate the effects of process variables on the yields of fullerenes through experimentation. This section will be divided into the following order of subjects:

3.2.1 Experimental Design and Selection of Variables

3.2.2 Running of Experiments

3.2.3 Collection and Extraction of Samples

3.2.4 Analysis of Samples

### 3.2.1 Experimental Design and Selection of Variables

The method of experimentation that was used in this work was a three level, three variable factorial design. If all of the combinations of the variables for this work were run, it would require a minimum of 27 separate experiments. Since the time required to get results for one condition is fairly long and labor intensive (not to mention the inevitable failure of equipment), and the need for replicate runs exists, the cost of time to perform an analysis of that size could be astronomical. When a full factorial design does become too costly to perform all experiments, an incomplete, or fraction of the design may be more desirable. However this cannot be done without some sacrifice of information.

When a factorial design is fractionated, confounding occurs within the variables. Confounding is an experimental arrangement in which certain effects cannot be distinguished from others (37). For the full $3^3$ factorial, there are 13 different effects each with two degrees of freedom: P, v, $\phi$, Pv, $Pv^2$, $P\phi$, $P\phi^2$, $v\phi$, $v\phi^2$, $Pv\phi$, $Pv^2\phi$, $Pv\phi^2$ and $Pv^2\phi^2$. In order to construct a design, any one of the $Pv\phi$ components may be used to confound the effects. This allows for 4 patterns, each with three different blocks for a total of twelve different and equally valid designs to be run. Unfortunately, this design is only practical if the interaction effects are small compared to the main effects.

For this work the $Pv\phi^2$ term was used for confounding. The aliases or terms that are then confounded together are the following: $P = Pv^2\phi = v\phi^2$, $v = Pv^2\phi^2 = P\phi^2$, $\phi = Pv = Pv\phi$, and $Pv^2 = P\phi = v\phi$. Basically what is meant is that upon confounding the linear effect of pressure cannot be distinguished from the effect of the interaction between a linear velocity and quadratic equivalence ratio term and so on. Consider the general linear model for the full factorial: $Y = \beta_0 + \beta_1 P + \beta_2 v + \beta_3 \phi + \beta_{12} Pv + \beta_{13} P\phi + \beta_{23} v\phi + \beta_{123} Pv\phi + \varepsilon$. Where the $\beta_\#$'s refer to the coefficient to that term and the $\varepsilon$ is the error. Upon confounding, what is lost is the information on the interactions between the variables. The resulting model is $Y = \beta_0 + \beta_1 P + \beta_2 v + \beta_3 \phi + \varepsilon$. As can be seen, this model is inadequate when there is considerable interaction between the variables and an optimal operating point within the experimental space is sought.

Initially the 1/3 fractional factorial was chosen to be run, or nine separate experimental conditions. Selection of the levels of the variables was accomplished first by determining appropriate ranges over which the variables should be studied. From earlier work (27-31), the variables of chamber pressure (P), cold gas velocity (v) and equivalence ratio ($\phi$) were shown to be appropriate and also indicated what ranges of these to investigate. The values chosen were the following: P, 20 to 50 torr; v, 30 to 50 cm/s; $\phi$, 2.375 to 2.75. Although in the early stages of this work, there were problems with controlling the process at some of the high pressure conditions, so the upper limit of the pressure was reduced to 35 torr. Later it appeared that a maximum yield with respect to carbon fed was not being reached. So the equivalence ratio range was shifted down one level to be 2.1875 to 2.5625. The final values for this work that were used are: P, 20, 27.5 and 35 torr; v, 30, 40 and 50 cm/s; $\phi$, 2.1875, 2.375 and 2.5625.

However, after the nine conditions were run, it was desired to perform a few more in order to enhance the plotting capability of the data. So a total of 15 different experimental conditions were run with replications on 8 of them. Replicate extractions were performed on the other 7 conditions. This gave a total of 31 experimental points (one condition had both a repeat run and extraction). The values of the variables for the different flame conditions are shown in Table 1. The first nine conditions are the original points, conditions 10 to 15 were added later.

Fortunately, with the addition of the extra experimental points the design now closely matches what is termed a face centered central composite design (38). These have the

Table 1 Experimental Conditions

| Experiment number | P (torr) | v (cm/s) | $\phi$ | repeat run | repeat extraction |
|---|---|---|---|---|---|
| 1 | 20 | 30 | 2.375 | | x |
| 2 | 20 | 40 | 2.5625 | x | |
| 3 | 20 | 50 | 2.1875 | x | |
| 4 | 35 | 40 | 2.375 | x | x |
| 5 | 35 | 50 | 2.5625 | x | |
| 6 | 35 | 30 | 2.1875 | x | |
| 7 | 27.5 | 50 | 2.375 | x | |
| 8 | 27.5 | 30 | 2.5625 | | x |
| 9 | 27.5 | 40 | 2.1875 | x | |
| 10 | 20 | 50 | 2.5625 | | x |
| 11 | 20 | 30 | 2.1875 | x | |
| 12 | 35 | 40 | 2.1875 | | x |
| 13 | 27.5 | 30 | 2.375 | | x |
| 14 | 35 | 50 | 2.375 | | x |
| 15 | 27.5 | 40 | 2.5625 | | x |

advantage similar to fractional factorials in that the full set need not be run, yet the interaction and higher order terms can still be estimated. The full quadratic model is:

$Y = \beta_0 + \beta_1 P + \beta_2 v + \beta_3 \phi + \beta_{11} P^2 + \beta_{22} v^2 + \beta_{33} \phi^2 + \beta_{12} Pv + \beta_{13} P\phi + \beta_{23} v\phi + \beta_{123} Pv\phi + \varepsilon.$

The central composite designs consist of two components, first a two-level full factorial used to estimate all the linear and interaction terms, the second component is the center and axial or star points used for estimation of the quadratic terms. Comparison of the original points to those required by the central composite design is shown in Table 2.

The coding of points used in Table 2 is such that -1, 0 and 1 represent the low, medium and high values respectively for the variables. For pressure, -1 = 20, 0 = 27.5 and 1 = 35 torr. Although the placement of the experimental points is not totally in line with those

Table 2 Comparison of Fractional Factorial and Central Composite Designs

| Exper. # | P | v | $\phi$ | P | v | $\phi$ | Match to # | Approx. to # |
|---|---|---|---|---|---|---|---|---|
| 1 | -1 | -1 | 0 | -1 | -1 | -1 | 11 | |
| 2 | -1 | 0 | 1 | -1 | -1 | 1 | | 1 |
| 3 | -1 | 1 | -1 | -1 | 1 | -1 | 3 | |
| 4 | 1 | 0 | 0 | -1 | 1 | 1 | 10 | |
| 5 | 1 | 1 | 1 | 1 | -1 | -1 | 6 | |
| 6 | 1 | -1 | -1 | 1 | -1 | 1 | | 12 |
| 7 | 0 | 1 | 0 | 1 | 1 | -1 | | 14 |
| 8 | 0 | -1 | 1 | 1 | 1 | 1 | 5 | |
| 9 | 0 | 0 | -1 | 0 | 0 | 0 | | 8 |
| 10 | -1 | 1 | 1 | -1 | 0 | 0 | | 2 |
| 11 | -1 | -1 | -1 | 1 | 0 | 0 | 4 | |
| 12 | 1 | 0 | -1 | 0 | -1 | 0 | 13 | |
| 13 | 0 | -1 | 0 | 0 | 1 | 0 | 7 | |
| 14 | 1 | 1 | 0 | 0 | 0 | -1 | 9 | |
| 15 | 0 | 0 | 1 | 0 | 0 | 1 | 15 | |

required by the central composite design, it will be assumed that it is sufficient enough to be used for the estimation of the linear and interaction effects between variables and fit the quadratic model.

### 3.2.2 Running of Experiments

An experiment began by first allowing the benzene vaporization unit to reach a steady state operating condition in terms of the temperature and pressure of the vessel for the selected flow rate. This would take anywhere from 1 to 3 hours depending on the flow rate. Longer times required for high flow rates. While this was occurring, the chamber would be sealed up and pressure tested to assure satisfactory vacuum conditions for the selected conditions, and the flow rates (upstream pressures) of the gasses would be set to their preselected values and turned off. A complete listing of the flow rates and pressures for the different experimental conditions are given in Appendix B.

Once everything was ready, the oxygen and argon gas flows to both the shield and core flames would be turned on, and the chamber pressure adjusted to between 60 to 70 torr. In this range the pressure is low enough so that the chances of a detonation upon ignition are minimal, yet high enough so that an electrical arc from the ignition wire could reach the surface of the burner. After these steps were completed the ethylene flow would be turned on and the shield flame ignited. With the shield flame started, the electrical arc would be discontinued, ignition wire moved away from the surface and the chamber pressure reduced to about 5 torr below the specified operating conditions.

At this point the benzene flow would be switched from recycling back to the bottle, to the mixing vessel with oxygen and argon and then directly to the burner. Simultaneously, the counter on the HPLC pump would be reset to record the cumulative benzene fed to the burner. Shortly after the flow was switched, the core flame would appear and stabilize in 3 to 5 seconds. The chamber pressure would then be adjusted to the specified level and the flow rates of the gasses checked. The length of the experiment would then be limited to the ability to control the chamber pressure to the specified level as the filter was being continuously plugged up by soot. This of course would depend on what the experimental conditions were. For a low pressure, high velocity, high equivalence ratio condition, the length of the experiment might be as short as 30 minutes. Whereas for a high pressure, low velocity, low equivalence ratio flame the time ran could exceed 3 hours.

Another factor that affected run time was the ability to keep the burner cooled. For some conditions, mostly low velocity and low equivalence ratio, there would be a higher heat load to the cooling fluid. Eventually the fluids inlet temperature would increase to a point that the heat absorbed in the cooling lines would cause it to vaporize and the burners temperature would increase dramatically. At this point if there was assumed to be enough soot produced, the experiment would be ended. If not, it would be shut down and stalled long enough that the fluid could cool and then be restarted.

When an experiment was ended, the benzene flow would be switched back to recycle causing the core flame to extinguish, the total benzene fed to the burner recorded and vaporizer turned off. The oxygen and ethylene gasses would be shut off and the cylinders closed, but argon allowed to purge the flow lines and chamber for approximately 5 minutes. The cooling fluid would be turned off after 10 to 15 minutes allowing the burner to cool down. However, a couple of hours would be required for the chamber walls to cool enough so that it could be opened and soot removed.

### 3.2.3 Collection and Extraction of Samples

When cleaning out the chamber, great care was taken to insure that a minimal amount of soot was lost to the surroundings or left within the chamber. First, one of the side flanges was removed and a foil pan placed on top of the burner to catch the soot that would fall off of the collection plates as they were removed. This was done so that no soot would fall down beside the burner and be lost to the bottom of the chamber. The top flange to which the collection plates are attached was removed carefully, set into a large pan and the soot scraped off the plates. The remainder of the chamber was scraped clean with a spatula and soot transferred to the large pan. The tubes that connected the filter to the top flange as well as the filter and its container were also scraped clean. After all surfaces had been scraped clean, the soot was placed inside a marked and weighed container and the weight of the collected soot recorded.

Concerning the filter itself, it was never able to be completely cleaned of the soot. There was always soot trapped within the fibers of the filter paper. This causes some additional error in the calculation of yield from carbon fed. Although the filter could be weighed before and after the experiment, their weight which averaged around 170 grams, exceeded the limit of the laboratory balance which was 160 grams. Another balance in the department was found which had a much larger limit, but it would only read to one decimal place and was very erratic. Therefore, it was decided that this value would be taken as a constant and added to the total value.

After collecting the soot, the fullerene fraction was extracted using toluene in a Soxhlet extraction unit. Approximately 2 grams of the soot were placed in a paper thimble, Whatman products, part # 2800339. If less than 4 grams were able to be collected, then only half of the soot would be used. This was done so that additional sample remained in case of an accident during the extraction (spill, glass breakage, etc.) and the experiment did not have to be needlessly re-ran. Approximately 300 ml of toluene was used for each extraction. The fresh solvent would be poured into the thimble containing the soot and allowed to drain into the empty flask. This decreased extraction times by 24 to 36 hours because a majority of the toluene soluble fraction was removed before actually running the unit. The usual time required to complete an extraction to solvent clarity was about 24 hours.

After the extraction was completed in the Soxhlet unit, the solvent rich in fullerenes was filtered through a 0.2 μm syringe filter, Gelman Acro-disc part # 4225. This removed any pieces of boiling stones or insoluble particles that passed through the thimble. The solvent would then be recovered by use of a rotary evaporator and remaining crystals taken to dryness. What remained at this time was reddish-black crystals adhered to the sides of a flask and sometimes an oily residue. The next step was to wash the sample with diethyl ether. About 80 to 100 ml of the solvent would be poured into the flask and then placed into a sonicating bath. This would then break the crystals off the sides of the flask as well as totally solublize the impurities.

Once this was done, the solution along with the insoluble fullerene crystals would be poured into a glass beaker, covered and the crystals allowed to settle out of the solution. This would take 12 to 18 hours. The ether solution would then be slowly poured off and filtered again through the same 0.2 μm syringe filter that was used after the Soxhlet extraction. The reason to filter it this time was to recover any fullerene particles suspended in the solution. The washed crystals would then be removed from the beaker and placed into an aluminum weighing boat. The beaker and syringe filter would then be rinsed with toluene and that solution poured into the weighing boat and set aside to evaporate overnight. After evaporation, the sample would be weighed, marked with an identification, covered and set aside to be analyzed for composition at a later date.

3.2.4 Analysis of Samples

Qualitative analysis of the powdered samples in KBr pellets was performed with FTIR. In early phases of this work, quantitative analysis of the samples was attempted with FTIR and proved little success. However, it did verify that fullerenes were being produced by the system.

Quantification of the amount of $C_{60}$ and $C_{70}$ in the samples were achieved with reverse phase high performance liquid chromatography. Standard samples of $C_{60}$ and $C_{70}$ were obtained from MER Inc. in Tucson, Arizona for use in calibration of the column. The calibration curves for the obtained samples are in Appendix C. A chromatogram of one of the calibration standards is shown in Figure 11.

The calibration solutions were made by combining both standards of $C_{60}$ and $C_{70}$ together into one solution. This enabled calibration time to be cut in half and the method developed for complete resolution of the peaks. The column was a Waters Symmetry $C_{18}$ column, 150 x 3.9 mm, 5 μm particle, part #542025. The mobile phase was an isocratic 60:40 methanol:toluene solution running at 1.0 ml/min. Spectra were taken with a Waters tunable UV absorbance spectrometer, model #484, at 305 nm. The chosen mobile phase and UV absorption level was recommended by Dr. Mike Alford, from TDA Research in Wheatridge, Colorado. The chromatogram in Figure 11 is from a solution with a composition of 0.21 mg/ml of $C_{60}$ and 0.28 mg/ml $C_{70}$. The retention time for the individual peaks are 8.7 minutes for $C_{60}$ and 16.2 minutes for $C_{70}$. The peak at 1.2 minutes is a system peak that is a result of the pressure pulse from injection of the sample.

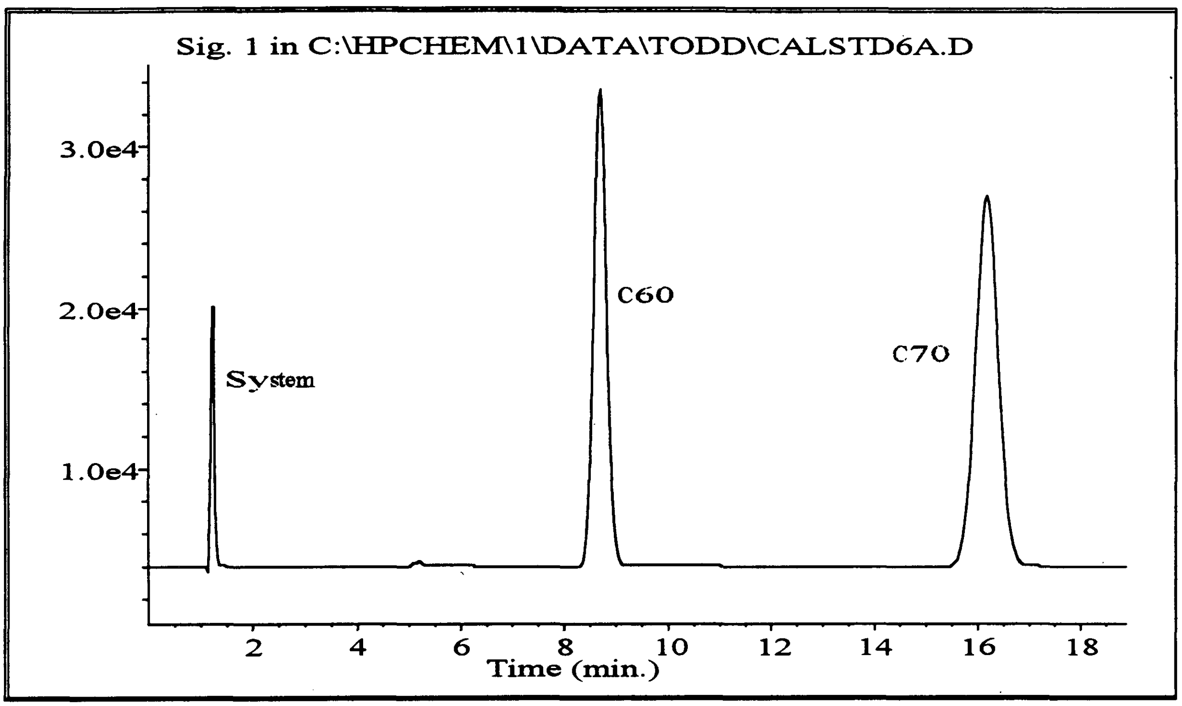


Figure 11 HPLC Calibration Standard

# Chapter 4

# RESULTS AND DISCUSSION

## 4.1 Measurements

This section is mainly for the presentation and general overview of all of the data taken in this study. Sections 4.2 and 4.3 will statistically examine the effect of process variables on different yields. In order to simplify the presentation of the data, this section will be broken up into the following main areas.

4.1.1 Experimental Runs

4.1.2 Extractions

4.1.3 HPLC

4.1.4 Temperature

### 4.1.1 Experimental Runs

The run-time and carbon conversion data for all fifteen experimental conditions plus replicates (23 total, separate runs) are shown in Table 3. Concerning the identification of the samples, the first number represents the experimental condition, the following letter signifies which set was from and the second number represents the extraction. The difference between sets c and d is that set d started when the equivalence ratio range was shifted, as explained in section 3.2.1. Sets a and b were used when the system was still in the construction phase. If an r follows either a c or a d, it signifies that the run is a replicate of that condition within that set. In order to be brief, the values for the second extractions were left out because they do not indicate any differences in the run time or carbon yield.

As shown in Table 3 and discussed in section 3.2.3, 100% of the soot produced by the flame could not be accounted for due to some entrapment in the filter and loss to surroundings during collection. Though great precaution and care was taken to minimize the loss to surroundings, that which was trapped in the filter was much more significant and had to be taken as a constant at 2.0 grams with a variability of 0.5 grams. The variability was included so that error bars could be calculated for in any values involving the total soot produced.

Other points to be noticed concerning Table 3 is the effect of the conditions on the run times and carbon yields. As a general trend, the run times are short and carbon yields high for conditions with high velocities and equivalence ratios. The opposite holds for low velocities and equivalence ratios. This is to be expected due to the nature of the system. Since the length of the experiment is dependent upon the pumps ability to pull

Table 3 Experimental Run Time and Carbon Yield

| ID | P | v | $\phi$ | min. | ml C6H | g C fed | Soot (g) collected | Soot (g) lost | Soot (g) total | % C yield |
|---|---|---|---|---|---|---|---|---|---|---|
| 1-c-1 | 20.0 | 30 | 2.3750 | 159.0 | 380.0 | 305.7 | 6.85 | 2.00 | 8.85 | 2.90 |
| 2-c-1 | 20.0 | 40 | 2.5625 | 33.7 | 113.3 | 91.2 | 1.54 | 2.00 | 3.54 | 3.89 |
| 2-d-1 | | | | 144.3 | 485.0 | 390.2 | 19.56 | 2.00 | 21.56 | 5.53 |
| 3-d-1 | 20.0 | 50 | 2.1875 | 228.5 | 850.0 | 683.8 | 2.88 | 2.00 | 4.88 | 0.71 |
| 3-dr-1 | | | | 215.1 | 800.0 | 643.6 | 3.40 | 2.00 | 5.40 | 0.84 |
| 4-c-1 | 35.0 | 40 | 2.3750 | 126.1 | 700.0 | 563.2 | 18.39 | 2.00 | 20.39 | 3.62 |
| 4-cr-1 | | | | 68.5 | 380.0 | 305.7 | 4.79 | 2.00 | 6.79 | 2.22 |
| 5-c-1 | 35.0 | 50 | 2.5625 | 21.1 | 155.0 | 124.7 | 9.78 | 2.00 | 11.78 | 9.44 |
| 5-d-1 | | | | 54.4 | 400.0 | 321.8 | 8.16 | 2.00 | 10.16 | 3.16 |
| 6-d-1 | 35.0 | 30 | 2.1875 | 153.5 | 600.0 | 482.7 | 5.63 | 2.00 | 7.63 | 1.58 |
| 6-dr-1 | | | | 102.3 | 400.0 | 321.8 | 3.52 | 2.00 | 5.52 | 1.71 |
| 7-c-1 | 27.5 | 50 | 2.3750 | 73.4 | 400.3 | 322.0 | 7.87 | 2.00 | 9.87 | 3.06 |
| 7-cr-1 | | | | 110.1 | 600.0 | 482.7 | 6.35 | 2.00 | 8.35 | 1.73 |
| 8-c-1 | 27.5 | 30 | 2.5625 | 72.3 | 250.0 | 201.1 | 15.11 | 2.00 | 17.11 | 8.50 |
| 9-d-1 | 27.5 | 40 | 2.1875 | 195.6 | 800.0 | 643.6 | 3.90 | 2.00 | 5.90 | 0.92 |
| 9-dr-1 | | | | 122.2 | 500.0 | 402.3 | 2.62 | 2.00 | 4.62 | 1.15 |
| 10-c-1 | 20.0 | 50 | 2.5625 | 61.9 | 260.0 | 209.2 | 14.32 | 2.00 | 16.32 | 7.80 |
| 11-d-1 | 20.0 | 30 | 2.1875 | 206.3 | 460.0 | 370.1 | 5.50 | 2.00 | 7.50 | 2.03 |
| 11-dr-1 | | | | 289.2 | 645.0 | 518.9 | 3.40 | 2.00 | 5.40 | 1.04 |
| 12-d-1 | 35.0 | 40 | 2.1875 | 128.6 | 670.0 | 539.0 | 4.13 | 2.00 | 6.13 | 1.14 |
| 13-d-1 | 27.5 | 30 | 2.3750 | 108.0 | 350.0 | 281.6 | 3.88 | 2.00 | 5.88 | 2.09 |
| 14-d-1 | 35.0 | 50 | 2.3750 | 68.6 | 476.0 | 382.9 | 4.82 | 2.00 | 6.82 | 1.78 |
| 15-d-1 | 27.5 | 40 | 2.5625 | 103.9 | 480.0 | 386.2 | 19.03 | 2.00 | 21.03 | 5.45 |

the filtered gasses through the filter at a rate that enables the pressure to remain constant, a high velocity, highly sooting flame will obviously have a shorter run time than the opposite.

4.1.2 Extractions

Extractions performed on the soot produced by the flames were carried out as a first step in the determination of the $C_{60} + C_{70}$ fractions. This is basically a gravimetric analysis and the data presented here are only meant to be used to examine the variability of the extraction step. The data shown in Table 4 is for all samples, therefore it is a little longer than Table 3. The additional samples have a 2 at the end of the id..

At inspection of the percent of solubles per gram of soot data in Table 4, it can be noticed that the degree of variability between samples of replicate extractions is not as great as those between replicate runs. The average of the sample standard deviations for each pair, are 0.86 and 3.00 for samples with replicate extractions and conditions with replicate runs respectively. This means that for the percentage of soluble mass extracted from the soot, a standard deviation of 0.86 percent can be expected for the extraction step. But a standard deviation of three percent is expected in the extracted mass of the soot between samples with replicate runs.

Table 4 Soluble Fractions of Soot

| ID | P | v | $\phi$ | g Soot | g net | % solubles/gram Soot | % solubles/gram C fed |
|---|---|---|---|---|---|---|---|
| 1-c-1 | 20 | 30 | 2.3750 | 2.357 | 0.146 | 6.19 | 0.18 |
| 1-c-3 | | | | 1.372 | 0.048 | 3.50 | 0.10 |
| 2-c-1 | 20 | 40 | 2.5625 | 1.079 | 0.077 | 7.14 | 0.28 |
| 2-d-1 | | | | 3.313 | 0.242 | 7.30 | 0.40 |
| 3-d-1 | 20 | 50 | 2.1875 | 1.446 | 0.379 | 26.21 | 0.19 |
| 3-dr-1 | | | | 1.760 | 0.312 | 17.73 | 0.15 |
| 4-c-1 | 35 | 40 | 2.3750 | 2.120 | 0.275 | 12.97 | 0.47 |
| 4-c-2 | | | | 2.835 | 0.283 | 9.98 | 0.36 |
| 4-cr-1 | | | | 2.403 | 0.236 | 9.82 | 0.22 |
| 5-c-1 | 35 | 50 | 2.5625 | 2.515 | 0.078 | 3.10 | 0.29 |
| 5-d-1 | | | | 2.210 | 0.262 | 11.86 | 0.37 |
| 6-d-1 | 35 | 30 | 2.1875 | 2.028 | 0.332 | 16.37 | 0.26 |
| 6-dr-1 | | | | 1.713 | 0.283 | 16.52 | 0.28 |
| 7-c-1 | 27.5 | 50 | 2.3750 | 2.790 | 0.461 | 16.52 | 0.51 |
| 7-cr-1 | | | | 2.414 | 0.362 | 15.00 | 0.26 |
| 8-c-1 | 27.5 | 30 | 2.5625 | 3.043 | 0.041 | 1.35 | 0.11 |
| 8-c-2 | | | | 2.383 | 0.032 | 1.34 | 0.11 |
| 9-d-1 | 27.5 | 40 | 2.1875 | 2.069 | 0.450 | 21.75 | 0.20 |
| 9-dr-1 | | | | 1.179 | 0.165 | 13.99 | 0.16 |
| 10-c-1 | 20 | 50 | 2.5625 | 3.063 | 0.062 | 2.02 | 0.16 |
| 10-c-2 | | | | 2.084 | 0.021 | 1.01 | 0.08 |
| 11-d-1 | 20 | 30 | 2.1875 | 2.118 | 0.388 | 18.32 | 0.37 |
| 11-dr-1 | | | | 2.356 | 0.338 | 14.35 | 0.15 |
| 12-d-1 | 35 | 40 | 2.1875 | 1.961 | 0.412 | 21.01 | 0.24 |
| 12-d-2 | | | | 1.878 | 0.368 | 19.60 | 0.22 |
| 13-d-1 | 27.5 | 30 | 2.3750 | 1.732 | 0.127 | 7.33 | 0.15 |
| 13-d-2 | | | | 1.713 | 0.117 | 6.83 | 0.14 |
| 14-d-1 | 35 | 50 | 2.3750 | 2.035 | 0.380 | 18.67 | 0.33 |
| 14-d-2 | | | | 1.763 | 0.313 | 17.75 | 0.32 |
| 15-d-1 | 27.5 | 40 | 2.5625 | 3.247 | 0.198 | 6.10 | 0.33 |
| 15-d-2 | | | | 3.461 | 0.218 | 6.30 | 0.34 |

Comparing of some of the data between Tables 3 and 4, it is seen that as the carbon yield for a sample decreases, its percentage of solubles per gram of soot increases. This is shown graphically in Figure 12. The error bars that have been placed on the points in Figure 12 are due to the variability in the extraction step (Y bars), and the deviation in the total soot produced (X bars). Considering the error bars on the carbon yield, some points have noticeably larger error than others. Since the soot lost was taken as a constant, the error associated with loss will be larger for runs where little soot was collected. In Table 3 it can be seen that there are a few runs where the assumed soot loss is comparable to that which was collected and therefore will have larger errors associated with the carbon yield for that run.

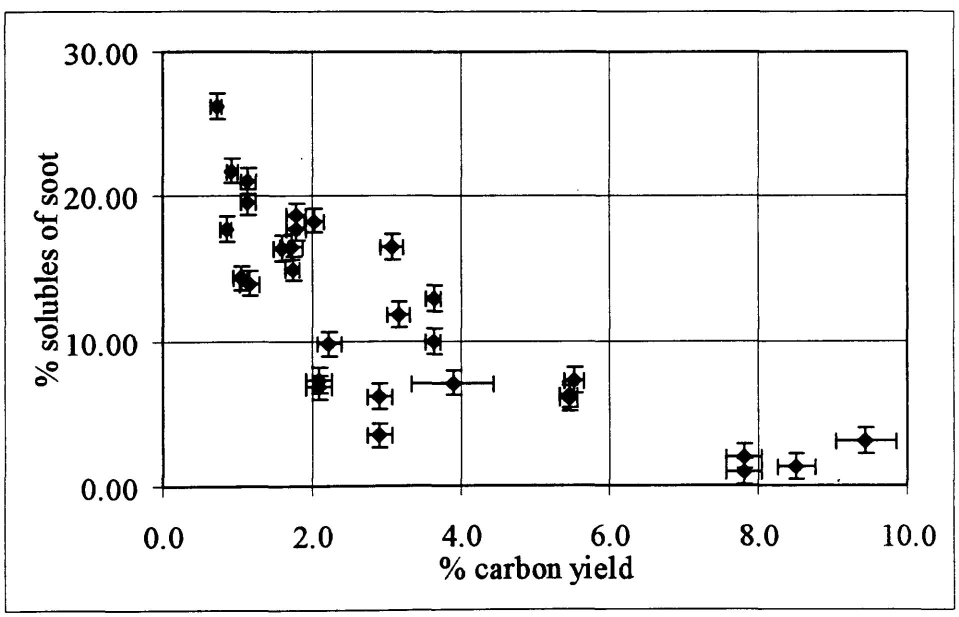


Figure 12 Soluble Fraction of Soot from Carbon Yield

As it will be discussed in the HPLC section 4.1.3, the samples are mostly composed of fullerenes and a small fraction of polycyclic aromatic hydrocarbons (PAH). Since separation is a major factor to be considered in any reaction/chemical production scheme, Figure 12 should indicate that in order to maximize the fraction of the soot that contains fullerenes, a low carbon yield flame should be selected. On inspection of Figure 12, one might also conclude that there is a lot more noise associated with these data than that which the error bars predict. Though there is wide variation in the data points between 1 to 4 percent carbon yield, it should not be taken only as noise. Since the data are a function of three different variables, and carbon yield is dependent mainly on the equivalence ratio and the chamber pressure, the data should be looked at as the ability to select a certain percentage of extractable soot mass over a wide range of carbon yields. It should be noted again that all data will be treated in greater detail in sections 4.2 and 4.3.

As noted earlier in section 3.2.4, FTIR was used to make a qualitative analysis of the samples for the presence of $C_{60}$ and $C_{70}$. Figure 13 is an absorption spectrum of sample 7-c-1. The peaks at 1428, 1182, 577 and 526 $cm^{-1}$ are from the presence of $C_{60}$. $C_{70}$ has been assigned the peaks at 795, 674, 642, 565 and 535 $cm^{-1}$. The other peaks have not been assigned and are thought to be from the larger fullerenes. Not seen in Figure 13 are peaks around 3000 $cm^{-1}$ that are due to PAH compounds. The spectrum was limited to the range of 400 to 1450 $cm^{-1}$ in order to magnify the fullerene peaks.

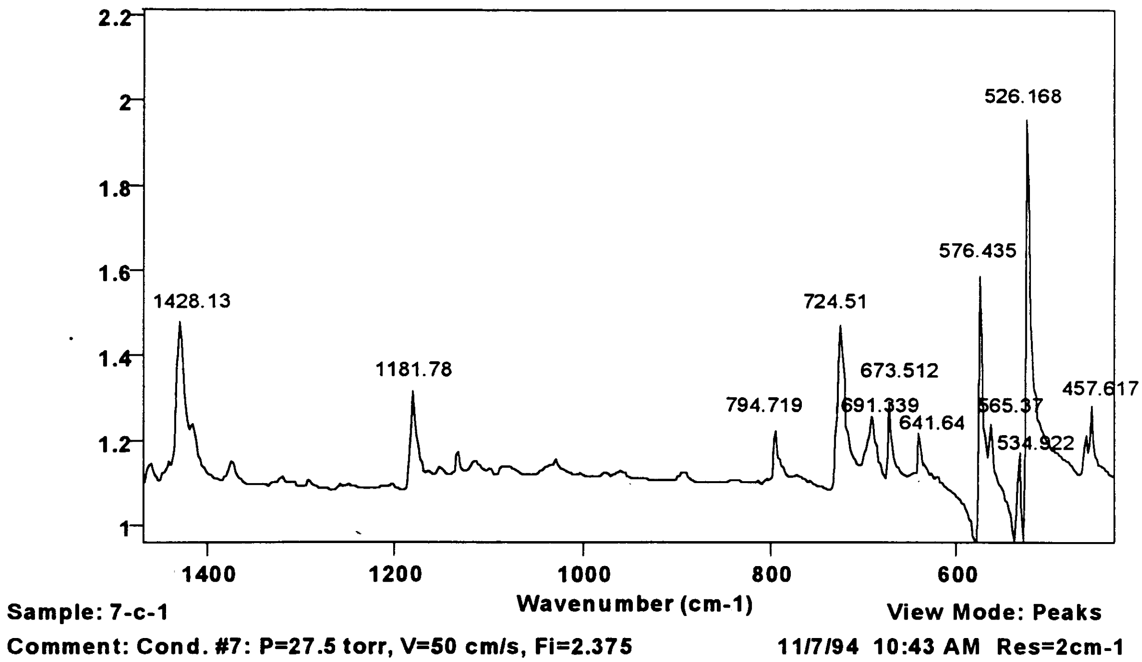


Figure 13 FTIR spectrum of sample 7-c-1 for qualitative analysis

4.1.3 HPLC

High performance liquid chromatography was the method by which the samples were analyzed for composition. An example chromatogram of sample 12-d-1 is shown in Figure 14 and is a fairly good representation of all of the samples. The $C_{60}$ and $C_{70}$ peaks are completely resolved at retention times of 9.1 and 17.1 minutes respectively and the mass fractions calculated from the calibration are 0.49 and 0.44 respectively.

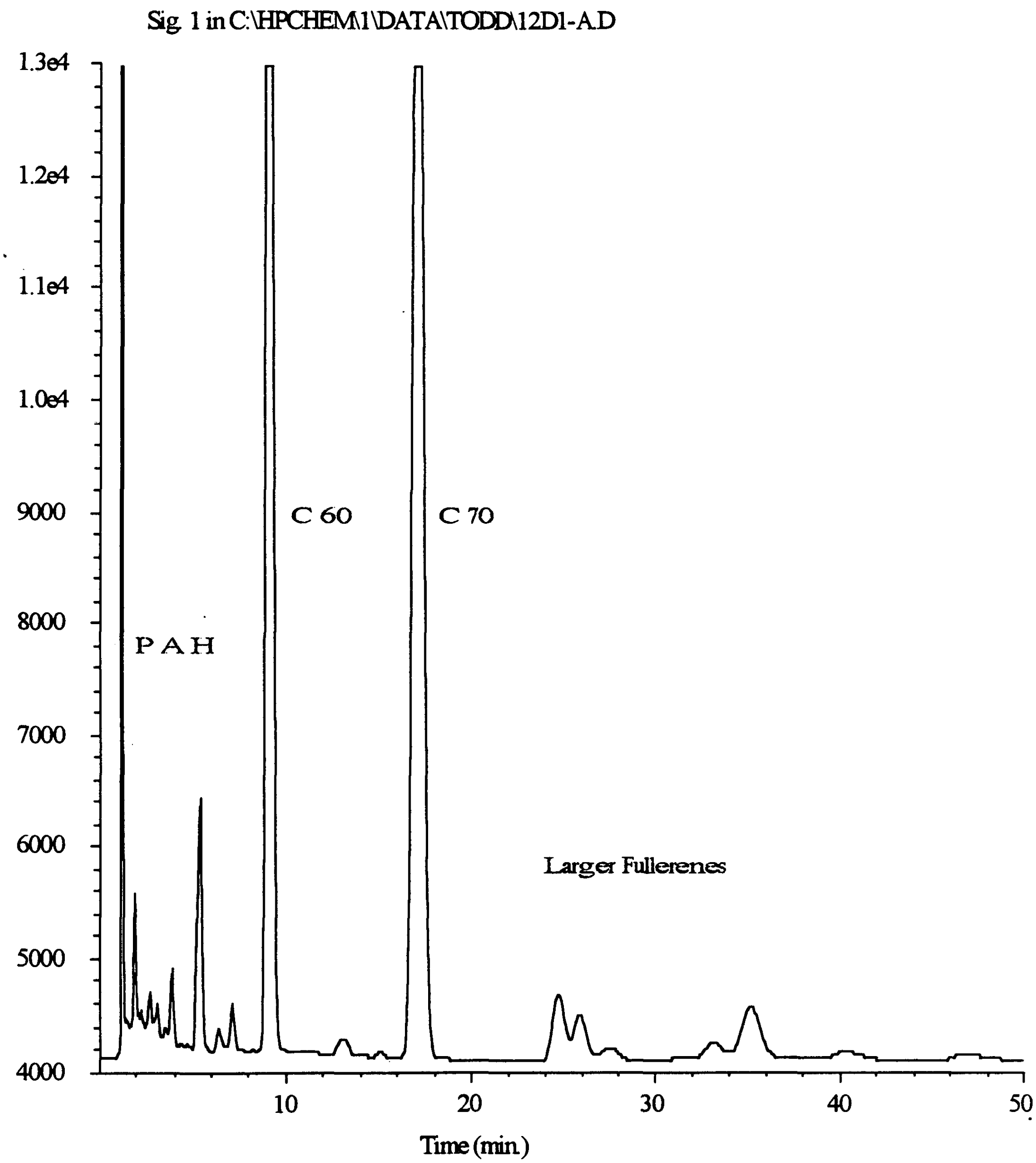


Figure 14 Example Chromatogram, Sample 12-d-1

Upon comparison to the chromatogram of calibration standard #6 in section 3.2.4, it is noticed that there is a number of additional peaks present. There is a slight change in the retention times of $C_{60}$ and $C_{70}$ due to a different batches of mobile phase solvent being used between calibration and the analysis of that sample. However, what is interesting is the number of other compounds that are present in the samples.

The peaks that come after $C_{70}$ are larger fullerenes (39). With respect to retention times, the peaks have been assigned to be the following compounds: 24.7 min., $C_{76}$; 25.9 and 27.5 are isomers of $C_{78}$; 33.2, $C_{82}$; 35.2, $C_{84}$. The peaks at 40.2 and 46.8 minutes are probably $C_{86}$ and $C_{88}$ respectively, but no work was found identifying these. There is also a third isomer of $C_{78}$ among the larger fullerene peaks, but due to the composition of the mobile phase and column temperature, this component is not resolved. Accurate identification and quantification of the larger fullerene peaks for this work would involve a much more thorough analysis and/or calibration with very expensive standards. But since the focus of this research was to quantify the yields of $C_{60}$ and $C_{70}$, no investigation into the larger fullerenes was made. It should also be mentioned that further extraction on the soot residue with trichlorobenzene yields higher concentrations of the fullerenes larger than $C_{70}$ (32).

The grouping of peaks between the system peak and that of $C_{60}$ are PAH compounds that have very little retention to the stationary non-polar phase of the column. This is mainly due to their high solubility in the toluene fraction of the mobile phase. These compounds are most likely to be things like benzo[ghi]fluorathene and coranulene (31). Oxides of $C_{60}$ and $C_{70}$ are very likely to be present in the samples and have slightly shorter retention times than their non-oxides. One of the peaks in the PAH range is $C_{60}O$ and the small peak between $C_{60}$ and $C_{70}$ is probably $C_{70}O$. Dr. Mike Alford from TDA Research was consulted for the identification of the extra peaks in the samples.

Table 5 is a summary of the HPLC analysis. The mass fraction of the solubles is from the actual injection of the extracted sample and thus computed directly from the calibration and the concentration of the sample solution. The molar C70/C60 ratio is computed through the calibration and molecular weights. The mass fractions of the soot is calculated by multiplying the fractions of solubles to the soluble fraction of the soot. Data consisting of the areas of the $C_{60}$ and $C_{70}$ peaks for all injections and other related information are given in Appendix D.

Due to the mass of information that is contained in Table 5, inspection of it is cumbersome and the relations to other data in previous tables might be overlooked. Figure 15 exhibits how the individual fractions of $C_{60}$ and $C_{70}$ change with respect to their total for the extracted fraction of the soot. Or basically, columns 2 and 3 against column 4 from Table 5. There seems to be a direct relationship between the fraction of $C_{60} + C_{70}$ and the individual fraction of $C_{60}$ in the extracted sample. As the total fraction of $C_{60}$ + $C_{70}$ in the soluble fraction of the soot increases, the fraction of $C_{60}$ increases also. However the fraction of $C_{70}$ in the soluble fraction of the soot remains relatively

Table 5 HPLC Analysis of Sample Composition

| ID | Mass fraction of solubles C60 | C70 | Total | Molar C70/C60 | Mass fraction of soot C60 | C70 | Total |
|---|---|---|---|---|---|---|---|
| 1-c-1 | 0.367 | 0.353 | 0.720 | 0.823 | 0.023 | 0.022 | 0.045 |
| 1-c-3 | 0.280 | 0.446 | 0.727 | 1.365 | 0.010 | 0.016 | 0.025 |
| 2-c-1 | 0.385 | 0.343 | 0.727 | 0.764 | 0.027 | 0.024 | 0.052 |
| 2-d-1 | 0.308 | 0.341 | 0.649 | 0.950 | 0.022 | 0.025 | 0.047 |
| 3-d-1 | 0.367 | 0.337 | 0.704 | 0.785 | 0.096 | 0.088 | 0.185 |
| 3-dr-1 | 0.335 | 0.289 | 0.624 | 0.741 | 0.059 | 0.051 | 0.111 |
| 4-c-1 | 0.410 | 0.368 | 0.778 | 0.770 | 0.053 | 0.048 | 0.101 |
| 4-c-2 | 0.479 | 0.374 | 0.853 | 0.670 | 0.048 | 0.037 | 0.085 |
| 4-cr-1 | 0.494 | 0.358 | 0.852 | 0.622 | 0.048 | 0.035 | 0.084 |
| 5-c-1 | 0.366 | 0.413 | 0.779 | 0.967 | 0.011 | 0.013 | 0.024 |
| 5-d-1 | 0.536 | 0.345 | 0.881 | 0.553 | 0.064 | 0.041 | 0.104 |
| 6-d-1 | 0.386 | 0.436 | 0.822 | 0.968 | 0.063 | 0.071 | 0.135 |
| 6-dr-1 | 0.312 | 0.409 | 0.721 | 1.125 | 0.052 | 0.068 | 0.119 |
| 7-c-1 | 0.465 | 0.347 | 0.812 | 0.639 | 0.077 | 0.057 | 0.134 |
| 7-cr-1 | 0.502 | 0.320 | 0.822 | 0.547 | 0.075 | 0.048 | 0.123 |
| 8-c-1 | 0.242 | 0.420 | 0.661 | 1.489 | 0.003 | 0.006 | 0.009 |
| 8-c-2 | 0.215 | 0.448 | 0.663 | 1.786 | 0.003 | 0.006 | 0.009 |
| 9-d-1 | 0.452 | 0.438 | 0.890 | 0.831 | 0.098 | 0.095 | 0.194 |
| 9-dr-1 | 0.355 | 0.437 | 0.791 | 1.055 | 0.050 | 0.061 | 0.111 |
| 10-c-1 | 0.358 | 0.419 | 0.777 | 1.003 | 0.007 | 0.008 | 0.016 |
| 10-c-2 | 0.313 | 0.476 | 0.789 | 1.305 | 0.003 | 0.005 | 0.008 |
| 11-d-1 | 0.406 | 0.465 | 0.871 | 0.981 | 0.074 | 0.085 | 0.160 |
| 11-dr-1 | 0.343 | 0.407 | 0.750 | 1.017 | 0.049 | 0.058 | 0.108 |
| 12-d-1 | 0.494 | 0.437 | 0.930 | 0.758 | 0.104 | 0.092 | 0.195 |
| 12-d-2 | 0.472 | 0.455 | 0.927 | 0.827 | 0.092 | 0.089 | 0.182 |
| 13-d-1 | 0.371 | 0.462 | 0.833 | 1.069 | 0.027 | 0.034 | 0.061 |
| 13-d-2 | 0.383 | 0.469 | 0.853 | 1.050 | 0.026 | 0.032 | 0.058 |
| 14-d-1 | 0.542 | 0.383 | 0.925 | 0.606 | 0.101 | 0.072 | 0.173 |
| 14-d-2 | 0.564 | 0.381 | 0.945 | 0.579 | 0.100 | 0.068 | 0.168 |
| 15-d-1 | 0.361 | 0.381 | 0.742 | 0.904 | 0.022 | 0.023 | 0.045 |
| 15-d-2 | 0.352 | 0.364 | 0.716 | 0.887 | 0.022 | 0.023 | 0.045 |

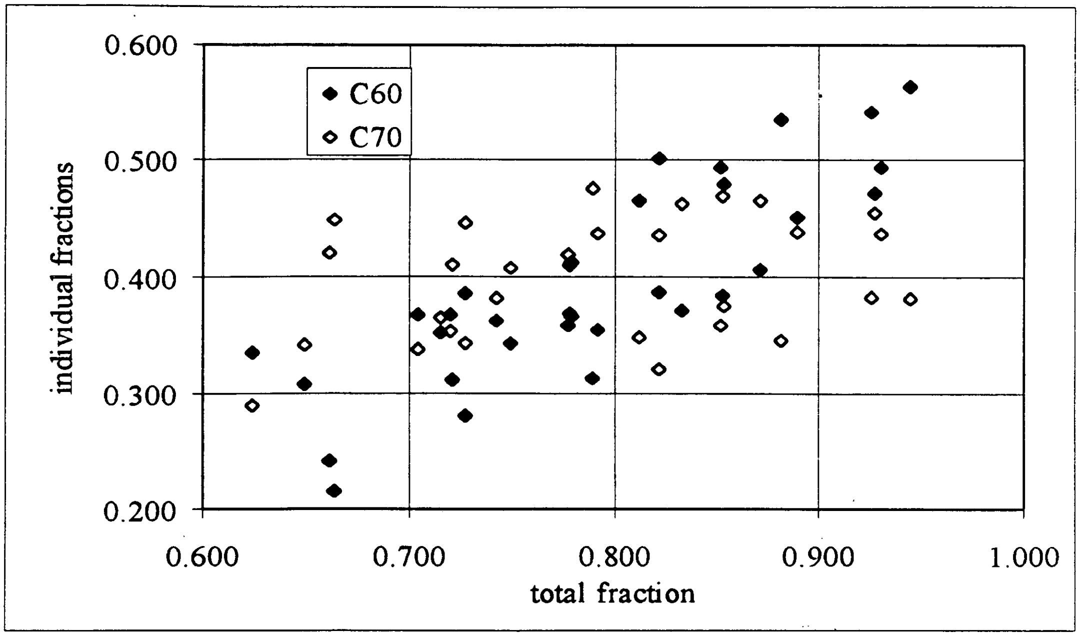


Figure 15 $C_{60}$ and $C_{70}$ vs. $C_{60}$+$C_{70}$ for extractable fraction

fixed at around 40% of the sample. Therefore, changes in the total fraction of $C_{60}$ and $C_{70}$ in the soluble fraction extracted from the soot is mainly due to a reflective change in the $C_{60}$ fraction.

Figure 16 is a plot of columns 6 and 7 against column 8 from Table 5 and presented to show how the fractions of $C_{60}$ and $C_{70}$ change relative to each other in a gram of soot. Figure 16 does not reflect the same information as that in Figure 15. Both $C_{60}$ and $C_{70}$ have a direct relationship to their total with respect to a mass of soot. However, there does seem to be some separation between the two components as their total fraction of the soot increases. The exact reasons for the differences between Figures 15 and 16 are

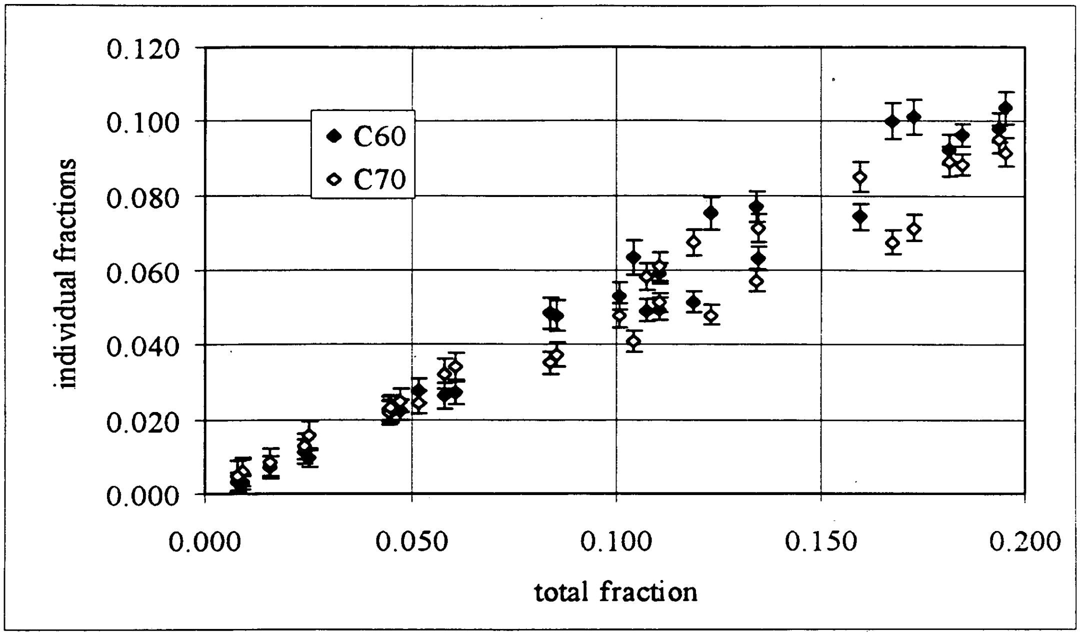


Figure 16 Individual Fractions vs. Total Fraction of Soot

not apparent. Except to state that there may be some competing factors between fullerene production and production of all other components in the extractable fraction of the soot.

A number of different plots were presented by Howard et al. (31) regarding values of the total $C_{60} + C_{70}$ in soot, $C_{70}/C_{60}$ molar ratio, total $C_{60} + C_{70}$ from carbon fed, the production rate of $C_{60} + C_{70}$ and the carbon yield. For comparison, similar plots have been constructed from this work as well as plots where the individual fractions of $C_{60}$ and $C_{70}$ are shown. Comparison plots are shown in Figures 17, 19, 21, 23 and 25. Plots that have been broken into the individual fractions are shown in Figures 18, 20, 22, 24 and 26.

Comparison of Figures 17, 19, 21, 23 and 25 with those by Howard et al. (31), show that the data taken in this study are not significantly different. Figure 17 is qualitatively the same as Figure 12, except that the data plotted in Figure 17 have been reduced by the mass fraction of $C_{60}$ and $C_{70}$ in the extracted sample as listed in column 4 of Table 3. A difference from Howard's work that should be noticed is that data taken in this work have higher $C_{60}$ + $C_{70}$ percentages of soot for carbon yields greater than 2 %. When broken down and plotted as individual components as seen in Figure 18, the highest percentage of $C_{60}$ in the soot is 10.5 at a carbon yield of 1.1 percent for sample 12-d-1. For $C_{70}$, a maximum of 9.5 percent of soot at a carbon yield of 0.9 percent for sample 9-d-1.

Figure 19 shows the greatest deviation from the work of Howard et al.. All data taken in this work are clustered around the highest measurements made by Howards group. Though it should noted that for their work, any measurements regarding $C_{60}$ and $C_{70}$ as a percentage of carbon fed was made by probe sampling. This allows calculations based on a known volume of the flame gas for the mass of product collected and ultimately reducing the error associated with the collection of soot from the inside of the chamber by a substantial amount. Assuming that the errors taken into account for soot collection with this work are sufficient, the highest yield of $C_{60}$ + $C_{70}$ as a fraction of carbon fed was 0.41 % for a total yield of 13.4 % from soot for sample 7-c-1. Sample 12-d-1 had 0.22 % for the highest percentage of soot at 19.5 %. There is no substantial information

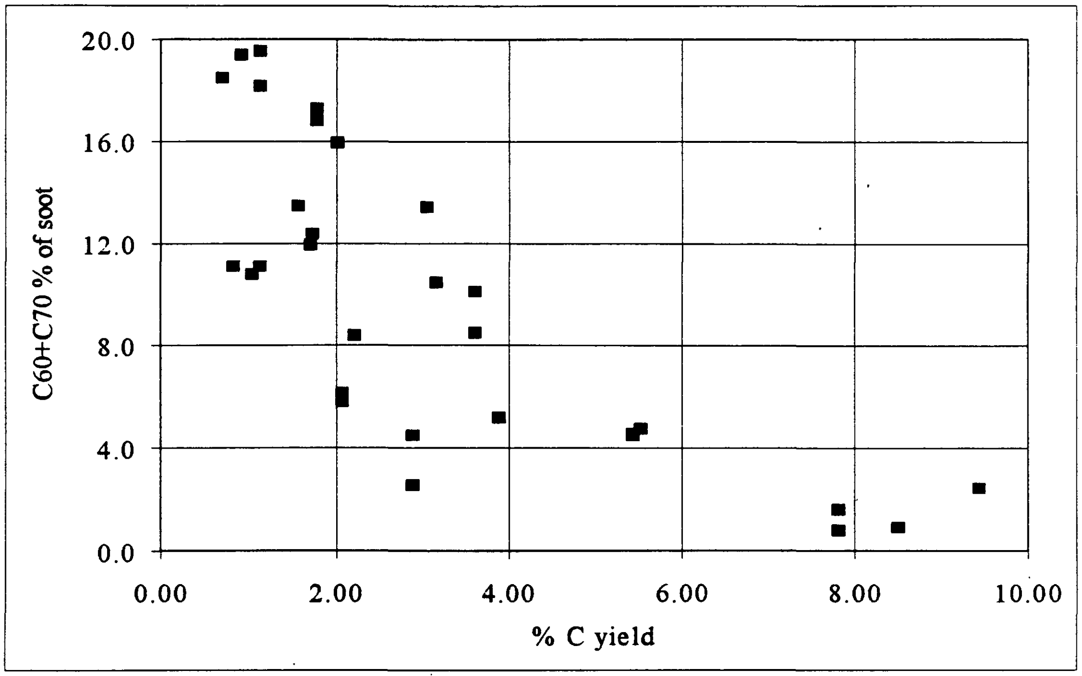


Figure 17 Fullerenes from Soot vs. Soot from Carbon

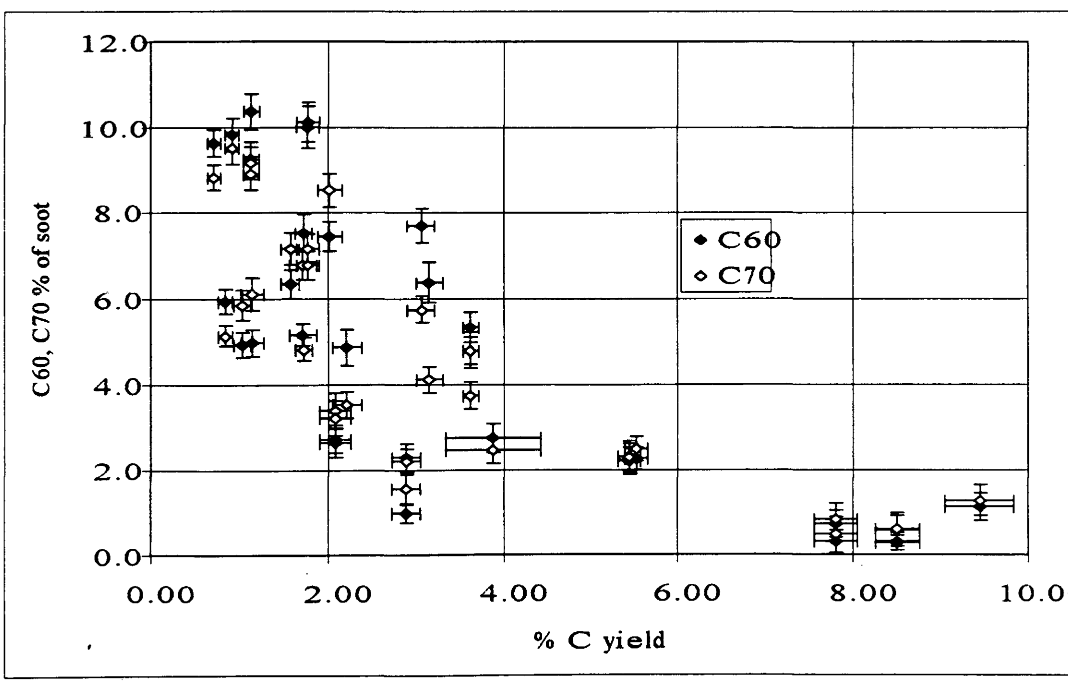


Figure 18 Individual Fullerenes from Soot vs. Soot from Carbon

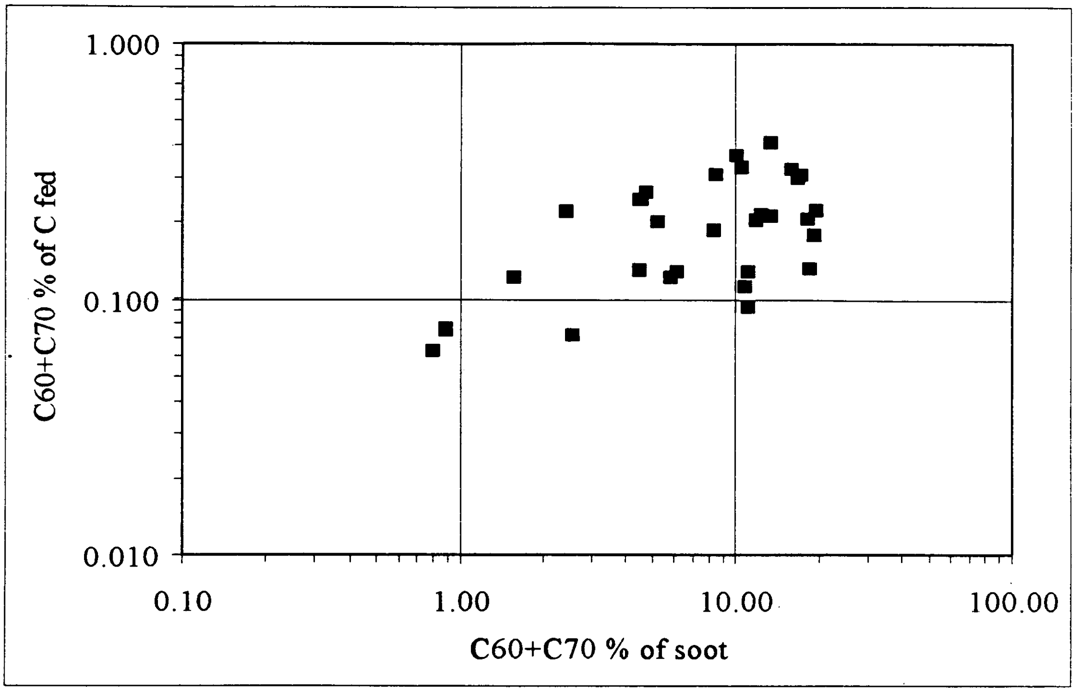


Figure 19 Fullerenes as a Percentage of Carbon Fed and of Soot

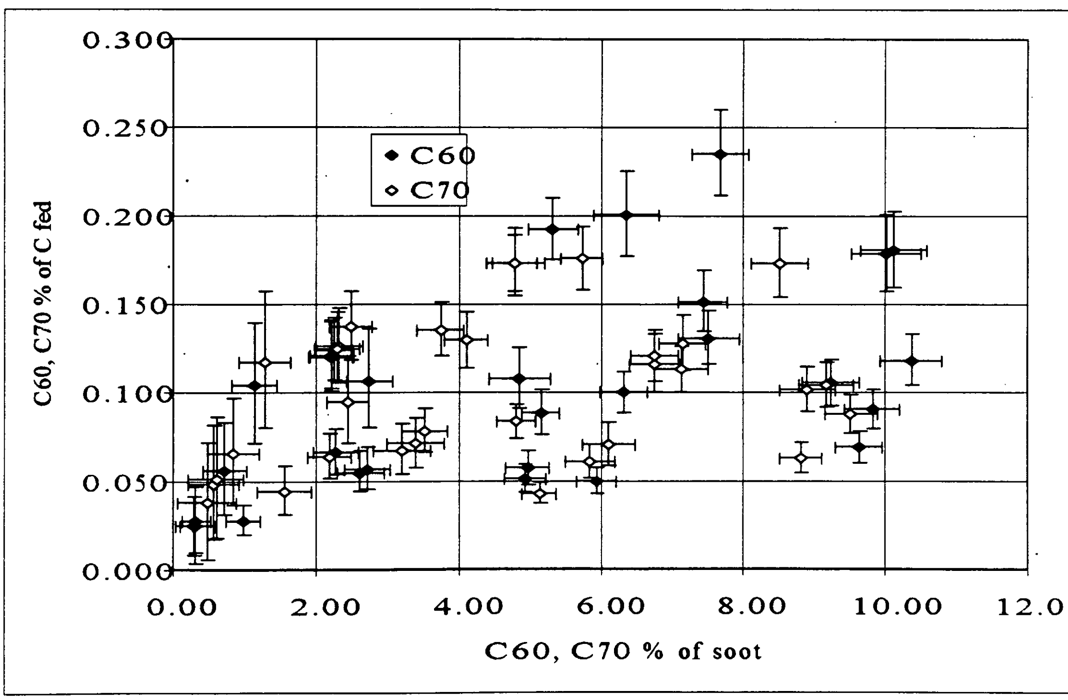


Figure 20 Individual Fullerenes as a Percentage of Carbon Fed and of Soot

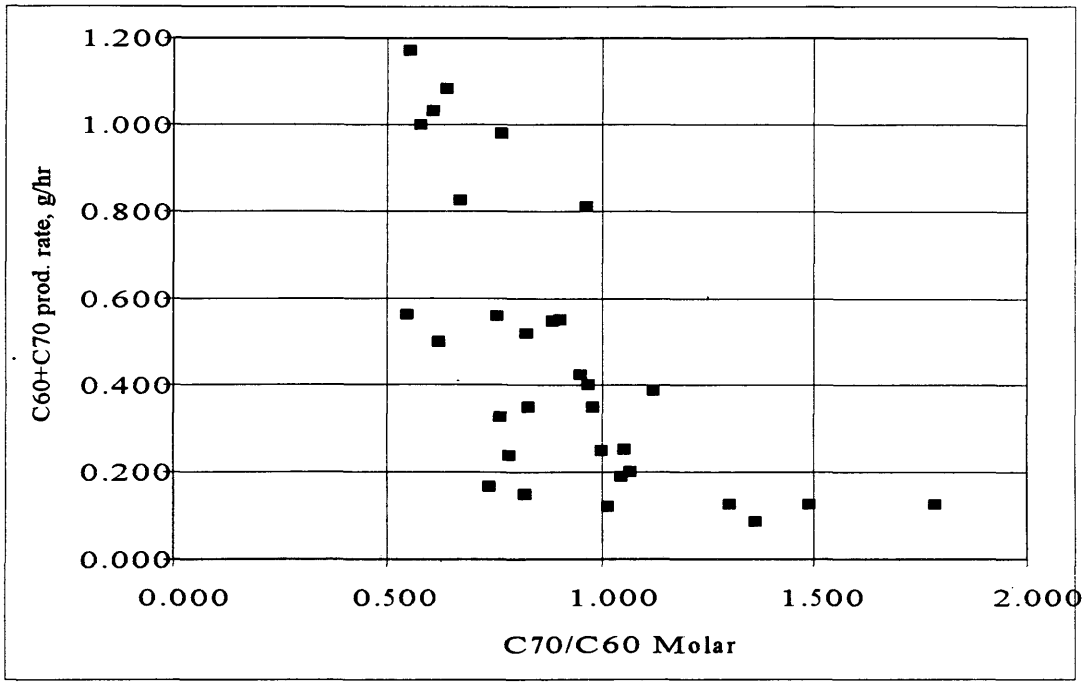


Figure 21 Fullerene Production Rate vs. $C_{70}/C_{60}$ Molar Ratio of Sample

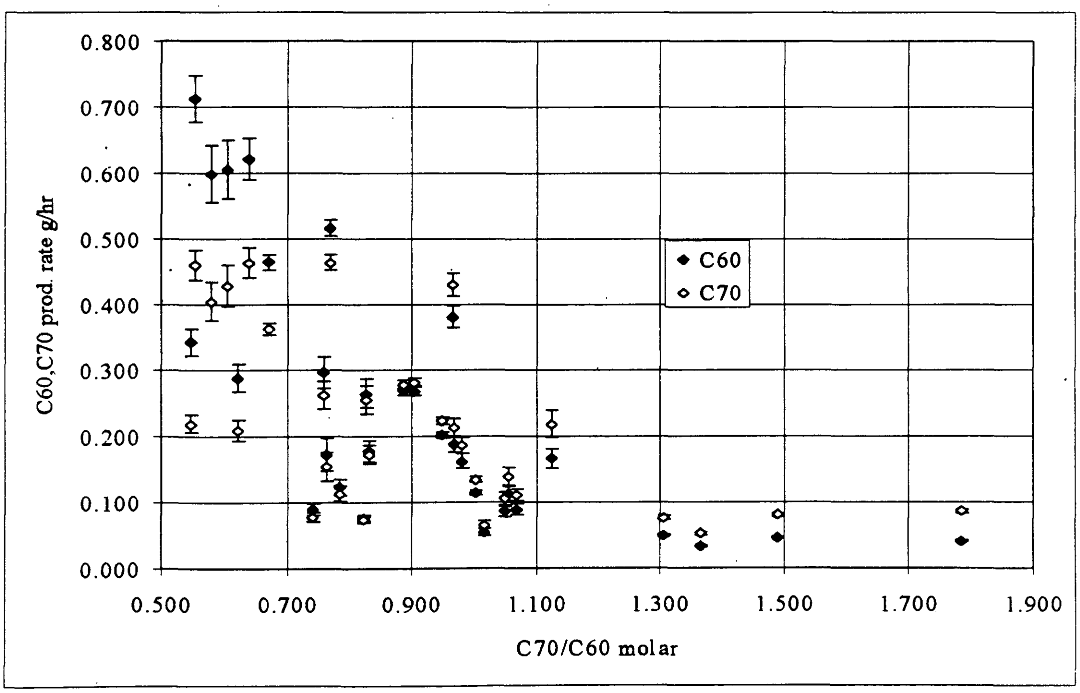


Figure 22 Individual Production Rate vs. $C_{70}/C_{60}$ Molar Ratio of Sample

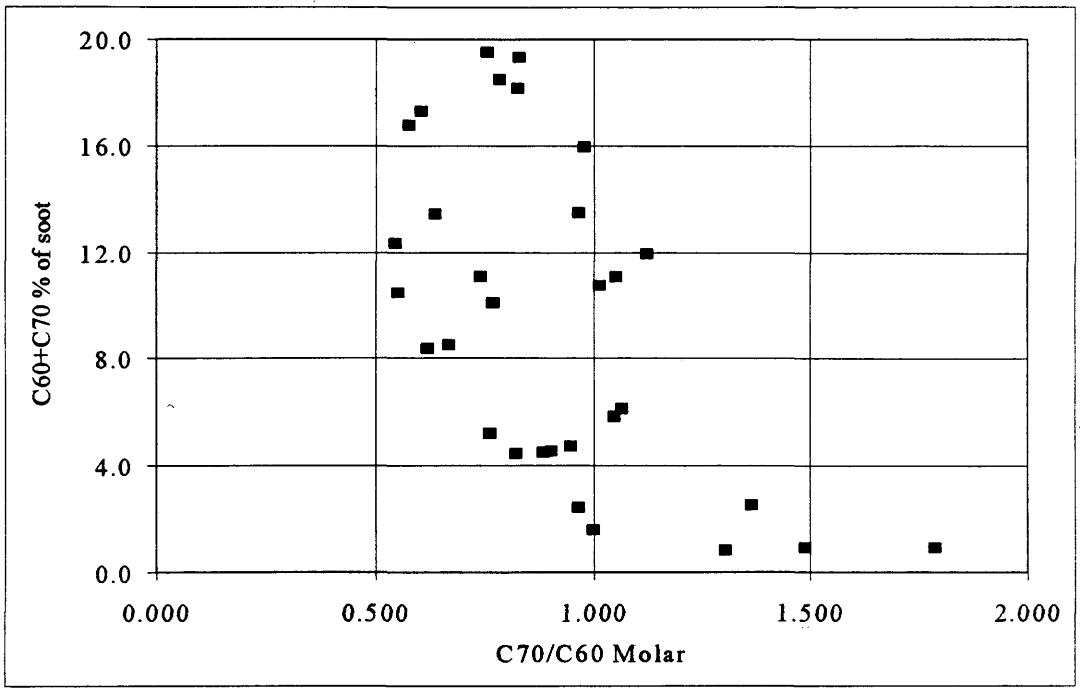


Figure 23 Fullerene Percent of Soot vs. $C_{70}/C_{60}$ Molar Ratio

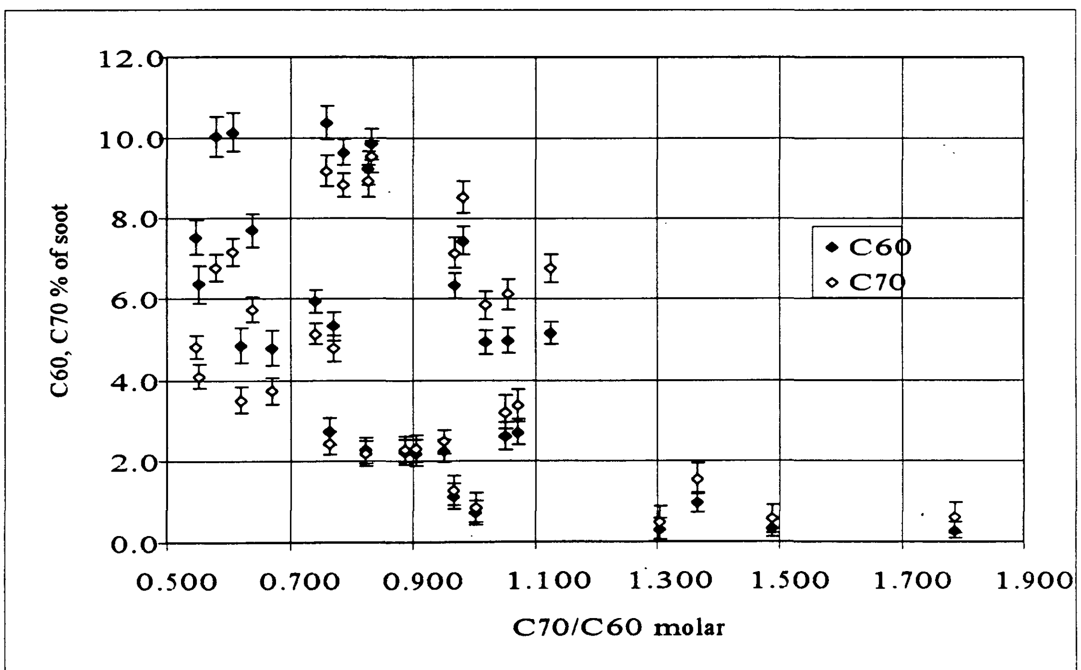


Figure 24 Individual Percent of Soot vs. $C_{70}/C_{60}$ Molar Ratio

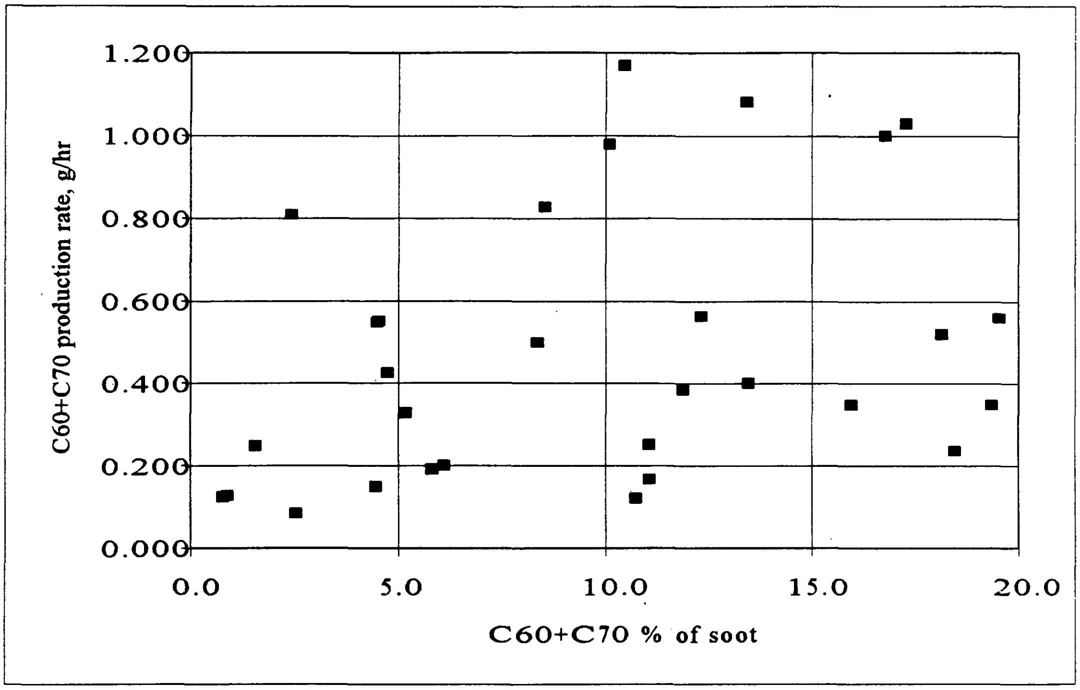


Figure 25 Fullerene Production Rate and Percent of Soot

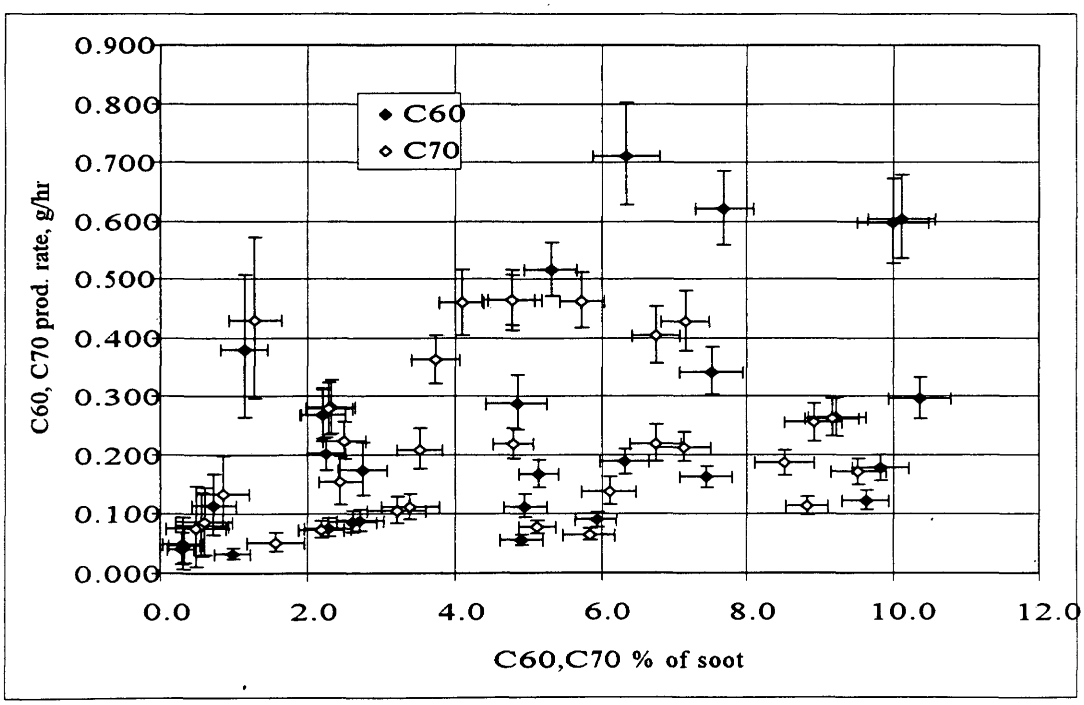


Figure 26 Individual Production Rate and Percent of Soot

gained by breaking up the samples into their separate components as done in Figure 20. The same general trend of higher yields from C fed as the fractions in the soot increases is seen. The change in the scale from log to normal was done so that error bars associated with the points could be appropriately compared.

Figures 21 and 23, when compared to the work of Howard et al. exhibit much of the same information except for a consistently lower $C_{70}/C_{60}$ molar ratio. Almost as if the data set had been shifted. Though one major point does stand out. This work produced a maximum production rate of 1.17 grams of $C_{60}$ + $C_{70}$ per hour at a $C_{70}/C_{60}$ molar ratio of 0.55 in sample 5-d-1. The Howard group saw a maximum of only 0.45 grams/hour at a $C_{70}/C_{60}$ molar ratio near 1.5. By plotting the individual fractions, seen in Figures 22 and 24, intuitive suspicions are confirmed. At lower $C_{70}/C_{60}$ ratios the production rate of $C_{60}$ is substantially higher than that of $C_{70}$, and likewise for the individual percentages in the soot, though not quite as enhanced.

The last comparison to the work of Howard et al. seen in figure 25 is again similar, though much more spread out in the direction of increasing production rate as noted by the differences seen Figure 21. Plotting of the individual fractions in Figure 26 is somewhat redundant. The same general trend is seen with a maximum production rate of 0.71 grams of $C_{60}$ per hour for a 6.4 percent fraction of the soot in sample 5-d-1. Although samples 14-d-1,2 have production rates that are somewhat smaller at 0.6 grams/hour, their fraction in the soot is substantially increased to 10 percent. In this same sample, the production of $C_{70}$ is around 0.42 grams per hour at 7 percent of the soot. Higher production at 0.46 grams per hour is seen at 4.1, 4.8 and 5.7 percent of the soot for samples 5-d-1, 4-c-1 and 7-c-1 respectively.

Presently the data indicate that a high fraction of $C_{60}$ and $C_{70}$ in the soot results in high production rates and yields from carbon fed, Figures 26 and 20 respectively. This is somewhat intuitive. Consequently, Figure 18 shows that the highest fractions of $C_{60}$ and $C_{70}$, are from flames with a low carbon yield. However, there is a difference between the overall carbon yield of a flame and its rate of soot production. There must be some trade off between carbon yield and soot production that in turn will affect the $C_{60}$ and $C_{70}$ rate of production and yield from carbon fed.

Figures 27 and 28 plot how soot production and carbon yield affect the rate of $C_{60}$ and $C_{70}$ production. Figures 29 and 30 are plots of the soot production and carbon yield effect on the $C_{60}$ and $C_{70}$ yield from carbon fed. In each of the figures a maximum is present. Near 10 grams per hour with respect to the rate of soot production and around 3 percent for the carbon yield. These indicate that an optimum operating point for $C_{60}$ and $C_{70}$ production is present within the experimental space.

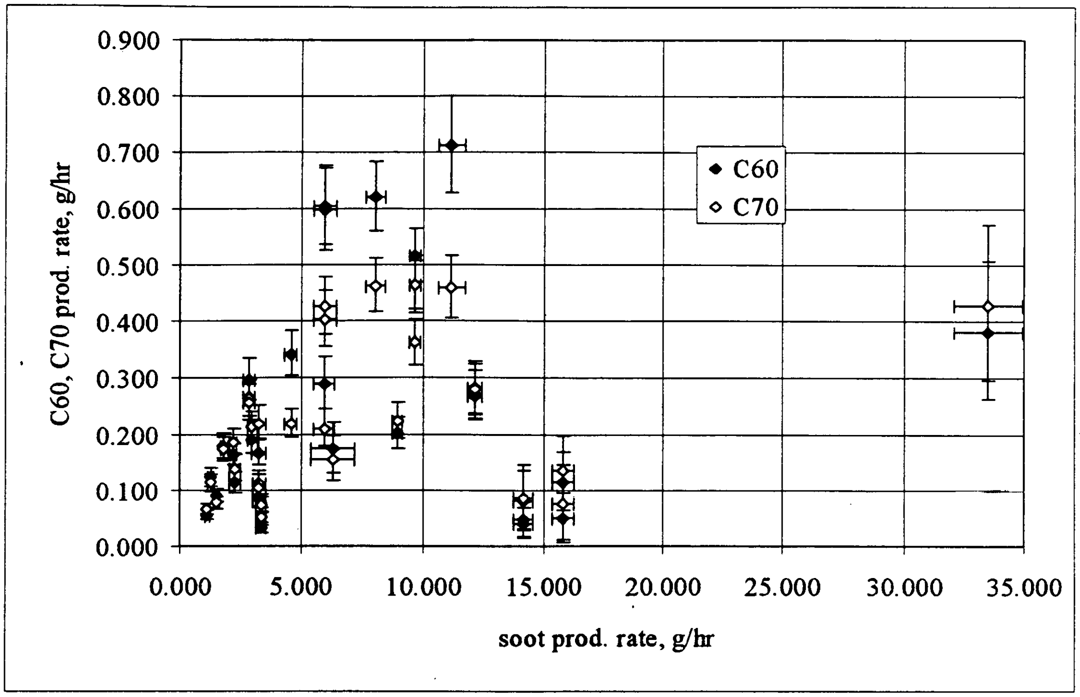


Figure 27 Production Rates of $C_{60}$ and $C_{70}$ vs. Soot Production Rate

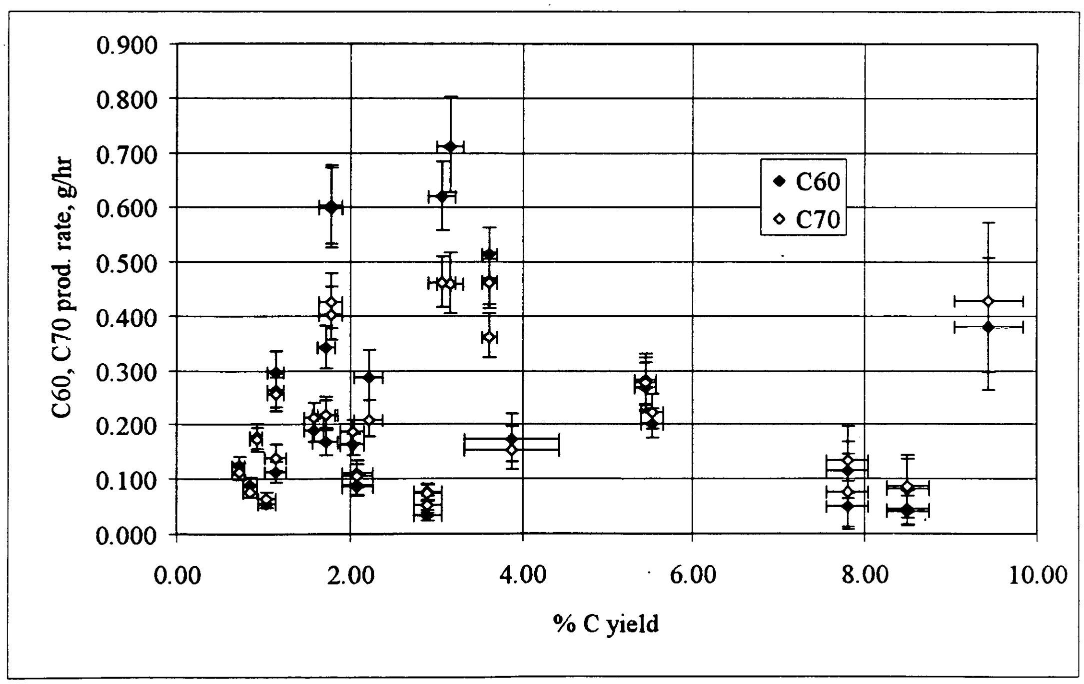


Figure 28 Production Rates of $C_{60}$ and $C_{70}$ vs. Percent Carbon Yield

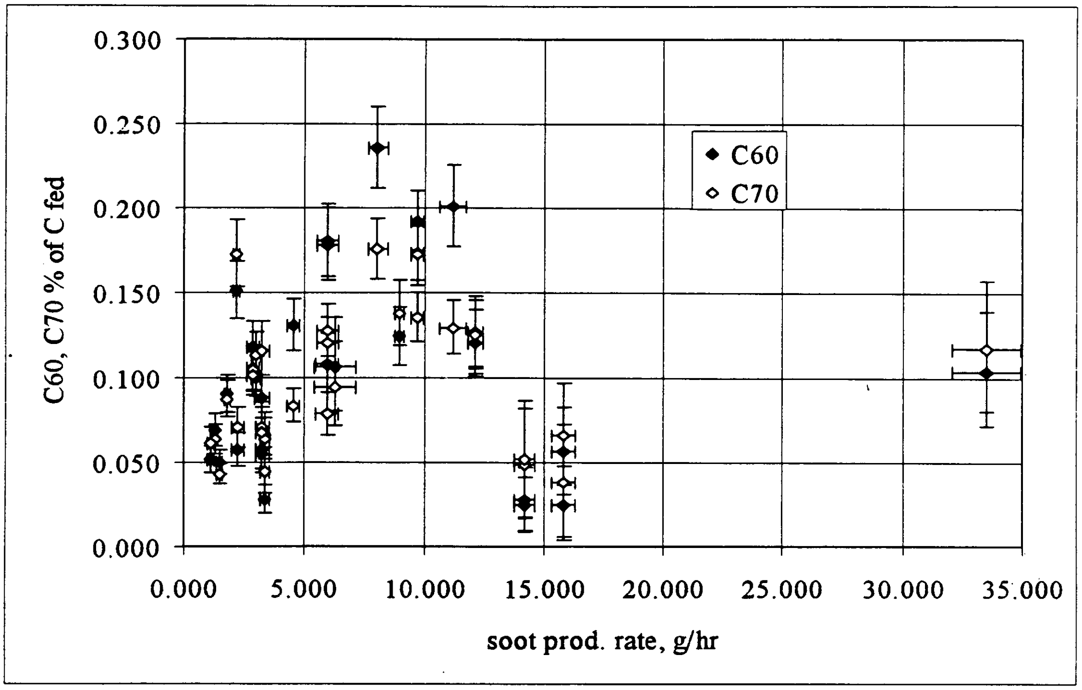


Figure 29 $C_{60}$ and $C_{70}$ Percent of Carbon Fed vs. Soot Production Rate

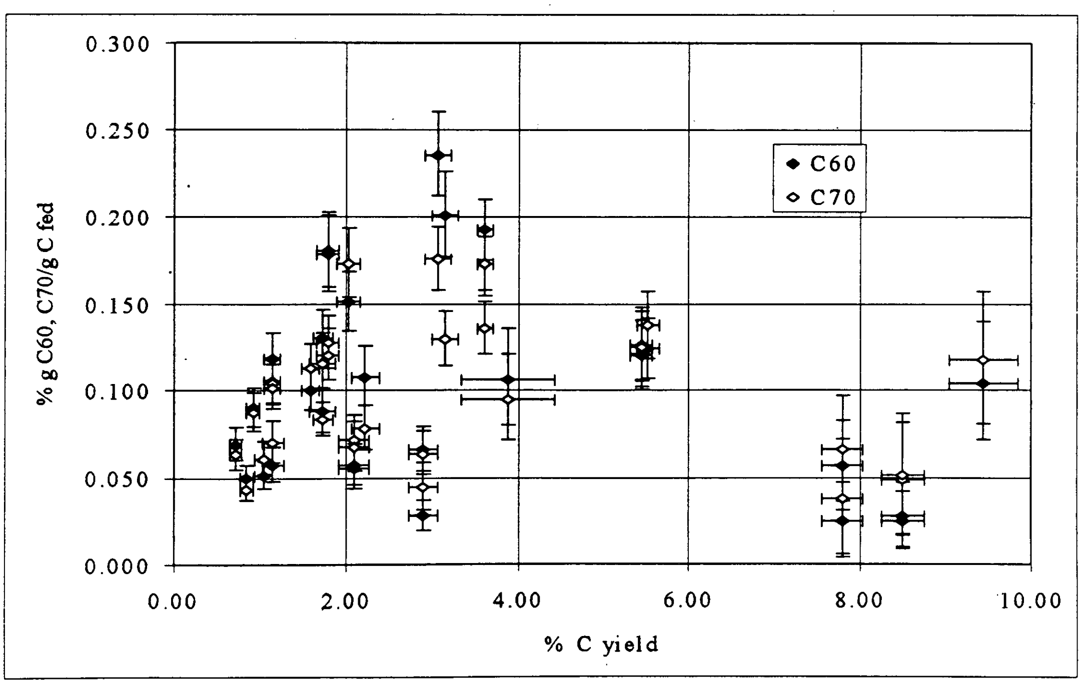


Figure 30 $C_{60}$ and $C_{70}$ Percent of Carbon Fed vs. Carbon Yield

Since there is an apparent optimum condition present in the experimental space, the next logical step would be to investigate the effect of the process variables on the various yields and production rates. Most importantly, the rates of fullerene and soot production per hour, the percent of $C_{60}$ and $C_{70}$ in the soot, the percent yield of $C_{60}$ and $C_{70}$ from carbon fed and carbon yield to soot. These will be covered in section 4.2.

### 4.1.4 Temperature

The effect of the flame temperature on the product distribution in the soot is important, yet not directly controllable. It can be affected by changes in the equivalence ratio and gas velocity. Higher velocities result in an increase of flame temperature. This is due to an increased distance between the flame and the burner surface. A decrease in the equivalence ratio, or increasing the oxygen content of the feed results in increases of the flames temperature by favoring a more complete combustion which has a higher heat of reaction.

The ability to make these measurements was achieved in the latter stages of this project and therefore only a couple were completed. Temperature measurements were made by insertion of a thermocouple into the flame and measuring the distance between the thermocouples junction and the burner surface. This of course can produce a plot of temperature versus distance for a given flame, indicating what and where the maximum temperature of the flame is. There are however a few corrections that need to be made to the measurement so that a more accurate value for the flame temperature can be achieved.

The thermocouple in the flame is heated by convection from the hot gasses and cooled by a combination of radiation to the surroundings and conduction to the supporting leads. If the loss due to conduction and radiation is large enough, temperatures above the melting point of the thermocouple can be measured. However this is usually more of a burden than a benefit. A method for calculating the errors due to radiation and conduction loss was created by Bradley et al. (40), and used here.

The method begins with an energy balance on the wire, Equation 1, then simplifies it to Equation 2 that is used for the radiation correction. Equation 2 is dependent upon the emissivity of the wire and the convective heat transfer coefficient of the gas. However both of these values must be estimated by assumptions on the characteristics of the system. The heat transfer coefficient is attained by calculation of the Nusselt number in Equation 3, for which the values within the Prandtl and Reynolds numbers are estimated by an assumption of the composition of the gas. The value for the emissivity of the wire is also subject to estimation by visual inspection of the wires surface and making an educated guess as to what the emissivity should be. This is somewhat unscientific, but at least it is known that the value is bounded between zero and one.

$$k\frac{d^2T}{dx^2} + \frac{4h}{D}\left(T_G - T_\infty\right) - \frac{4\sigma}{D}\left(\varepsilon T_\infty^4 - \alpha T_b^4\right) = 0 \qquad (1)$$

$$T_G = T_\infty + \frac{\sigma \varepsilon T_\infty^4}{h} \tag{2}$$

$$Nu = 0.42\,Pr^{0.2} + 0.57\,Pr^{0.33}\,Re^{0.5} \tag{3}$$

For this work the composition of the gas was roughly calculated to consist mainly of argon, carbon monoxide, water and ethylene. Although the products of the flame are numerous, the individual fractions of all the components other than what is being considered, are negligible and will not have a noticeable impact on the estimated properties of the gas. The argon fraction is easily calculated by the orifice calibration. The fractions of carbon monoxide, water and ethylene were solved by an atomic balance that minimized the fraction of ethylene in the product.

The methods that were employed to calculate the properties of the gas in the paper by Bradley et al. were also used here and can be found in the text by Reid et al. (41) along with polynomial constants and critical values for the components. Concerning the emissivity of the wire, only after a few moments in the flame the wire could be seen to be noticeably blackened by oxidation and/or soot accumulation. Therefore it could be safely assumed to not be at a value listed for the clean wire which is 0.10 for platinum at 810 K. Instead the radiation correction was carried out for a range of emissivities that seemed plausible (0.8 ± 0.15). The magnitude of the corrections that were made due to radiation varied from 519 K at an emissivity of 0.65, to over 782 K at an emissivity of 0.95 for conditions 14 and 3 respectively. A sample spreadsheet for the calculation of the radiation correction can be found in Appendix E.

The calculation for the error due to conductive cooling proved quite a bit more difficult. The method outlined in the paper by Bradley is very laborious and used to produce the plots presented in that article. An attempt to solve the energy equation for the probe as constructed resulted in an integral in temperature for which its form could not be found in the integral tables, nor software such as Mathematica could solve. Therefore an attempt to use the charts presented in the Bradley article was made. This was done by scaling the geometry's of the wire to be representative of a diameter to length ratio. For a given diameter wire, as the length is increased linearly, the error due to conductive cooling decreases exponentially. This is the nature of the shape of the curves presented so the assumption seems appropriate for a rough calculation.

For the thermocouple used in this work, the D/L ratio is 0.025. In the figure that corresponds to a platinum-10 percent rhodium wire, the error from conductive cooling could be from 1 to 5 percent depending on the temperature of the main lead or support. For the way in that error has been defined for the charts, this leads to an error in the equilibrium wire temperature between 13 to 71 K for a junction temperature of 1350 K. This means that for a measured temperature of 1350 K, in the absence of conductive cooling, the measurement could be between 1363 to 1421 K. Compared to the magnitude of the errors due to radiation, this correction seems negligible and will not be considered in the overall correction. The temperature versus height plots for conditions #3 and #14 are shown in Figures 31 and 32 respectively. The figures show the measured points and correction curves relative to the measurements for three emissivities of 0.65, 0.80 and 0.95.

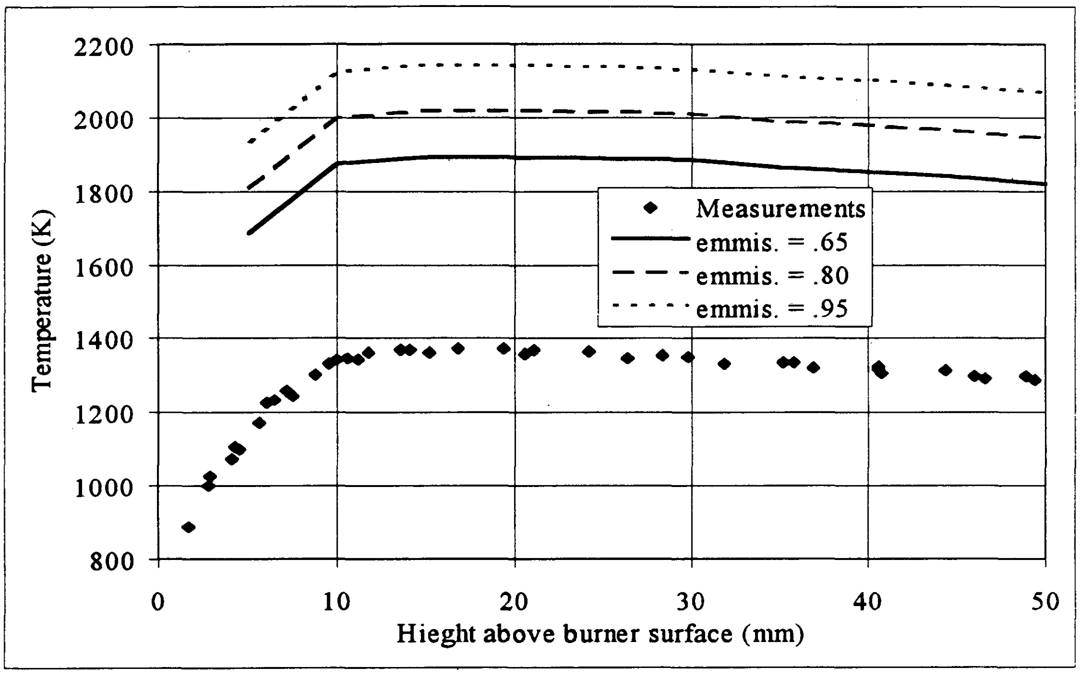


Figure 31 Flame temperature for condition #3

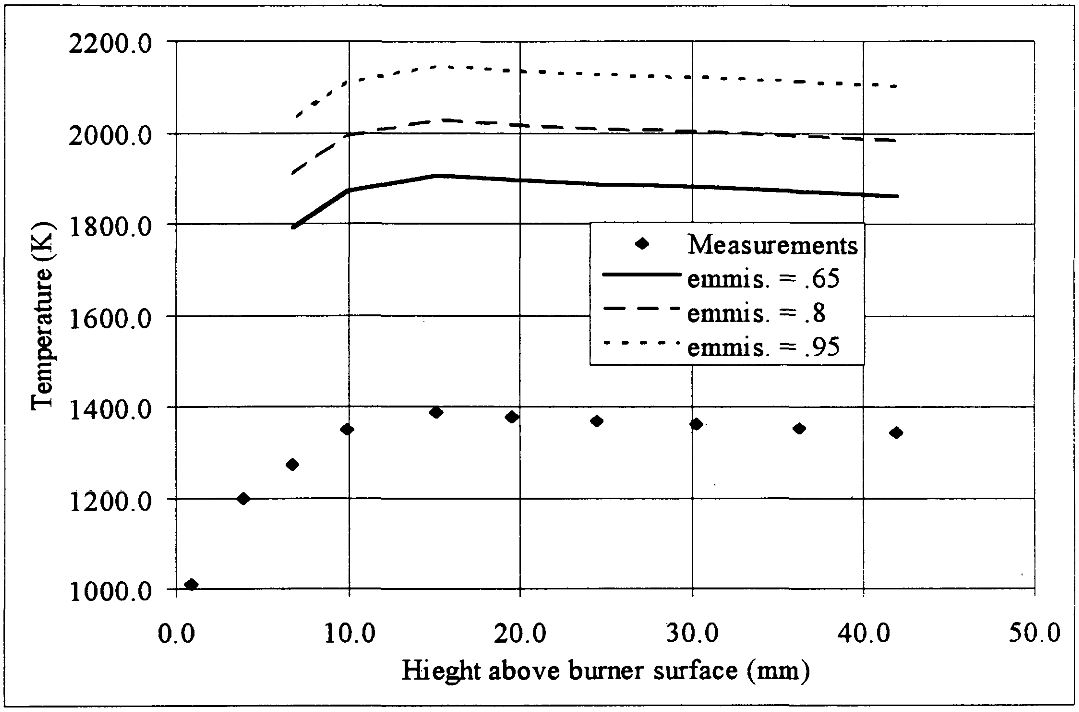


Figure 32 Flame temperature for condition #14

Both figures 31 and 32 show relatively the same information. A peak temperature is reached near 15 mm above the burner surface. The correction curves were not extended below 5 mm because the flame front existed in this region and the assumptions of the composition of the gas changed to the known reactant composition and the temperature in this region is of no interest for this work. Both figures also show the importance of the emissivity value. The range of the correction for both conditions is more than 300 K. The expected peak temperatures for flames of this type are around 2100 K. Therefore, under the assumption that the composition of the major components in the product gas is not far off and the conduction cooling error is indeed negligible, emissivities in the neighborhood of 0.85 would produce the expected values for the flame temperature.

It should be reminded however, that this method has made quite a few assumptions, and that in order to attain a more exact correction, the composition of the product gas should be known to a higher degree and more importantly, a value for the emissivity of the wire under the sooting flame conditions should have a smaller range than that used here. Also the conduction cooling error should be calculated more exactly, but this may be over ridden by using a smaller diameter wire so that the figures presented in the Bradley method could be used without an assumed scaling factor.

### 4.2 Data analysis

The main goal of this study was to find empirical relationships for the yields of fullerenes dependent upon the three process variables: chamber pressure, cold gas velocity and equivalence ratio. These relationships could be used in the future to determine the best operating conditions when certain forces such as the cost of separation, cost of fuel and other general operating costs become more or less important. As stated in Chapter 3, a quadratic model is used for fitting of the data. In order to determine how well a model fits the data, the coefficient of determination, $R^2$, is frequently used. However it is always possible to fit a polynomial of degree n-1 to n data points and obtain a perfect fit, the use of too many regressor variables should be avoided and can be misleading as to the true functional relationship of the variables to the measured output (42). To be more exact, the coefficient of determination is a measure of the proportion of the variability in the data explained or accounted for by the regression model. Therefore, for any data with appreciable variability, a model with many terms and a coefficient of determination close to one will be of little use when used for prediction, process control or process optimization.

One of the first steps in the decision of what terms should be used in a model is the construction of an anova (analysis of variance) table . The information gained from the anova table is how strongly the measured variable is affected by each of the components and their interactions with each other (43). In Chapter 3 it was mentioned that with the original 1/3 fraction factorial, much information about the effects is lost or confounded with multiple effects so that the anova is of little use. For the central composite design, an anova table can give some meaningful information about the effects of the variables. Though these values are not used in the actual fit model, they do enhance which terms should be used. Only the linear and the two-factor interaction terms were considered in the anova tables that were constructed for this study. The three-factor interaction term was neglected because it was decided that the term would not be considered in the model. The anova tables for $C_{60}$, $C_{70}$ and $C_{60}$+$C_{70}$ for the yields in soot, yields from carbon fed and the production rates are given in Appendix F. The tables were constructed by methods found in most texts concerning experimental design and analysis.

The software used to handle the data for this work was Excel, the spreadsheet package from Microsoft, and Mathematica, a program that is used for advanced mathematical computations and its excellent graphical capabilities. A linear regression package that is included with Excel served the purpose of fitting the data and Mathematica was used to produce 3-dimensional plots. The best fit equations were built by performing linear regression first on the linear terms only, then adding the interaction and quadratic terms individually. The error sum of squares for the model with the added term must be reduced by an amount equal to or larger than the original error mean square, otherwise the new model will have a larger error mean square than the old model due to the loss of one degree of freedom.

Therefore, starting with the basic linear equation, one term was added, and the new model regressed. If the error sum of squares had been reduced by the original error mean square, the term was kept. If not, the term was dropped and a different term was attempted. The following equations are the best fit to the data. Equations 4, 5 and 6 relate the variables to the percent yield of $C_{60}$, $C_{70}$ and total $C_{60}$ + $C_{70}$ in the soot respectively. Equations 7, 8 and 9 to the percent yield from carbon fed, and 10, 11 and 12 to the rates of production in grams per hour. The regression output for the fit parameters to the equations are given in Appendix G.

$$Ys = 45.943 + 0.793P + 0.719v - 43.204\phi - 0.475v\phi + 0.023Pv - 0.668P\phi + 13.170\phi^2 \qquad (4)$$

$$Ys = 187.267 + 0.651P + 0.149v - 149.909\phi - 0.188v\phi + 0.015Pv - 0.487P\phi + 32.312\phi^2 \qquad (5)$$

$$Ys = 233.210 + 1.443P + 0.868v - 193.113\phi - 0.663v\phi + 0.037Pv - 1.155P\phi + 45.482\phi^2 \quad (6)$$

$$Yc = -3.674 - 0.008P - 0.005v + 3.328\phi + 0.009v\phi + 0.0003Pv - 0.0003v^2 - 0.782\phi^2 \quad (7)$$

$$Yc = -0.344 - 0.004P - 0.008v + 0.544\phi + 0.010v\phi + 0.0002Pv - 0.0002v^2 - 0.202\phi^2 \quad (8)$$

$$Yc = -4.018 - 0.013P - 0.013v + 3.872\phi + 0.019v\phi + 0.0004Pv - 0.0005v^2 - 0.984\phi^2 \quad (9)$$

$$Yp = -9.767 - 0.029P - 0.032v + 8.905\phi + 0.015v\phi + 0.001Pv - 1.991\phi^2 - 0.0003v^2 \quad (10)$$

$$Yp = -2.364 - 0.013P - 0.023v + 2.404\phi + 0.018v\phi + 0.0006Pv - 0.637\phi^2 - 0.0003v^2 \quad (11)$$

$$Yp = -12.131 - 0.042P - 0.056v + 11.308\phi + 0.032v\phi + 0.002Pv - 2.628\phi^2 - 0.0006v^2 \quad (12)$$

Figures 33 to 50 are curve fit plots for comparison to the data. It is reminded that the curves are fit to data in three different planes with only different 5 conditions per plane. In each figure curves are represented for three different equivalence ratios varying over the velocity all at a constant pressure. The experimental points have been coded to match with a certain curve in order to examine the fit.

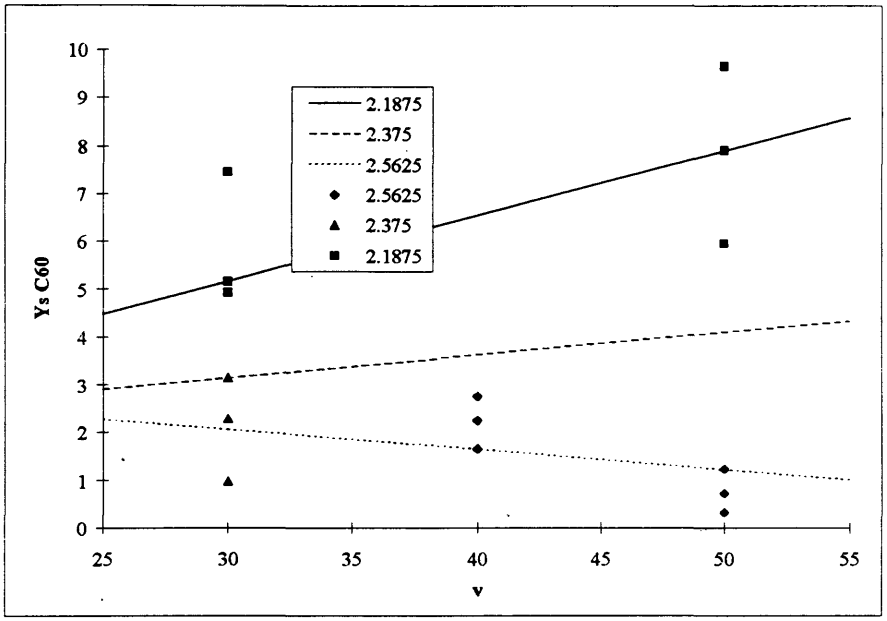


Figure 33 Curve Fit for $C_{60}$ Yield in Soot at 20 Torr

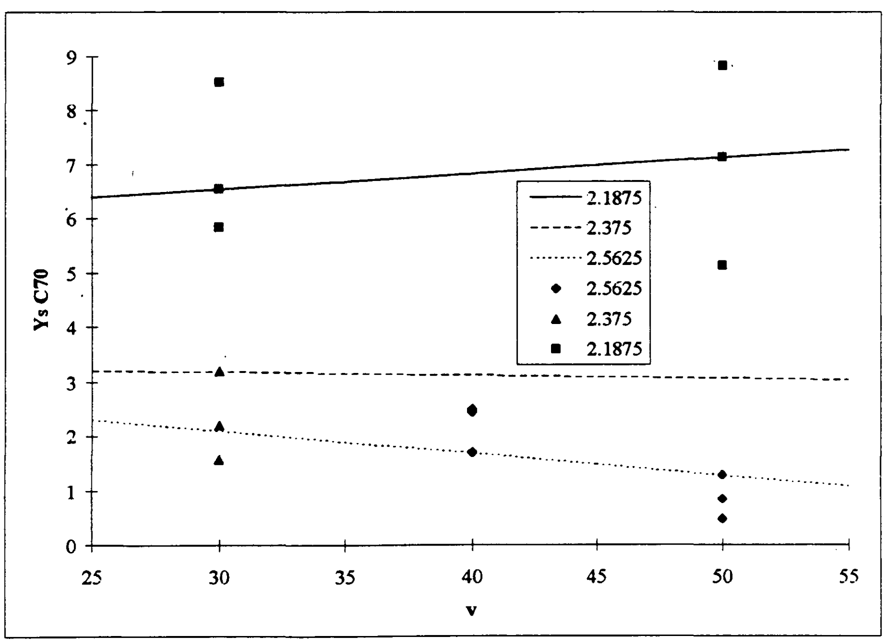


Figure 34 Curve Fit for $C_{70}$ Yield in Soot at 20 Torr

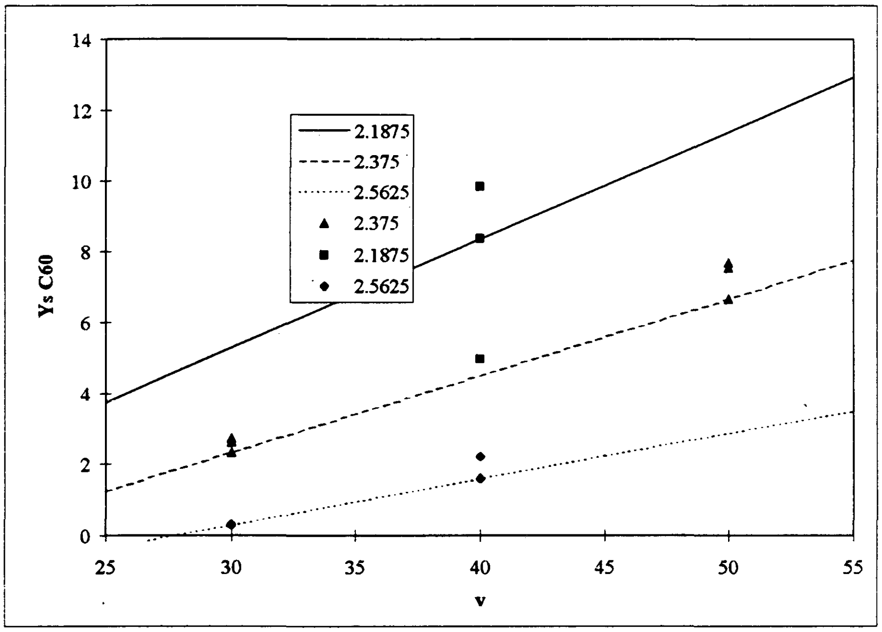


Figure 35 Curve Fit for $C_{60}$ Yield in Soot at 27.5 Torr

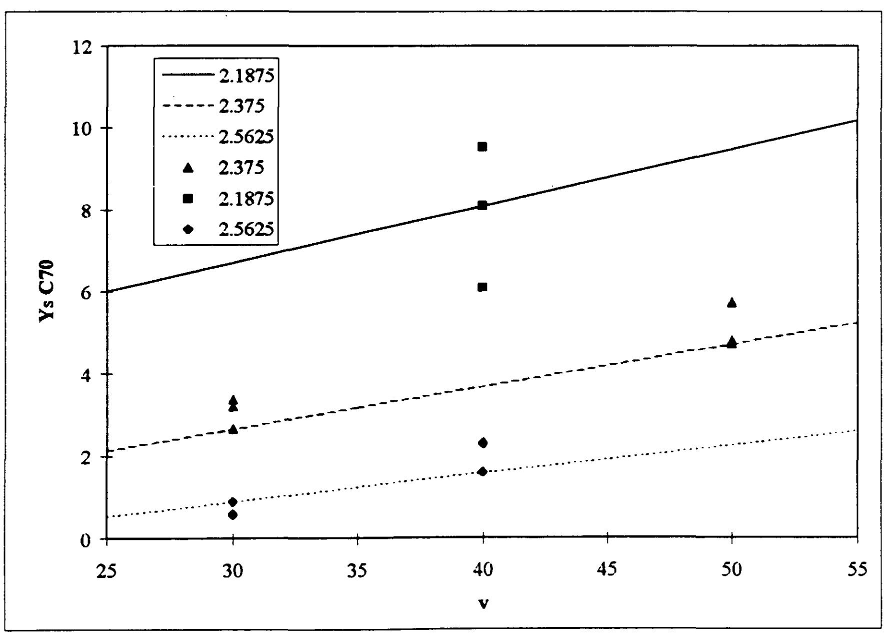


Figure 36 Curve Fit for $C_{70}$ Yield in Soot at 27.5 Torr

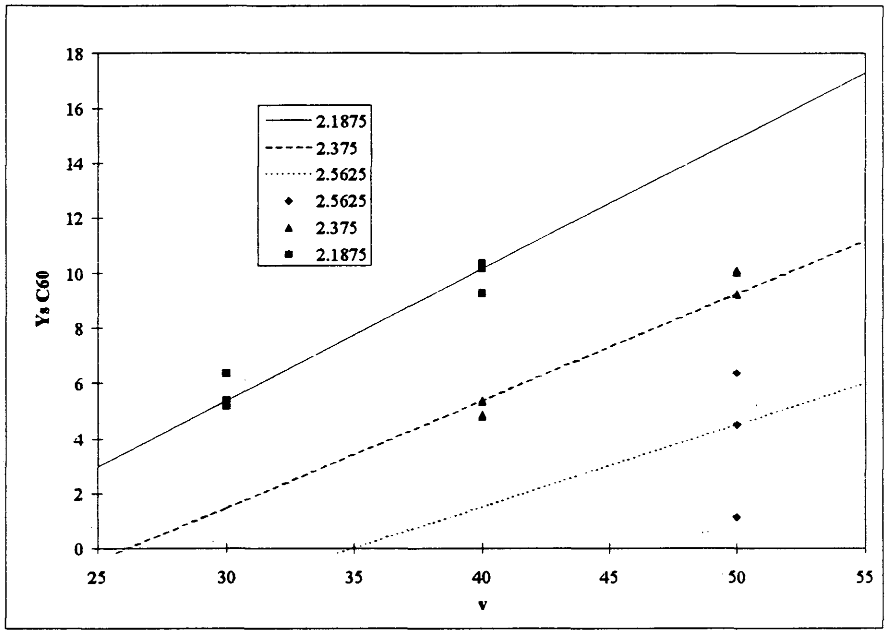


Figure 37 Curve Fit for $C_{60}$ Yield in Soot at 35 Torr

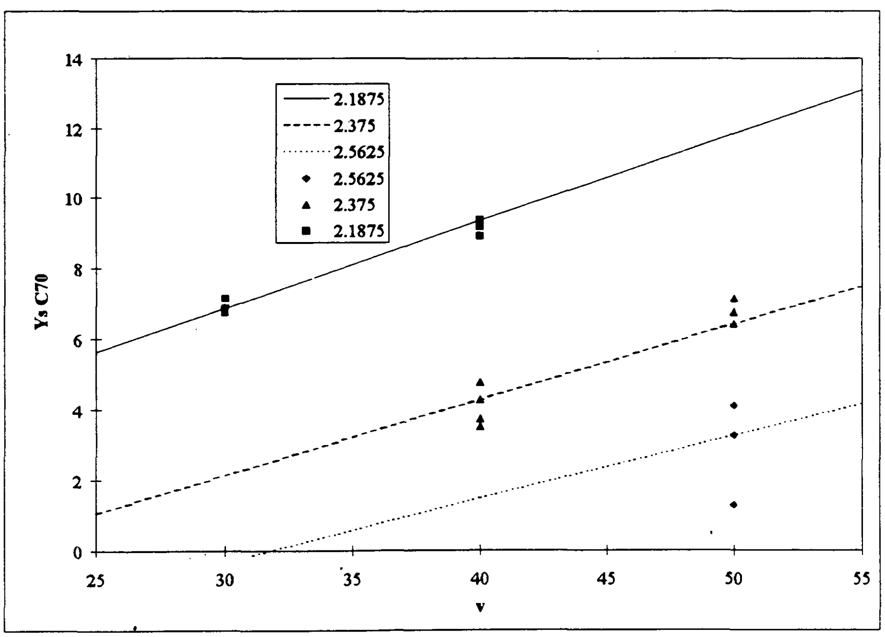


Figure 38 Curve Fit for $C_{70}$ Yield in Soot at 35 Torr

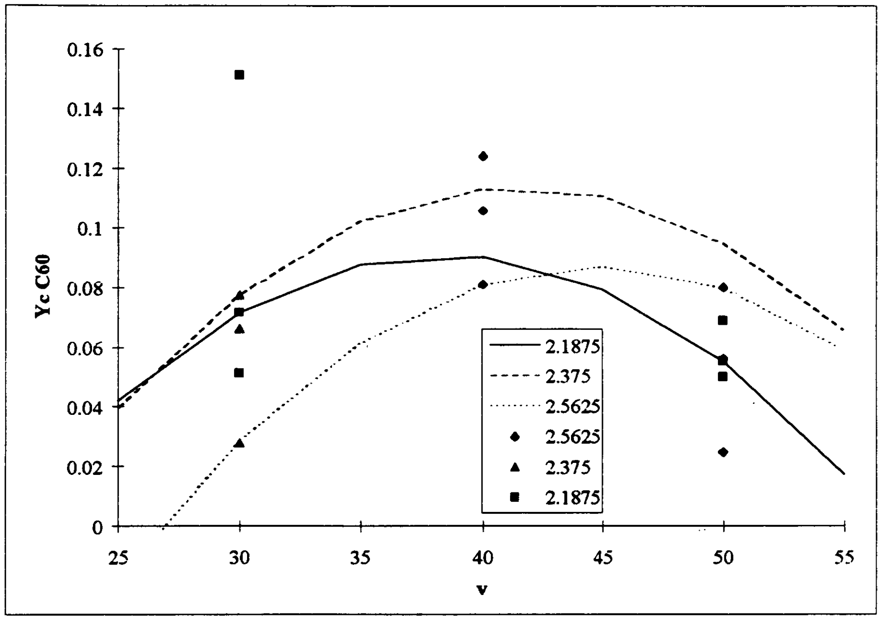


Figure 39 Curve Fit for $C_{60}$ Yield from Carbon Fed at 20 Torr

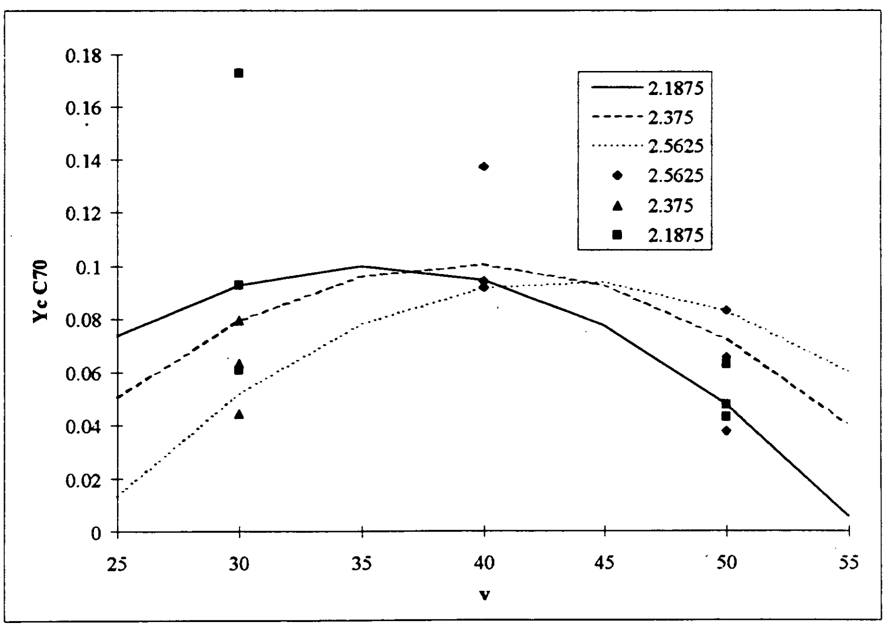


Figure 40 Curve Fit for C70 Yield from Carbon Fed at 20 Torr

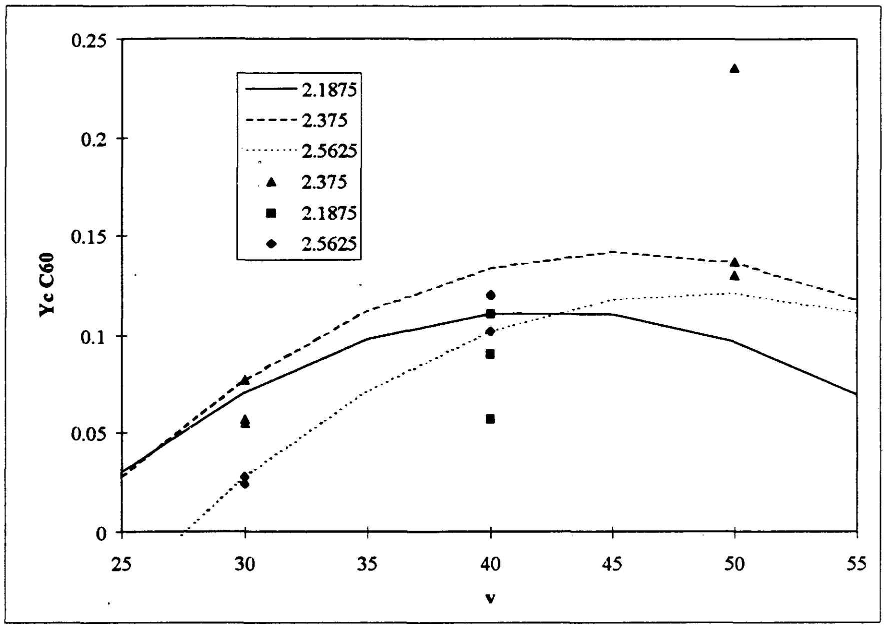


Figure 41 Curve Fit for $C_{60}$ Yield from Carbon Fed at 27.5 Torr

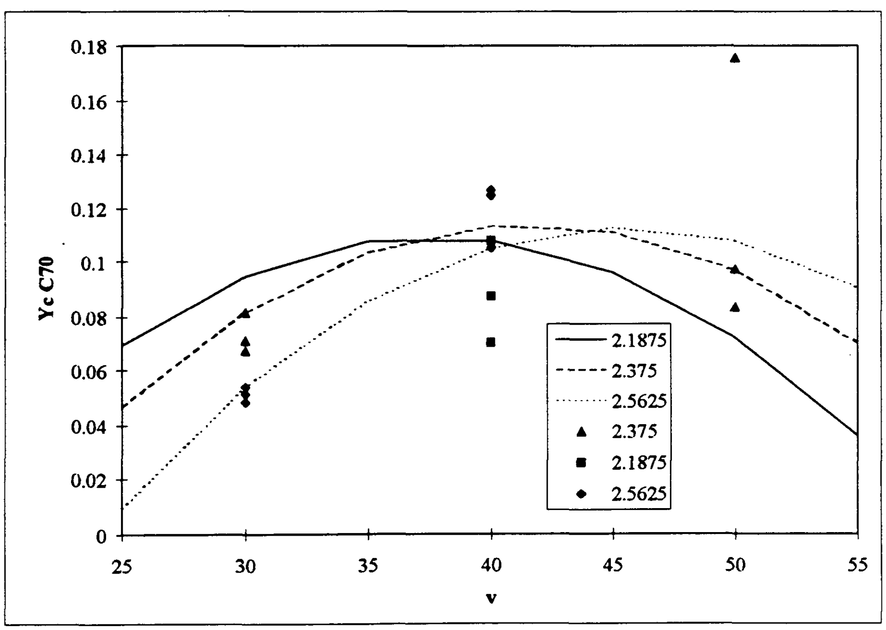


Figure 42 Curve Fit for $C_{70}$ Yield from Carbon Fed at 27.5 Torr

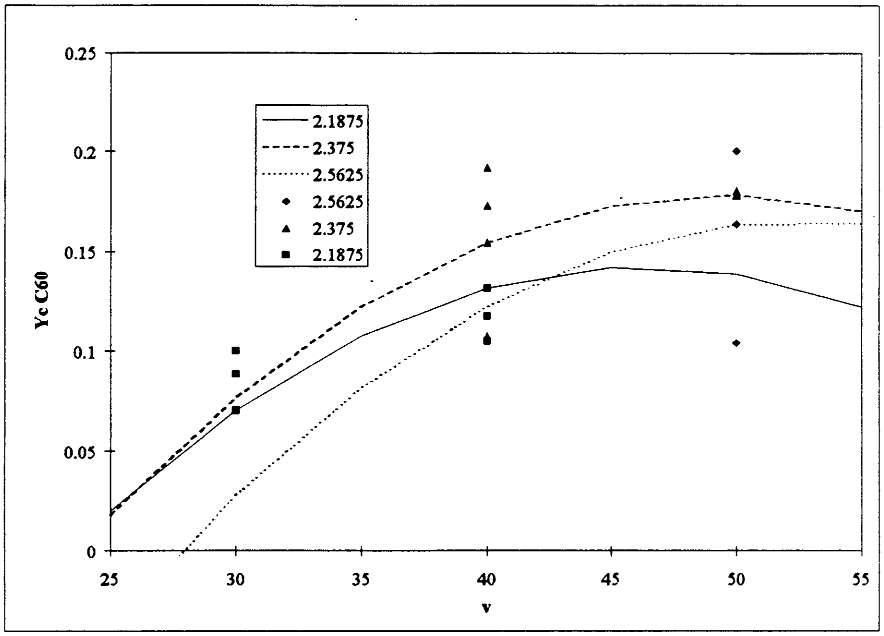


Figure 43 Curve Fit for $C_{60}$ Yield from Carbon Fed at 35 Torr

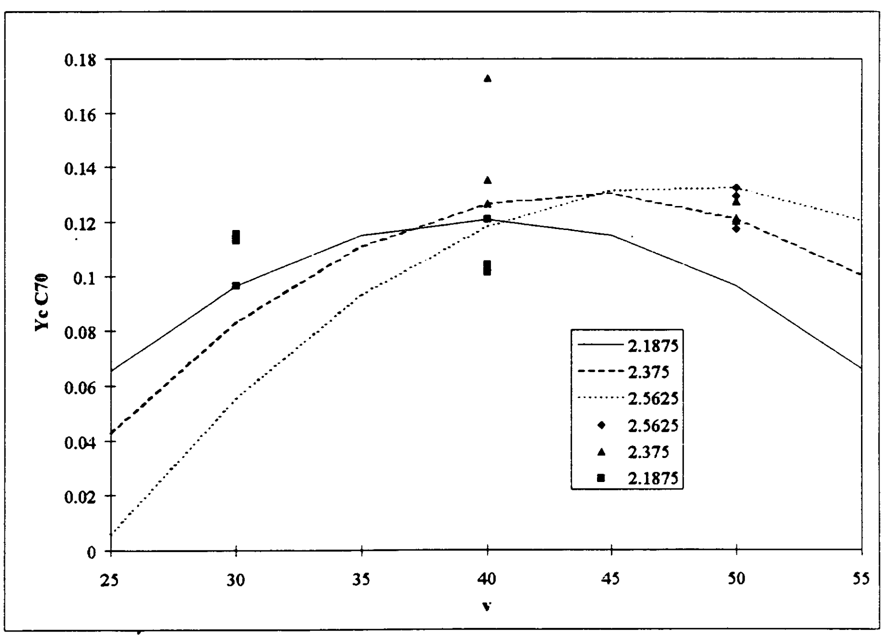


Figure 44 Curve Fit for $C_{70}$ Yield from Carbon Fed at 35 Torr

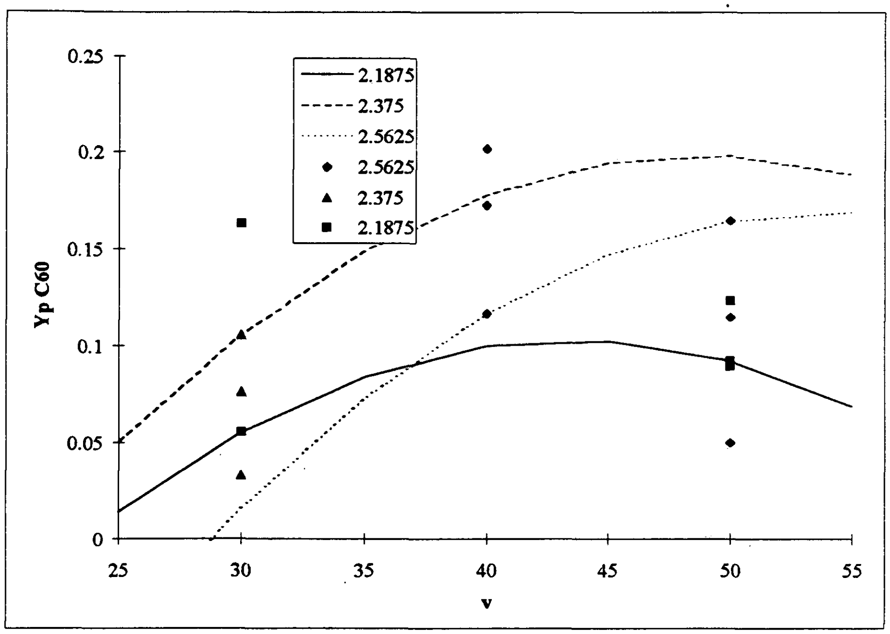


Figure 45 Curve Fit for $C_{60}$ Production Rate at 20 Torr

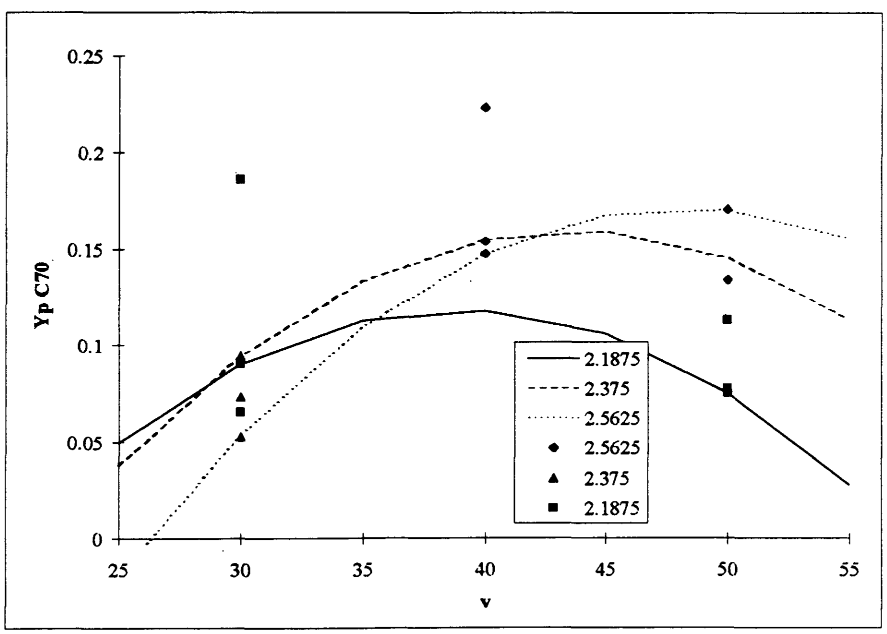


Figure 46 Curve Fit for $C_{70}$ Production Rate at 20 Torr

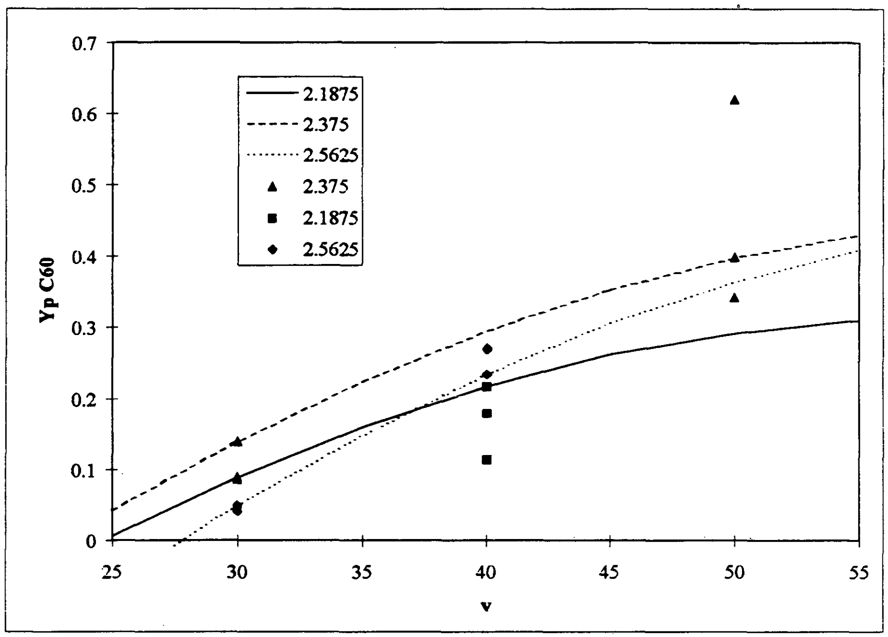


Figure 47 Curve Fit for $C_{60}$ Production Rate at 27.5 Torr

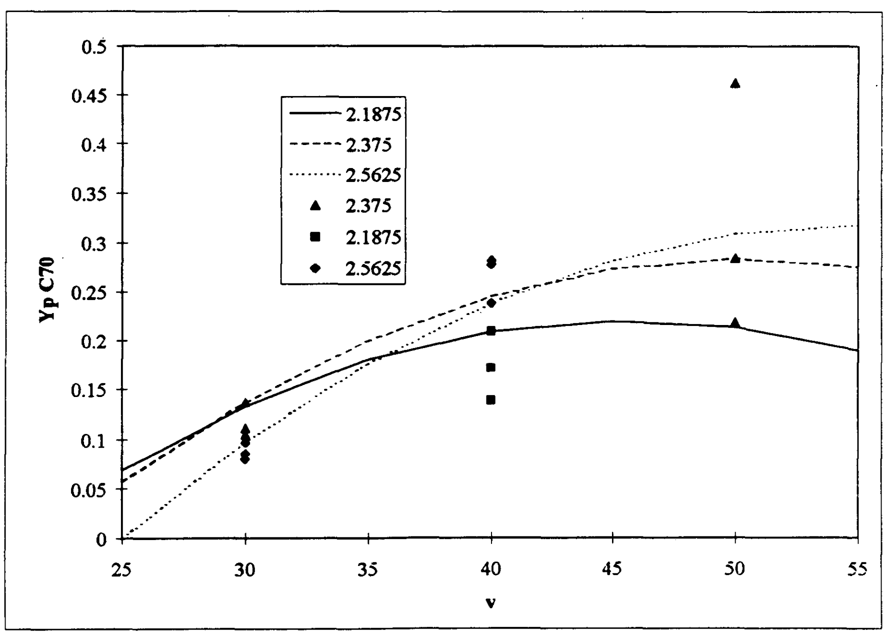


Figure 48 Curve Fit for $C_{70}$ Production Rate at 27.5 Torr

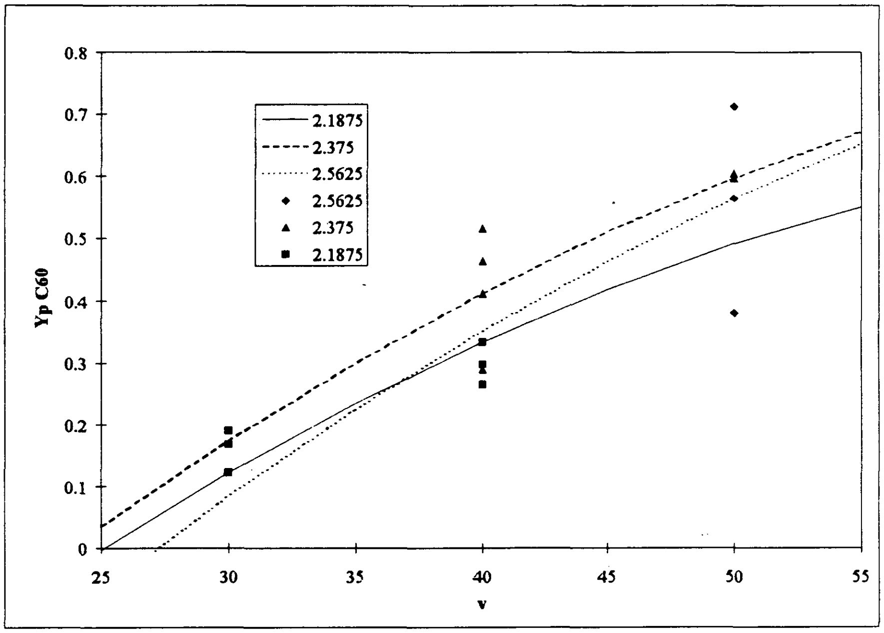


Figure 49 Curve Fit for $C_{60}$ Production Rate at 35 Torr

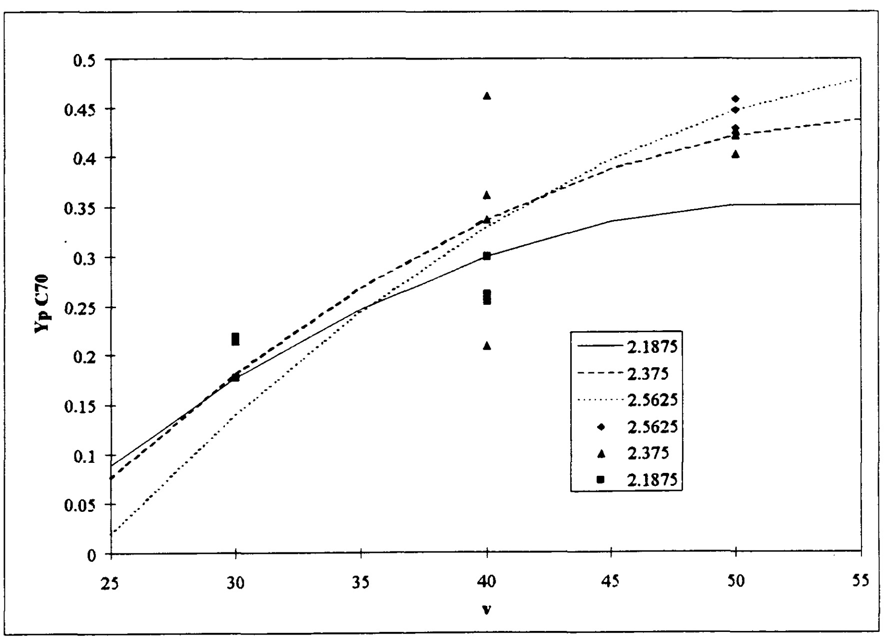


Figure 50 Curve Fit for $C_{70}$ Production Rate at 35 Torr

On inspection of the previous figures, those of 33 to 38 compare how the yields of $C_{60}$ and $C_{70}$ in the soot are affected by the process conditions. It is clear and unarguable that soots with the highest percentage of fullerenes are produced by flames with low equivalence ratios. Increases in the cold gas velocity also tend to increase the $C_{60}$ and $C_{70}$ yields. Though the effect is not as strong at low pressures. Examining the differences between the yields of $C_{60}$ and $C_{70}$, $C_{70}$ seems to be less affected by increases in the velocity but perhaps more by decreases in the equivalence ratio.

Figures 39 to 44 relate the variables to the fullerene yields from carbon fed to the burner. In all plots the curves reveal the significant quadratic effect of both the velocity and equivalence ratio. The yields tend to peak at velocities of 40 to 50 cm/s as the pressure is increased. At each of the areas of highest yields for $C_{60}$, the equivalence ratio curve which stands out is 2.375, indicating that maximum yields occurs near that equivalence ratio. This effect is not seen in the $C_{70}$ yields from carbon fed, yet velocity is still significant. Another note on the $C_{70}$ curves, there seems to be somewhat of an inflection in the equivalence ratio effect. At low velocities, $C_{70}$ yields from carbon are higher for low equivalence ratios, whereas the opposite is true for high velocities. This inflection occurs near the peak in the velocity effect.

The production rates of $C_{60}$ and $C_{70}$ and the fitted curves are given in Figures 45 to 50. Similar to the yields from carbon fed, there exists a quadratic effect in the velocity. This should be expected since their models contain the same terms. For both $C_{60}$ and $C_{70}$, higher rates of production are favored by high pressures. For the experimental space studied, a peak production rate only occurs at low pressures. However, this peak is not as great as that measured and predicted at higher pressures. For both $C_{60}$ and $C_{70}$, higher rates of production could be expected outside the space studied as both pressure and velocity is increased.

The previous two-dimensional plots are useful for comparison and examining general trends in the data. In order to visualize the effects of the variables more closely, three-dimensional plots relating the three variables to curves of constant yields and production rates have been constructed. Using the fit equations, these plots were built by solving for one of the variables at a constant yield. This resulted in a two-factor equation that could be plotted in three-dimensional space. So the curves are actually all values of the third variable which give the intended yield. These are shown in Figures 51 through 59.

The true benefit of these plots is an ability to visualize how to manipulate all the variables at once and keep an intended output. The contour plots for the mean yields of $C_{60}$ and $C_{70}$ in soot, shown in Figures 51, 52 and 53 expose how this is possible. If the process is currently giving a certain yield and it is desired to run at a higher pressure, the same yield may be attained by increasing the equivalence ratio, decreasing the velocity or a combination of both. There does not seem to be any major differences between the response surfaces of $C_{60}$ and $C_{70}$ for the yields in soot. Although for a given condition, the yields of $C_{60}$ will be slightly higher than that of $C_{70}$.

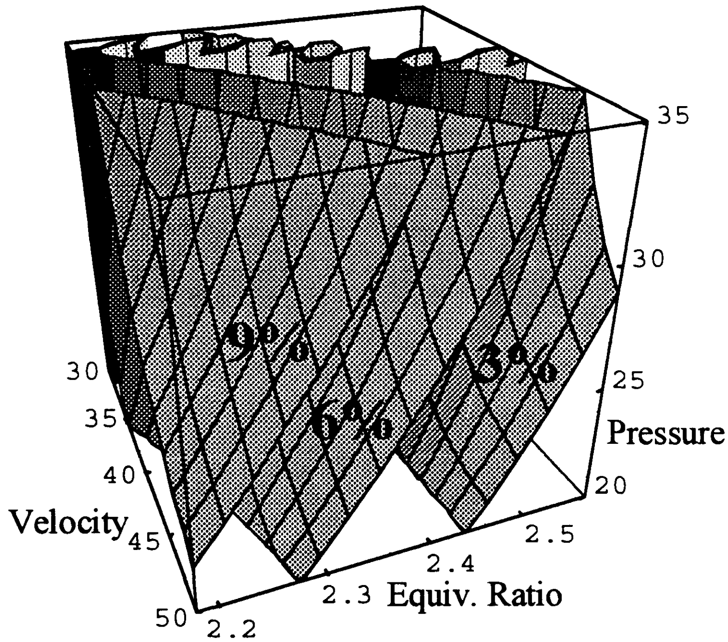


Figure 51 Mean Yield Contours for $C_{60}$ in Soot

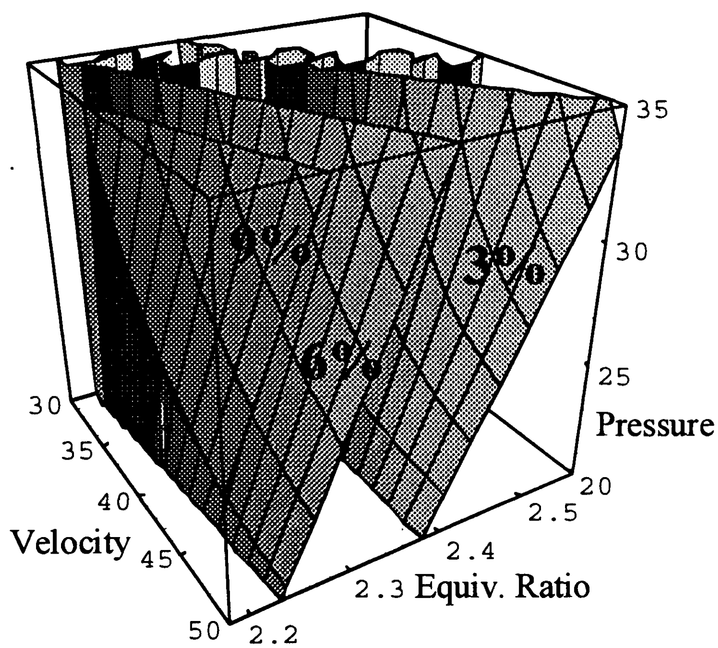


Figure 52 Mean Yield Contours for $C_{70}$ in Soot

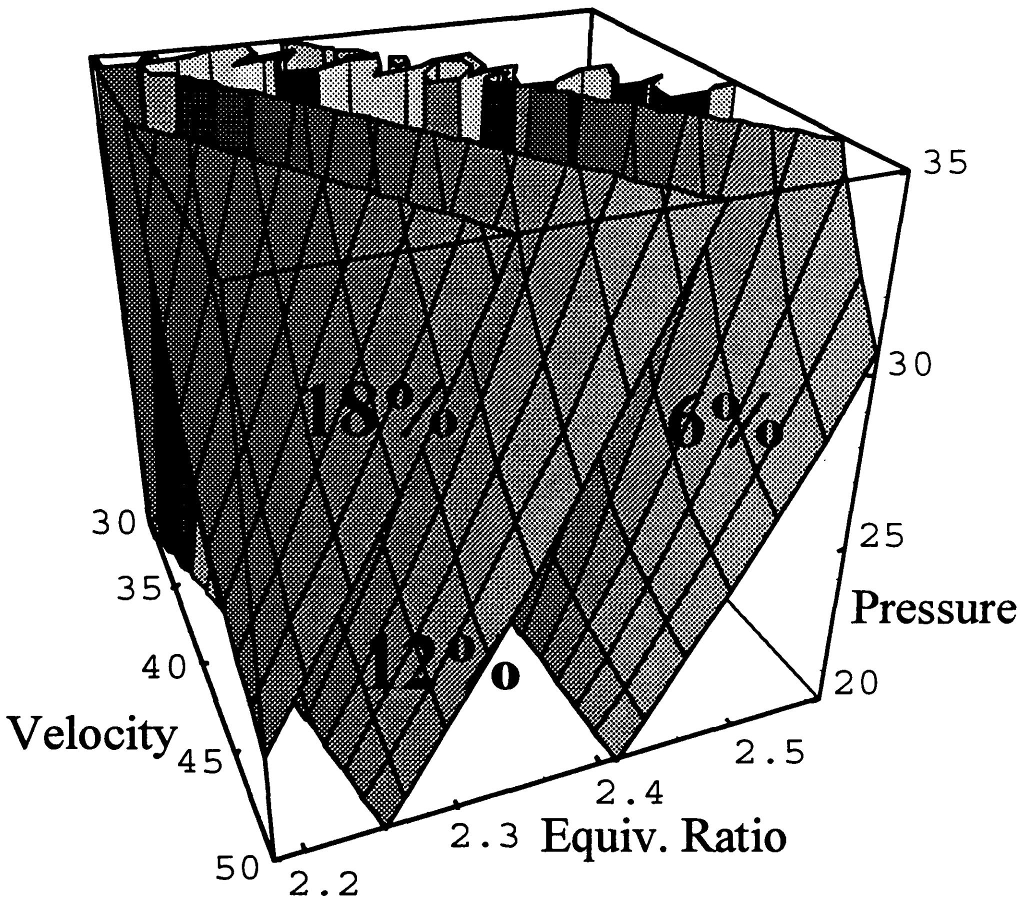


Figure 53 Mean Yield Contours for Total $C_{60}$ and $C_{70}$ in Soot

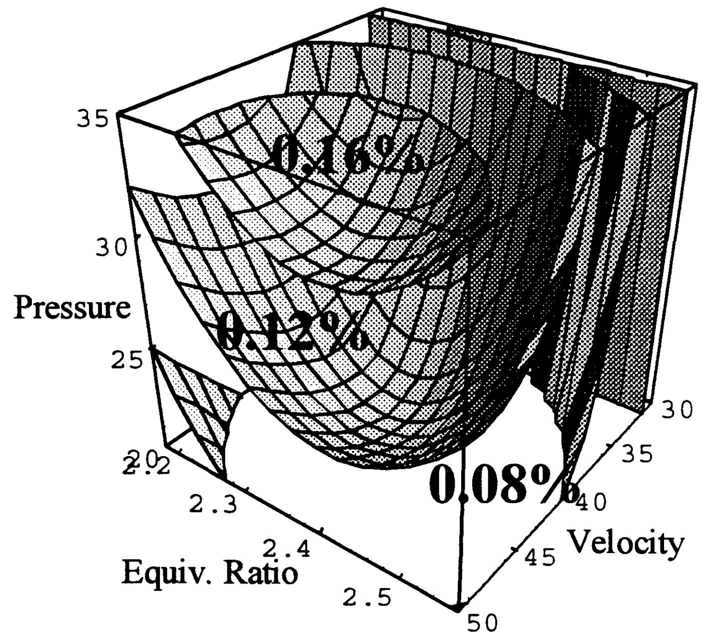


Figure 54 Mean Yield Contours for $C_{60}$ from Carbon Fed

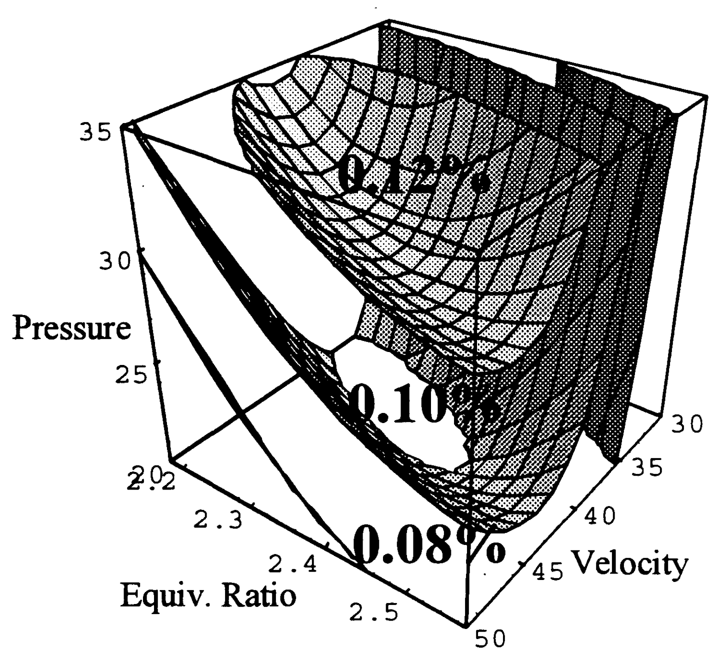


Figure 55 Mean Yield Contours for $C_{70}$ from Carbon Fed

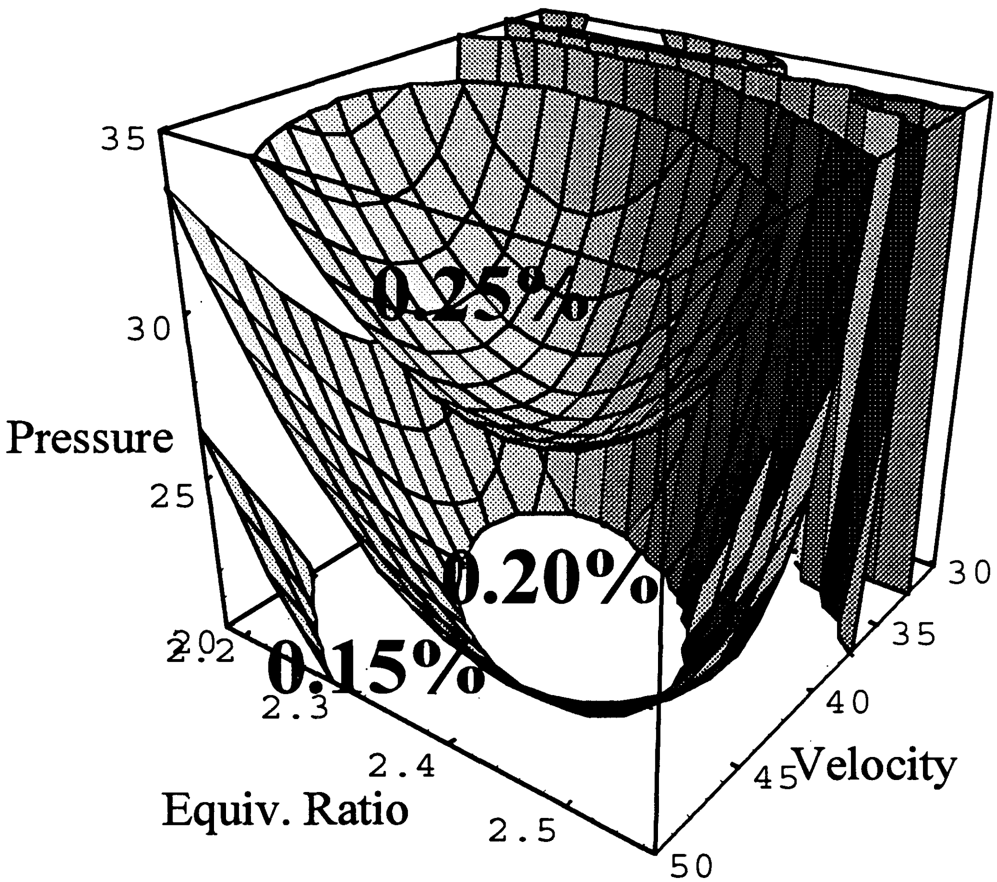


Figure 56 Mean Yield Contours for Total $C_{60}$ and $C_{70}$ from Carbon Fed

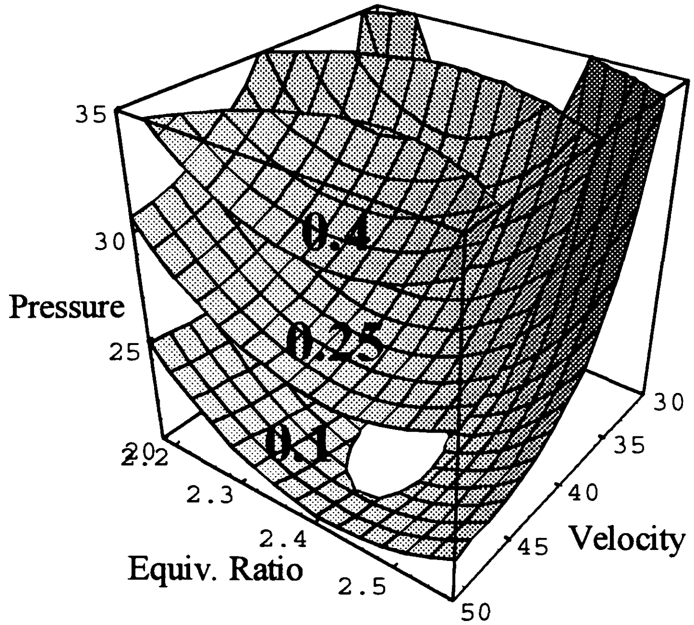


Figure 57 Mean Production Rate for $C_{60}$ (g/hr)

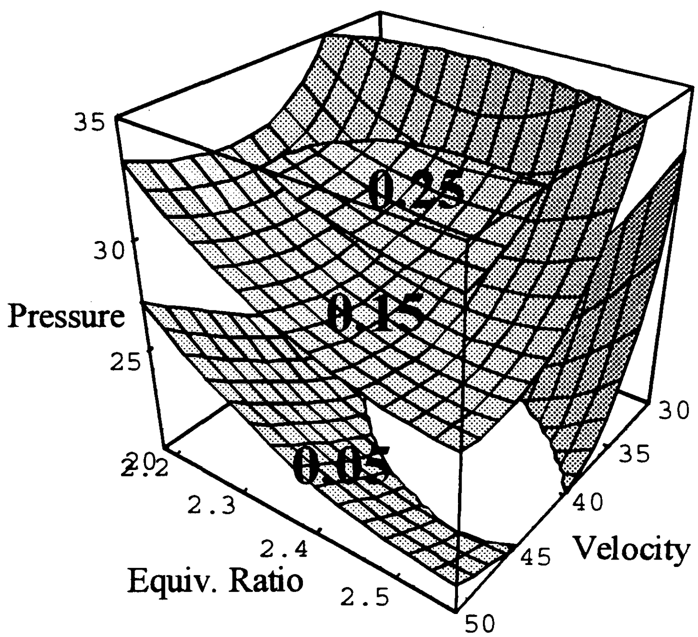


Figure 58 Mean Production Rate for $C_{70}$ (g/hr)

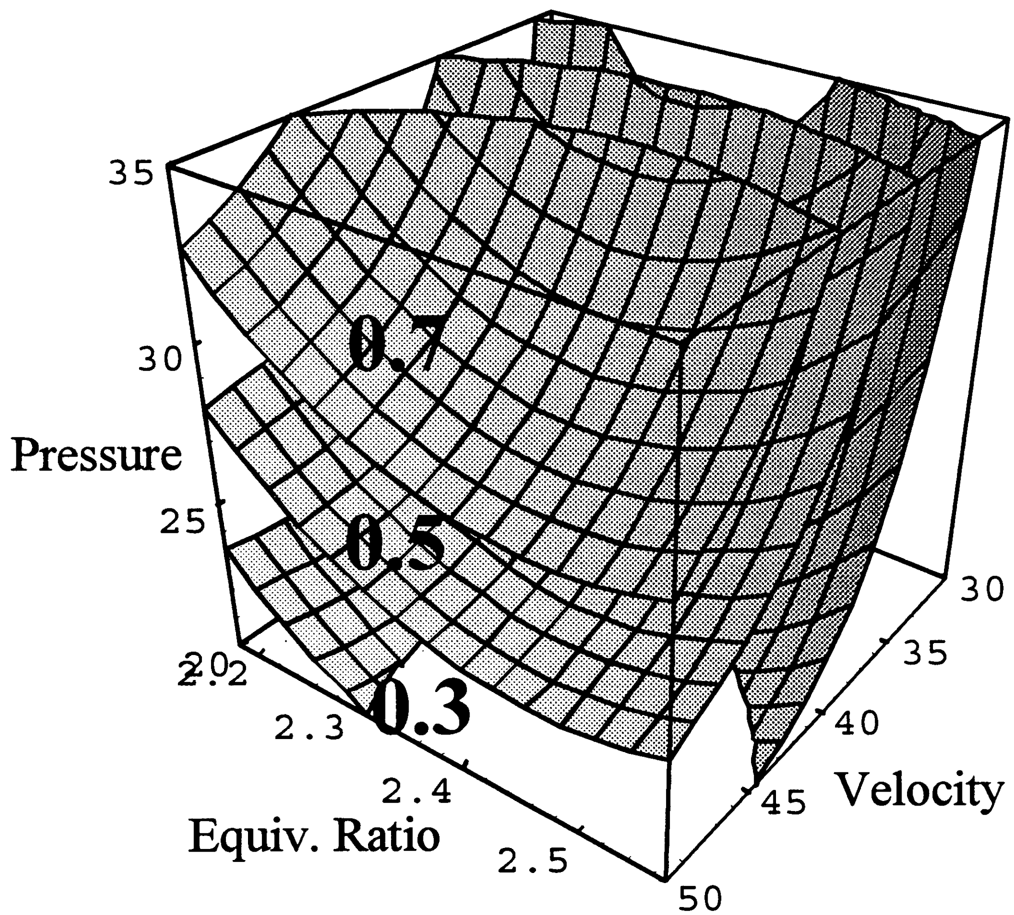


**Figure 59 Mean Total Production Rate of $C_{60}$ and $C_{70}$ (g/hr)**

The same cannot be said for the yields from carbon fed. As seen in Figures 54, 55 and 56, for any given condition the models predict that the yields of $C_{70}$ could be significantly higher than that of $C_{60}$. For both $C_{60}$ and $C_{70}$ the increases tend towards higher velocities and pressures Though for $C_{60}$ the effect of equivalence ratio is more apparent than $C_{70}$. Within the space studied, a maximum occurs for the yield of $C_{60}$ from carbon fed near an equivalence ratio of 2.4. The quadratic effect of velocity on both yields is also very apparent. In consideration of production rates, Figures 57, 58 and 59 indicate that increases in the velocity and pressure also lead to an increase in the rate of production of both $C_{60}$ and $C_{70}$. In a similar manner as in the yields from carbon fed, a peak in the equivalence ratio occurs near a value of 2.4 for both $C_{60}$ and $C_{70}$.

Although these plots seems to imply a lot of information, they should not be taken as accurate response surfaces much past the local experimental space studied. A local maximum has been found in the equivalence ratio and in some areas the velocity is also seen to pass through a point of maximum effect. However not much information has been gained about the effect of pressure. It is expected that as the pressure is increased there will eventually be a decrease in the yield from soot.

## 4.3 Data Evaluation

The constructed models will be used here to give estimations to the material cost of producing of $C_{60}$ and $C_{70}$. Since the cost of separation is a completely different issue, the

Table 6 Cost of Production for Various Considerations

| | Benzene flow rate (ml/min) | Mass of fuel (g/h) | Cost of fuel $/h | Mass produced (g/h) C60 | C70 | Cost of prod. ($/g) C60 | C70 |
|---|---|---|---|---|---|---|---|
| High yield in soot | 6.6 | 344.52 | 0.10 | 0.4 | 0.32 | 0.26 | 0.32 |
| High yield from C fed | 6.4 | 334.08 | 0.10 | 0.66 | 0.46 | 0.15 | 0.22 |
| High prod. rate | 7.2 | 375.84 | 0.11 | 0.66 | 0.46 | 0.17 | 0.25 |

information given here is the cost of producing a soot with different $C_{60}$ and $C_{70}$ content. Also, since the models are assumed to be dependable only within the experimental space studied, conditions that lie within it will only be used in the calculations.

Table 6 is a rough calculation of the cost of producing soots with various process goals taken into consideration. An industrial bulk cost estimate of $0.30/kg of fuel was used to arrive at the figures. The values used in the calculations all come from a common area of the experimental space, high pressures and velocities The flow rate of fuel relies on both the equivalence ratio and the cold gas velocity. For the outputs considered, the conditions do not change appreciably, so therefore the cost of fuel is relatively constant. What does change is the masses of $C_{60}$ and $C_{70}$ produced in the soot.

At first glance it may appear that the masses of $C_{60}$ and $C_{70}$ produced in the soot for a high soot yield are lower than those for high carbon yields and production rates. Really what has happened is that there was less soot produced overall since high soot yields occur with low equivalence ratios or low sooting conditions. This results in a 50 to 100 percent increase in the cost of producing the fullerenes from conditions of high yields from carbon fed and production rates. By extrapolating the costs to kilogram quantities, $C_{60}$ and $C_{70}$ could have costs between \$150 to \$260 and \$220 to \$320 respectively.

It should be reminded that these are basement level costs associated only with the cost of fuel. No considerations have been made towards the cost of other process chemicals such as oxygen and argon, or other operational costs such as electricity needed to run the system. The largest of all costs that has been neglected is the cost of separation. A mentioned previously, this is could be a whole different optimization study. The cheapest level of separation could be achieved by a simple solvent wash and recovery on the soot. Costs should increase significantly from there as the individual fullerenes are separated from each other. In spite of all that, these neglected costs would have to be over 1000 times the cost of the fuel alone in order to raise the price to a level comparable to the current arc produced fullerenes.

# Chapter 5

# CONCLUSIONS

## 5.1: Fullerenes as f(P, v, $\phi$)

The experimental design used in this study has provided clues as to where optimal operating conditions for the production of the fullerenes $C_{60}$ and $C_{70}$ by combustion at reduced pressures. What has been found is that the equivalence ratio strongly affects the yields and production rates. For a given chamber pressure and cold gas velocity, the yields from carbon fed and production rate will increase until the equivalence ratio reaches a level near 2.4. The same effect is seen in the cold gas velocity for a given chamber pressure and equivalence ratio.

The equivalence ratio does not exhibit a maximum with respect to the yields from soot. As it is decreased. the yields in the soot increase steadily. The yields from soot appear to increase without bound towards levels of higher chamber pressure and cold gas velocity and lower equivalence ratio. This should not be the case. Eventually the equivalence ratio will reach a point of non-sooting conditions and all production will cease. The same could be said for increases in the velocity. Eventually the velocity will reach a point where the flame is no longer stable and it will simply blow out. This could not be said for yields from carbon fed and production rates where a significant quadratic effect has been measured.

It is expected that the main benefit of this study will be to point future research in proper directions as to investigate other important process considerations.

## 5.2: Flame Temperature

The importance of the flame temperature on the effects cannot be over stated. Though it cannot be controlled directly, changes in the cold gas velocity and equivalence ratio will influence it. Measurements of it were attempted by insertion of a thermocouple probe directly into the flame. Even though this method is low cost and relatively easy, there are many different considerations and errors in the measurement that need to be addressed before any dependable values can be extracted.

What is known is that the flames expected peak temperature near 2100 K is within the error curves estimated by the radiation and conduction corrections. There are however, a few major assumptions concerning the gas composition and emissivity of the thermocouple wire that disallow an estimation to within ⇧ 50 K of the true flame temperature. This is a major obstacle to measuring the temperature effects on the fullerene yields.

# Chapter 6

## RECOMMENDATIONS

Regarding a process optimization, further studies should be done to expand the experimental space to areas of increasing cold gas velocity and chamber pressure. Also within the space more points should be investigated near an equivalence ratio of 2.4 in order to know more exactly the value that is critical to the cost of producing fullerenes. Also, further investigations should be made to correct the thermocouple measurements so that a temperature effect study could be carried out. Other methods for temperature measurements in flames are available, such as the use of lasers and optical sensors but the equipment is much more expensive and more involved than thermocouples.

Quantification of the higher fullerenes that are also present in the flame samples should also carried out. This could be done as easily as assuming a response curve equal to that of C60 and C70 and using the peak areas recorded in the original HPLC work or actually calibrating the column. Though calibration standards for the higher fullerenes are likely to be too expensive.

Considering the experimental system itself, more work could be put into the soot collection system. A filtering apparatus that is lighter and a more consistent weight other than the automotive air filter that was used could lead to a significant decrease in the error associated with the yield from carbon fed. This area should also be of concern to any party that wishes to produce fullerenes on a commercial basis. Soot loss though the filter to the vacuum pumps only results in lost profits and frequent changing of pump oil. If a filter has too fine of a nominal pore size, it will cake up with soot too quickly resulting in lost operational time due to too frequent change overs.

Also of concern is control of the burners temperature. Currently the cooling lines are to small of diameter and the flow rate of coolant is not sufficient to keep the temperature stable. For certain conditions where there is much heat soaked up by the burner surface, such as low velocity or low equivalence ratio flames, the rate of cooling is not sufficient to keep the temperature at a steady level. Combine the low coolant flow rate and the high rate of heat transfer to the cooling lines and eventually the coolant fluid starts to vaporize in the lines. At this point the burner must be shut down and allowed to cool. Otherwise over heating of the burner could result in damage to internal gaskets and the feed lines attached to it.

# REFERENCES CITED


1. Kroto, H. W., J. R. Heath, S. C. O'Brien, R. F. Curl and R. E. Smalley. 1985. Nature 318: 162-163.

2. Kraetschmer, W., L. D. Lamb, K. Fostiropoulos, D. R. Huffman. 1990. Nature 347: 354-358.

3. Huffman, D. R.. 1994. The Almost (but never quite) Complete Buckminsterfullerene Bibliography. Anonymous ftp site, physics.arizona.edu. email to tinker@physics.arizona.edu for information.

4. Huffman, D. R. 1994. Materials Letters 21: 127-129.

5. Baum, R. M. 1993. Chemical and Engineering News (November 22): 8-18.

6. Curl, R. F., R. E. Smalley. 1991. Scientific American (October) 265: 54-63.

7. Baum, R. M. 1993. Chemical and Engineering News (August 2): 3-4.

8. Hebard, A. F., M. J. Rosseinsky, R. C. Haddon, D. W. Murphy, S. H. Glarum, T. T. M. Palstra, A. P. Ramirez, A. R. Kortan. 1991. Nature 350: 600.

9. Geake, E. 1993. New Scientist 138: 18-18

10. Jones, D. E. H. 1966. New Scientist 32: 245.

11. Osawa, E. 1970. Kagaku (Kyoto) 25: 854.

12. Yoshida, Z., E. Osawa. 1971. Aromaticity (Kyoto) 174-178.

13. Bochvar, D. A., E. G. Gal'pern. 1973. Proc. Acad. Sci. USSR 209: 239-241.

14. Hoffman, R., 1993. Scientific American 66

15. Jones, D. E. H., 1982. The Inventions of Daedalus. San Francisco: W. H. Freeman, Oxford: 118-119.

16. Kroto, H. W., A. W. Allaf, S. P. Balm. 1991. Chemical Reviews 91, 6: 1213-1235.

17. Kroto, H. W. 1992. Angewandte Chemie - International Edition In English 31, 2: 111-129.

18. Gerhardt, P., S. Loffler, K. H. Homann. 1987. Chemical Physics Letters 137, 4: 306-310.

19. Gerhardt, P., S. Loffler, K. H. Homann. 1988. 22nd International Syposium on Combustion 395-401.

20. Loffler, S., K. H. Homann. 1990. 23rd International Syposium on Combustion 355-362.

21. Coulombeau, C., A. Rassat. 1987. Journal De Chimie Physique Et De Physico-Chimie Biologique 84, 7-8: 875-882.

22. Luthi, H. P., J. Almlof. 1987. Chemical Physics Letters 135, 4: 357-360.

23. Rosen, A., B. Waestberg. 1988. Journal of the American Chemical Society 110, 26: 8701-8703.

24. Creasy, W. R. 1990. Journal of Chemical Physics 92, 12: 7229-7233.

25. Feng, J. K., J. Li, Z. Li, M. C. Zerner. 1993. International Journal of Quantum Chemistry 29, 3: 331-344.

26. Kraetschmer, W., K. Fostiropoulos, D. R. Huffman. 1990. Chemical Physics Letters 170, 2: 167-170.

27. Howard, J. B., J. T. McKinnon, Y. Makarovsky, A. L. Lafleur, M. E. Johnson. 1991. Nature 352: 139-141.

28. Howard, J. B., J. T. McKinnon, M. E. Johnson, Y. Makarovsky, A. L. Lafleur. 1992. Journal of Physical Chemistry 96, 16: 6657-6662.

29. McKinnon, J. T., 1991. Journal of Physical Chemistry 95, 22: 8941-8944.

30. McKinnon, J. T., W. L. Bell, R. M. Barkley. 1992. Combustion and Flame 88, 1: 102-112.

31. Howard, J. B., A. L. Lafleur, Y. Makarovsky, S. Mitra, C. J. Pope, T. K. Yadav. 1992. Carbon 30, 8: 1183-1201.

32. Ebbesen, T. W., J. Tabuchi, K. Tanigaki. 1992. Chemical Physics Letters 191, 3: 336-338.

33. Pope, C. J., J. A. Marr, J. B. Howard. 1993. Journal of Physical Chemistry 97, 42: 11001-11013.

34. Lamb, L. D., D. R. Huffman. 1993. Journal of Physics and Chemistry of Solids 54, 12: 1635.

35. Anacleto, J. F., H. Perreault, R. K. Boyd, S. Pleasance, M. A. Quilliam, P. G. Sim, J. B. Howard, Y. Makarovsky, A. L. Lafleur. 1992. Rapid Communications in Mass Spectroscopy 6, 3: 214-220.

36. Anacleto, J. F., R. K. Boyd, S. Pleasance, M. A. Quilliam, J. B. Howard, A. L. Lafleur, Y. Makarovsky. 1992. Canadian Journal of Chemistry 70, 10: 2558-2658.

37. Hicks, C. R.. 1973. Fundamental Concepts in the Design of Experiments. New York: Holt, Rinehart and Winston: 305

38. Lorenzen, T. J., V. L. Anderson. 1993. Design of Experiments, A No-Name Approach. New York: Marcel Dekker, Inc. 328-334.

39. Jinno, K., T. Uemura, H. Ohta, H. Nagashima, K. Itoh. 1993. Analytical Chemistry 65, 19: 2650-2654.

40. Bradley, D., K. J. Mathhews. 1968. Journal of Mechanical Engineering Science 65, 4. 299-305.

41. Reid, R. C., J. M. Prausnitz, B. E. Poling. 1987. The Properties of Gases and Liquids. New York: McGraw-Hill, Inc.

42. Montgomery, D. C..1991. Design and Analysis of Experiments. New York: John Wiley and Sons: 497.

43. Box, G. E. P., W. G. Hunter, J. S. Hunter. 1978. Statistics for Experimenters. New York: J. Wiley & Sons: 313.

# APPENDICES

## Appendix A: Orifice Calibrations

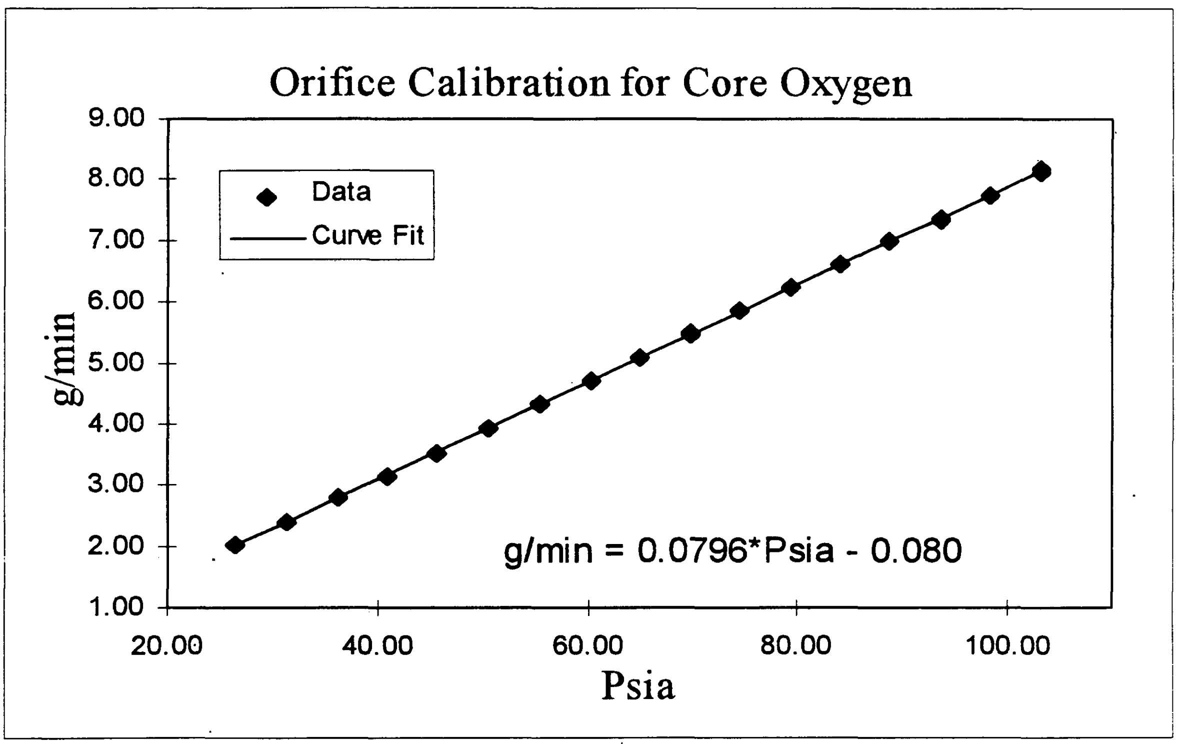

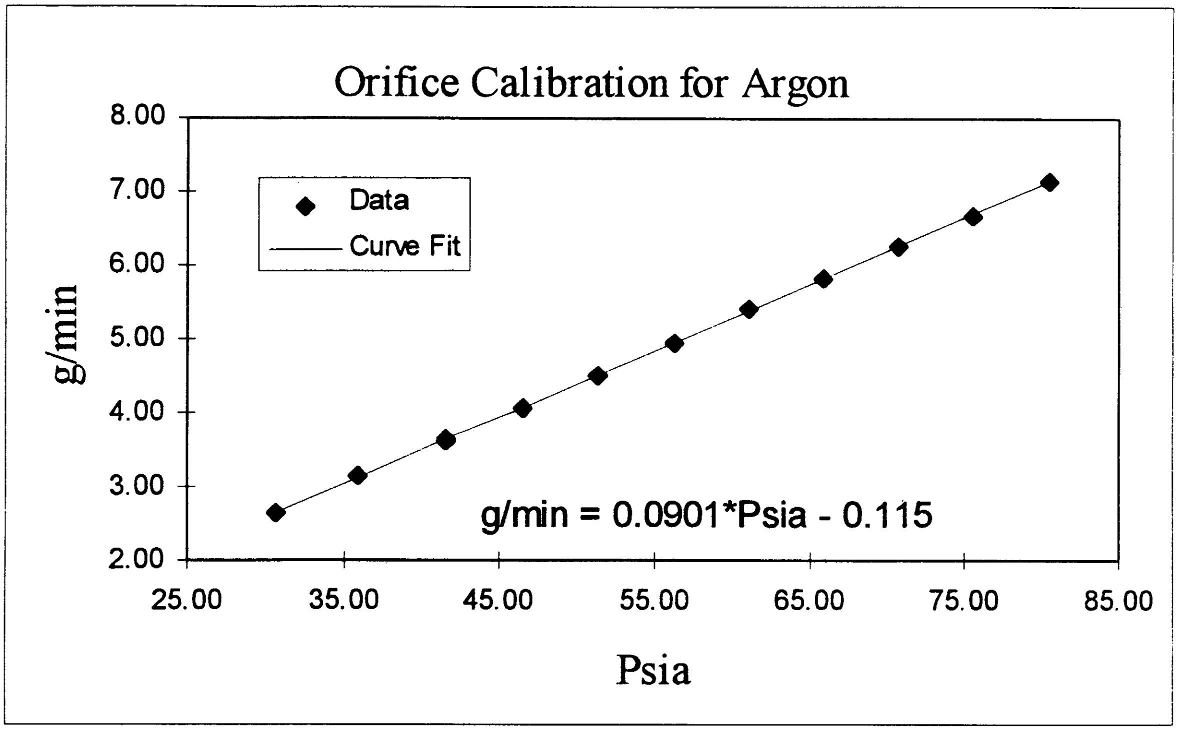
Orifice Calibration for Argon
8.00
7.00
6.00
5.00
4.00
3.00
2.00
g/min
Data
Curve Fit
g/min = 0.0901*Psia - 0.115
25.00
35.00
45.00
55.00
65.00
75.00
85.00
Psia

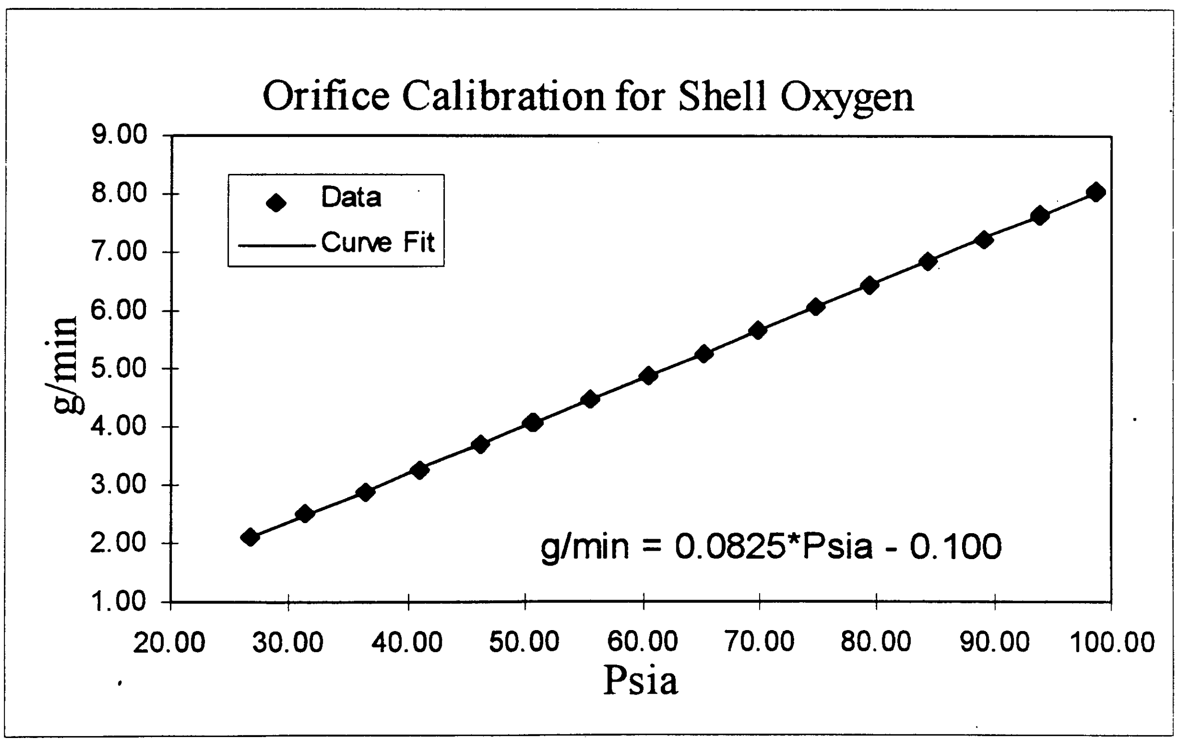
Orifice Calibration for Shell Oxygen
9.00
8.00
7.00
6.00
5.00
4.00
3.00
2.00
1.00
g/min
Data
Curve Fit
g/min = 0.0825*Psia - 0.100
20.00
30.00
40.00
50.00
60.00
70.00
80.00
90.00
100.00
Psia

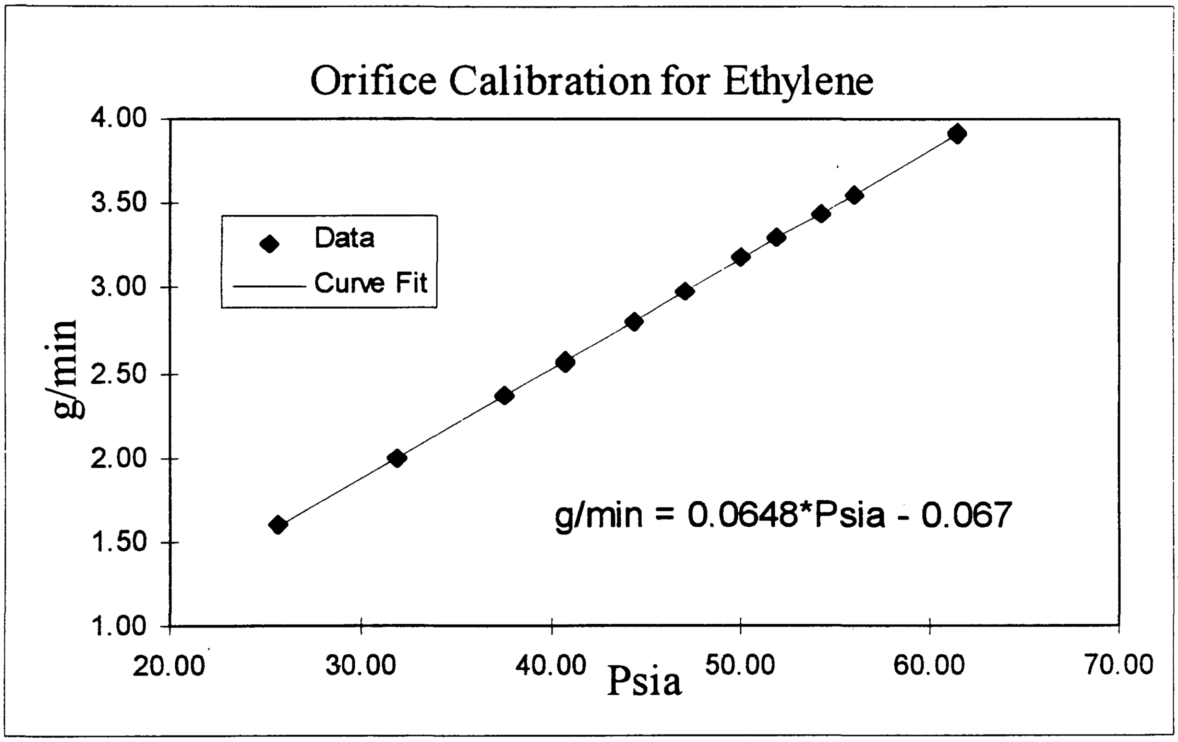
Orifice Calibration for Ethylene
Data
Curve Fit
g/min = 0.0648*Psia - 0.067
g/min
4.00
3.50
3.00
2.50
2.00
1.50
1.00
20.00
30.00
40.00
50.00
60.00
70.00
Psia

## Appendix B: Flow Rates and Pressures of Feeds for the Experimental Conditions

**Condition #1**

| | | | |
|---|---|---|---|
| Chamber Pressure | 20 Torr | C6H6 | 2.39 ml/min |
| Cold Gas Velocity | 30 cm/s | Core O2 | 33.7 psia |
| Equivalence Ratio | 2.375 | Core Ar | 17.2 psia |
| | | Sheild O2 | 27.1 psia |
| | | Sheild C2H4 | 11.0 psia |

**Condition #2**

| | | | |
|---|---|---|---|
| Chamber Pressure | 20 Torr | C6H6 | 3.36 ml/min |
| Cold Gas Velocity | 40 cm/s | Core O2 | 43.7 psia |
| Equivalence Ratio | 2.563 | Core Ar | 22.4 psia |
| | | Sheild O2 | 35.5 psia |
| | | Sheild C2H4 | 14.1 psia |

**Condition #3**

| | | | |
|---|---|---|---|
| Chamber Pressure | 20 Torr | C6H6 | 3.72 ml/min |
| Cold Gas Velocity | 50 cm/s | Core O2 | 56.2 psia |
| Equivalence Ratio | 2.188 | Core Ar | 27.5 psia |
| | | Sheild O2 | 43.9 psia |
| | | Sheild C2H4 | 17.2 psia |

**Condition #4**

| | | | |
|---|---|---|---|
| Chamber Pressure | 35 Torr | C6H6 | 5.55 ml/min |
| Cold Gas Velocity | 40 cm/s | Core O2 | 76.6 psia |
| Equivalence Ratio | 2.375 | Core Ar | 37.8 psia |
| | | Sheild O2 | 60.7 psia |
| | | Sheild C2H4 | 23.4 psia |

**Condition #5**

| | | | |
|---|---|---|---|
| Chamber Pressure | 35 Torr | C6H6 | 7.35 ml/min |
| Cold Gas Velocity | 50 cm/s | Core O2 | 93.6 psia |
| Equivalence Ratio | 2.563 | Core Ar | 46.7 psia |
| | | Sheild O2 | 75.4 psia |
| | | Sheild C2H4 | 28.9 psia |

**Condition #6**

| | | | |
|---|---|---|---|
| Chamber Pressure | 35 Torr | C6H6 | 3.91 ml/min |
| Cold Gas Velocity | 30 cm/s | Core O2 | 58.9 psia |
| Equivalence Ratio | 2.188 | Core Ar | 28.8 psia |
| | | Sheild O2 | 46.0 psia |
| | | Sheild C2H4 | 18.0 psia |

**Condition #7**

| | | | |
|---|---|---|---|
| Chamber Pressure | 27.5 Torr | C6H6 | 5.45 ml/min |
| Cold Gas Velocity | 50 cm/s | Core O2 | 75.3 psia |
| Equivalence Ratio | 2.375 | Core Ar | 37.1 psia |
| | | Sheild O2 | 59.6 psia |
| | | Sheild C2H4 | 23.0 psia |

**Condition #8**

| | | | |
|---|---|---|---|
| Chamber Pressure | 27.5 Torr | C6H6 | 3.46 ml/min |
| Cold Gas Velocity | 30 cm/s | Core O2 | 45.0 psia |
| Equivalence Ratio | 2.563 | Core Ar | 23.0 psia |
| | | Sheild O2 | 36.5 psia |
| | | Sheild C2H4 | 14.5 psia |

**Condition #9**

| | | | |
|---|---|---|---|
| Chamber Pressure | 27.5 Torr | C6H6 | 4.09 ml/min |
| Cold Gas Velocity | 40 cm/s | Core O2 | 61.7 psia |
| Equivalence Ratio | 2.188 | Core Ar | 30.1 psia |
| | | Sheild O2 | 48.1 psia |
| | | Sheild C2H4 | 18.8 psia |

**Condition #10**

| | | | |
|---|---|---|---|
| Chamber Pressure | 20 Torr | C6H6 | 4.20 ml/min |
| Cold Gas Velocity | 50 cm/s | Core O2 | 52.1 psia |
| Equivalence Ratio | 2.563 | Core Ar | 24.8 psia |
| | | Sheild O2 | 38.0 psia |
| | | Sheild C2H4 | 14.6 psia |

**Condition #11**

| | | | |
|---|---|---|---|
| Chamber Pressure | 20 Torr | C6H6 | 2.23 ml/min |
| Cold Gas Velocity | 30 cm/s | Core O2 | 34.3 psia |
| Equivalence Ratio | 2.188 | Core Ar | 17.2 psia |
| | | Sheild O2 | 27.1 psia |
| | | Sheild C2H4 | 11.0 psia |

**Condition #12**

| | | | |
|---|---|---|---|
| Chamber Pressure | 35 Torr | C6H6 | 5.21 ml/min |
| Cold Gas Velocity | 40 cm/s | Core O2 | 78.1 psia |
| Equivalence Ratio | 2.188 | Core Ar | 37.8 psia |
| | | Sheild O2 | 60.7 psia |
| | | Sheild C2H4 | 23.4 psia |

**Condition #13**

| | | | |
|---|---|---|---|
| Chamber Pressure | 27.5 Torr | C6H6 | 3.27 ml/min |
| Cold Gas Velocity | 30 cm/s | Core O2 | 45.8 psia |
| Equivalence Ratio | 2.375 | Core Ar | 23.0 psia |
| | | Sheild O2 | 36.5 psia |
| | | Sheild C2H4 | 14.5 psia |

**Condition #14**

| | | | |
|---|---|---|---|
| Chamber Pressure | 35 Torr | C6H6 | 6.94 ml/min |
| Cold Gas Velocity | 50 cm/s | Core O2 | 95.4 psia |
| Equivalence Ratio | 2.375 | Core Ar | 46.7 psia |
| | | Sheild O2 | 75.4 psia |
| | | Sheild C2H4 | 28.9 psia |

**Condition #15**

| | | | |
|---|---|---|---|
| Chamber Pressure | 27.5 Torr | C6H6 | 4.62 ml/min |
| Cold Gas Velocity | 40 cm/s | Core O2 | 59.4 psia |
| Equivalence Ratio | 2.563 | Core Ar | 30.1 psia |
| | | Sheild O2 | 48.1 psia |
| | | Sheild C2H4 | 18.8 psia |

Appendix C: HPLC Calibrations

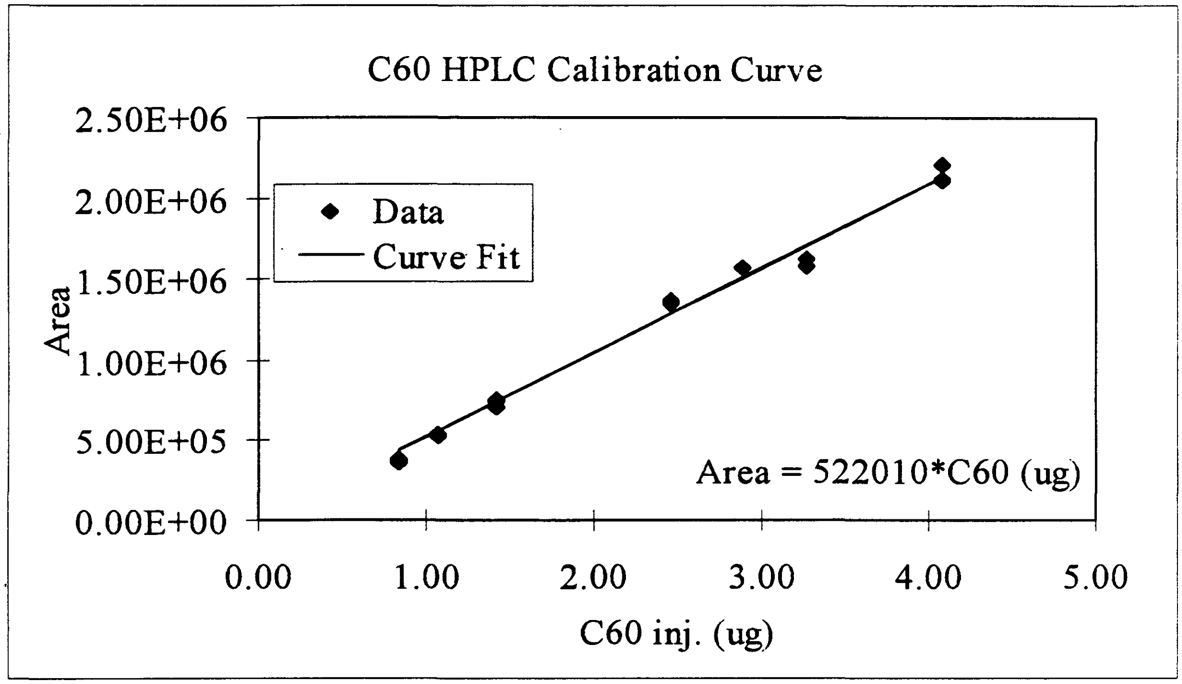


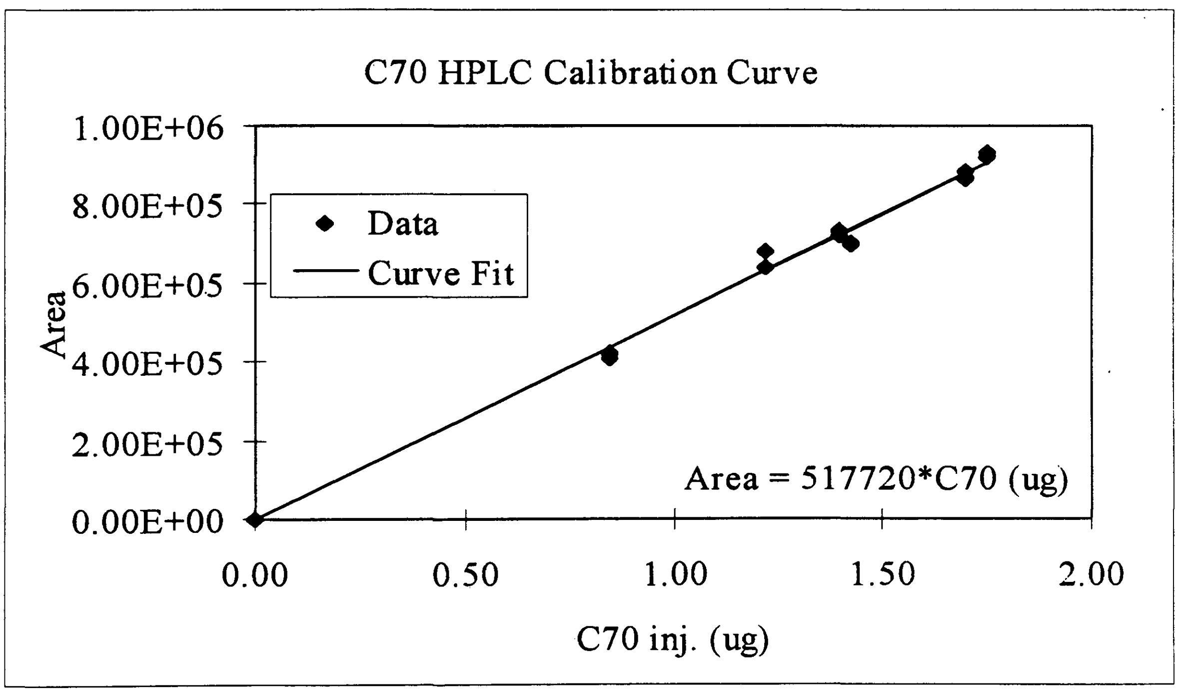

Appendix D: HPLC Analysis of Samples

| | | | Peak areas from samples | | | | Sample injection mass (ug) | | | |
|---|---|---|---|---|---|---|---|---|---|---|
| | conc. | Mass | Inj. 1 | | Inj. 2 | | Inj. 1 | | Inj. 2 | |
| ID | mg/ml | inj. (ug | C60 | C70 | C60 | C70 | C60 | C70 | C60 | C70 |
| 1-c-1 | 0.52 | 2.59 | 494593 | 470661 | 498150 | 474923 | 0.95 | 0.91 | 0.95 | 0.92 |
| 1-c-3 | 0.59 | 2.93 | 424278 | 670877 | 433244 | 683400 | 0.81 | 1.30 | 0.83 | 1.32 |
| 2-c-1 | 0.54 | 2.68 | 537108 | 475306 | 539747 | 476283 | 1.03 | 0.92 | 1.03 | 0.92 |
| 2-d-1 | 0.51 | 2.53 | 401955 | 444471 | 410195 | 448081 | 0.77 | 0.86 | 0.79 | 0.87 |
| 3-d-1 | 0.54 | 2.69 | 513564 | 472262 | 519513 | 466433 | 0.98 | 0.91 | 1.00 | 0.90 |
| 3-dr-1 | 0.56 | 2.80 | 493257 | 422574 | 485126 | 416266 | 0.94 | 0.82 | 0.93 | 0.80 |
| 4-c-1 | 0.58 | 2.92 | 633398 | 564329 | 616482 | 549349 | 1.21 | 1.09 | 1.18 | 1.06 |
| 4-c-2 | 0.53 | 2.64 | 653259 | 504580 | 664719 | 517207 | 1.25 | 0.97 | 1.27 | 1.00 |
| 4-cr-1 | 0.52 | 2.60 | 668004 | 479134 | 671196 | 483989 | 1.28 | 0.93 | 1.29 | 0.93 |
| 5-c-1 | 0.56 | 2.78 | 531828 | 593948 | 531953 | 596040 | 1.02 | 1.15 | 1.02 | 1.15 |
| 5-d-1 | 0.50 | 2.50 | 692952 | 441928 | 705655 | 452309 | 1.33 | 0.85 | 1.35 | 0.87 |
| 6-d-1 | 0.54 | 2.69 | 547721 | 614913 | 536937 | 599938 | 1.05 | 1.19 | 1.03 | 1.16 |
| 6-dr-1 | 0.51 | 2.55 | 413765 | 535798 | 415255 | 542901 | 0.79 | 1.03 | 0.80 | 1.05 |
| 7-c-1 | 0.54 | 2.71 | 655141 | 481586 | 663836 | 493519 | 1.26 | 0.93 | 1.27 | 0.95 |
| 7-cr-1 | 0.53 | 2.65 | 687737 | 434798 | 698973 | 443087 | 1.32 | 0.84 | 1.34 | 0.86 |
| 8-c-1 | 0.50 | 2.50 | 313034 | 544547 | 317772 | 542206 | 0.60 | 1.05 | 0.61 | 1.05 |
| 8-c-2 | 0.49 | 2.46 | 280620 | 576928 | 272906 | 566576 | 0.54 | 1.11 | 0.52 | 1.09 |
| 9-d-1 | 0.53 | 2.67 | 626654 | 601348 | 632741 | 609513 | 1.20 | 1.16 | 1.21 | 1.18 |
| 9-dr-1 | 0.50 | 2.48 | 455632 | 556340 | 462437 | 564825 | 0.87 | 1.07 | 0.89 | 1.09 |
| 10-c-1 | 0.54 | 2.69 | 502312 | 583777 | 502216 | 581807 | 0.96 | 1.13 | 0.96 | 1.12 |
| 10-c-2 | 0.48 | 2.40 | 389376 | 595670 | 393922 | 586832 | 0.75 | 1.15 | 0.75 | 1.13 |
| 11-d-1 | 0.55 | 2.73 | 588636 | 667825 | 568172 | 645093 | 1.13 | 1.29 | 1.09 | 1.25 |
| 11-dr-1 | 0.58 | 2.90 | 507015 | 603124 | 531197 | 618563 | 0.97 | 1.16 | 1.02 | 1.19 |
| 12-d-1 | 0.51 | 2.53 | 647591 | 569985 | 653572 | 571661 | 1.24 | 1.10 | 1.25 | 1.10 |
| 12-d-2 | 0.51 | 2.55 | 629745 | 601462 | 625811 | 599860 | 1.21 | 1.16 | 1.20 | 1.16 |
| 13-d-1 | 0.56 | 2.78 | 542544 | 666994 | 532008 | 662560 | 1.04 | 1.29 | 1.02 | 1.28 |
| 13-d-2 | 0.56 | 2.78 | 553518 | 668778 | 560306 | 684084 | 1.06 | 1.29 | 1.07 | 1.32 |
| 14-d-1 | 0.54 | 2.70 | 754905 | 534397 | 775791 | 538268 | 1.45 | 1.03 | 1.49 | 1.04 |
| 14-d-2 | 0.51 | 2.53 | 740977 | 491006 | 745735 | 504320 | 1.42 | 0.95 | 1.43 | 0.97 |
| 15-d-1 | 0.61 | 3.06 | 571754 | 596718 | 582586 | 610261 | 1.10 | 1.15 | 1.12 | 1.18 |
| 15-d-2 | 0.58 | 2.88 | 522759 | 534883 | 534404 | 550027 | 1.00 | 1.03 | 1.02 | 1.06 |

| | Mass fraction in sample | | | | | | | C70/C60 molar ratio | | |
|---|---|---|---|---|---|---|---|---|---|---|
| | C60 | | C70 | | Averaged | | | | | |
| ID | Inj. 1 | Inj. 2 | Inj. 1 | Inj. 2 | C60 | C70 | Total | Inj. 1 | Inj. 2 | ave. |
| 1-c-1 | 0.366 | 0.369 | 0.351 | 0.355 | 0.367 | 0.353 | 0.720 | 0.822 | 0.824 | 0.823 |
| 1-c-3 | 0.277 | 0.283 | 0.442 | 0.451 | 0.280 | 0.446 | 0.727 | 1.367 | 1.363 | 1.365 |
| 2-c-1 | 0.384 | 0.385 | 0.342 | 0.343 | 0.385 | 0.343 | 0.727 | 0.765 | 0.763 | 0.764 |
| 2-d-1 | 0.305 | 0.311 | 0.340 | 0.343 | 0.308 | 0.341 | 0.649 | 0.956 | 0.944 | 0.950 |
| 3-d-1 | 0.365 | 0.370 | 0.339 | 0.335 | 0.367 | 0.337 | 0.704 | 0.795 | 0.776 | 0.785 |
| 3-dr-1 | 0.337 | 0.332 | 0.292 | 0.287 | 0.335 | 0.289 | 0.624 | 0.740 | 0.742 | 0.741 |
| 4-c-1 | 0.415 | 0.404 | 0.373 | 0.363 | 0.410 | 0.368 | 0.778 | 0.770 | 0.770 | 0.770 |
| 4-c-2 | 0.475 | 0.483 | 0.370 | 0.379 | 0.479 | 0.374 | 0.853 | 0.668 | 0.672 | 0.670 |
| 4-cr-1 | 0.493 | 0.495 | 0.356 | 0.360 | 0.494 | 0.358 | 0.852 | 0.620 | 0.623 | 0.622 |
| 5-c-1 | 0.366 | 0.366 | 0.412 | 0.414 | 0.366 | 0.413 | 0.779 | 0.965 | 0.968 | 0.967 |
| 5-d-1 | 0.531 | 0.541 | 0.341 | 0.349 | 0.536 | 0.345 | 0.881 | 0.551 | 0.554 | 0.553 |
| 6-d-1 | 0.390 | 0.382 | 0.441 | 0.431 | 0.386 | 0.436 | 0.822 | 0.970 | 0.966 | 0.968 |
| 6-dr-1 | 0.311 | 0.312 | 0.406 | 0.412 | 0.312 | 0.409 | 0.721 | 1.119 | 1.130 | 1.125 |
| 7-c-1 | 0.462 | 0.469 | 0.343 | 0.351 | 0.465 | 0.347 | 0.812 | 0.635 | 0.643 | 0.639 |
| 7-cr-1 | 0.498 | 0.506 | 0.317 | 0.323 | 0.502 | 0.320 | 0.822 | 0.546 | 0.548 | 0.547 |
| 8-c-1 | 0.240 | 0.243 | 0.421 | 0.419 | 0.242 | 0.420 | 0.661 | 1.503 | 1.475 | 1.489 |
| 8-c-2 | 0.218 | 0.212 | 0.452 | 0.444 | 0.215 | 0.448 | 0.663 | 1.777 | 1.794 | 1.786 |
| 9-d-1 | 0.450 | 0.454 | 0.435 | 0.441 | 0.452 | 0.438 | 0.890 | 0.829 | 0.833 | 0.831 |
| 9-dr-1 | 0.352 | 0.357 | 0.433 | 0.440 | 0.355 | 0.437 | 0.791 | 1.055 | 1.056 | 1.055 |
| 10-c-1 | 0.358 | 0.358 | 0.420 | 0.418 | 0.358 | 0.419 | 0.777 | 1.004 | 1.001 | 1.003 |
| 10-c-2 | 0.311 | 0.315 | 0.480 | 0.473 | 0.313 | 0.476 | 0.789 | 1.322 | 1.287 | 1.305 |
| 11-d-1 | 0.413 | 0.399 | 0.473 | 0.457 | 0.406 | 0.465 | 0.871 | 0.980 | 0.981 | 0.981 |
| 11-dr-1 | 0.335 | 0.351 | 0.402 | 0.412 | 0.343 | 0.407 | 0.750 | 1.028 | 1.006 | 1.017 |
| 12-d-1 | 0.491 | 0.496 | 0.436 | 0.437 | 0.494 | 0.437 | 0.930 | 0.761 | 0.756 | 0.758 |
| 12-d-2 | 0.473 | 0.470 | 0.456 | 0.454 | 0.472 | 0.455 | 0.927 | 0.825 | 0.828 | 0.827 |
| 13-d-1 | 0.374 | 0.367 | 0.464 | 0.461 | 0.371 | 0.462 | 0.833 | 1.062 | 1.076 | 1.069 |
| 13-d-2 | 0.381 | 0.386 | 0.464 | 0.475 | 0.383 | 0.469 | 0.853 | 1.044 | 1.055 | 1.050 |
| 14-d-1 | 0.535 | 0.550 | 0.382 | 0.384 | 0.542 | 0.383 | 0.925 | 0.612 | 0.600 | 0.606 |
| 14-d-2 | 0.562 | 0.566 | 0.376 | 0.386 | 0.564 | 0.381 | 0.945 | 0.573 | 0.584 | 0.579 |
| 15-d-1 | 0.358 | 0.365 | 0.377 | 0.385 | 0.361 | 0.381 | 0.742 | 0.902 | 0.905 | 0.904 |
| 15-d-2 | 0.348 | 0.356 | 0.359 | 0.369 | 0.352 | 0.364 | 0.716 | 0.884 | 0.889 | 0.887 |

## Appendix E: Sample Calculations for Thermocouple Radiation Correction

*****Calculation of heat transfer coefficient through estimation of gas properties.

| | | |
|---|---|---|
| ** Measured temperature | 1325 | K |
| ** Assumed true temperature | 1750 | K |
| ** Calculation temperature | **1537.5** | K |

| | | | |
|---|---|---|---|
| diameter of bead = | 0.01 | in | 0.0254 cm |
| **cold gas velocity =** | **50** | **cm/s** | |
| **hot gas velocity =** | **298.482** | **cm/s** | |

Rough product mix for condition

| | **#14** | **#3** |
|---|---|---|
| Ar | 0.103 | 0.059 |
| CO | 0.350 | 0.199 |
| H2O | 0.119 | 0.076 |
| C2H4 | 0.056 | 0.024 |

| | moles | mol. frac. | mol. wt. |
|---|---|---|---|
| Ar | 0.103 | 0.163 | 39.948 |
| CO | 0.350 | 0.558 | 28.01 |
| H2O | 0.119 | 0.190 | 18.015 |
| C2H4 | 0.056 | 0.089 | 28.054 |
| total | 0.628 | | |
| | ave. mol. wt. prod. | | **28.1** |

---

**Density calculation**

*** Assume ideal gas conditions

$\rho = PM/RT$

| | | |
|---|---|---|
| **Chamber Pressure =** | **35** | **torr** |
| R = | 0.082058 | l atm / mol K |
| $\rho$ = | **1.02E-05** | **g/cm3** |

---

**Viscosity calculation**

pure species by corresponding states method (Reid, Prausnitz & Poling, pg 397)

| Critical values | Tc/K | Pc/bar | Zc |
|---|---|---|---|
| Ar | 150.8 | 48.7 | 0.291 |
| CO | 132.9 | 35 | 0.295 |
| H2O | 647.3 | 220.5 | 0.229 |
| C2H4 | 282.4 | 50.4 | 0.276 |

viscosity calculation continued...

| dipole moments | | |
|---|---|---|
| Ar | 0 | D |
| CO | 0.1 | D |
| H2O | 1.84 | D |
| C2H4 | 0 | D |

| reduced dipole moments | | Fp |
|---|---|---|
| Ar | 0 | 1 |
| CO | 0.00104 | 1 |
| H2O | 0.093468 | 1.29648531 |
| C2H4 | 0 | 1 |

| $\xi$ | | |
|---|---|---|
| Ar | 0.004817 | μP^-1 |
| CO | 0.007021 | μP^-1 |
| H2O | 0.003341 | μP^-1 |
| C2H4 | 0.006238 | μP^-1 |

| Dimensionless viscosity | |
|---|---|
| Ar | 3.403344 |
| CO | 3.680284 |
| H2O | 1.649834 |
| C2H4 | 2.286829 |

| Estimated viscosities | | | | |
|---|---|---|---|---|
| Ar | 706.5 μP | = | 0.07065 cP |
| CO | 524.2 μP | = | 0.05242 cP |
| H2O | 493.7 μP | = | 0.04937 cP |
| C2H4 | 366.6 μP | = | 0.03666 cP |

Estimation of gas mixture, Method of Wilke, (Reid, Prausnitz & Poling, pg 407)

| φij i\j | Ar | CO | H2O | C2H4 |
|---|---|---|---|---|
| Ar | 1.0000 | 1.0216 | 1.1978 | 0.8653 |
| CO | 0.9654 | 1.0000 | 1.1976 | 0.8424 |
| H2O | 0.7729 | 0.8177 | 1.0000 | 0.6937 |
| C2H4 | 1.1710 | 1.2063 | 1.4549 | 1.0000 |

| yjφij i\j | Ar | CO | H2O | C2H4 | sum |
|---|---|---|---|---|---|
| Ar | 0.1633 | 0.1668 | 0.1956 | 0.1413 | 0.6670 |
| CO | 0.5385 | 0.5578 | 0.6680 | 0.4699 | 2.2342 |
| H2O | 0.1468 | 0.1553 | 0.1900 | 0.1318 | 0.6239 |
| C2H4 | 0.1042 | 0.1073 | 0.1294 | 0.0890 | 0.4298 |

| | yiηi | iηi/Σ(yjφij) | |
|---|---|---|---|
| Ar | 0.0115 | 0.0173 | |
| CO | 0.0292 | 0.0131 | |
| H2O | 0.0094 | 0.0150 | |
| C2H4 | 0.0033 | 0.0076 | |
| | **ηm =** | **0.0530 cP** | Estimated mixture viscosity |

**Heat capacity calculation**
from polynomial, (Reid, Prausnitz & Poling, Appendix A)

| | A | B | C | D |
|---|---|---|---|---|
| Ar | 2.08E+01 | | | |
| CO | 3.09E+01 | -1.29E-02 | 2.79E-05 | -1.27E-08 |
| H2O | 3.22E+01 | 1.92E-03 | 1.06E-05 | -3.60E-09 |
| C2H4 | 3.806 | 1.57E-01 | -8.35E-05 | 1.76E-08 |

| | | | | yiCpi | |
|---|---|---|---|---|---|
| Ar | 20.800 | J/mol K | Ar | 3.396 | |
| CO | 30.812 | J/mol K | CO | 17.187 | |
| H2O | 47.068 | J/mol K | H2O | 8.941 | |
| C2H4 | 111.025 | J/mol K | C2H4 | 9.876 | |
| | | | **Cpm** | **39.400** | **J/mol K** |
| | | | | **1.404** | **J/g K** |

**Thermal conductivity calculation**
pure species from Table 10-3 (Reid, Prausnitz & Poling, pg 514)

| | A | B | C | D | range |
|---|---|---|---|---|---|
| Ar | 2.71E-03 | 5.54E-05 | -2.72E-08 | 5.53E-12 | 115-1470 |
| CO | 5.07E-04 | 9.13E-05 | -3.52E-08 | 8.20E-12 | 115-1670 |
| H2O | 7.34E-03 | -1.01E-05 | 1.80E-07 | -9.10E-11 | 273-1070 |
| C2H4 | -1.76E-02 | 1.20E-04 | 3.34E-08 | -1.37E-11 | 200-1270 |

| | | |
|---|---|---|
| Ar | 0.0437 | W/m K |
| CO | 0.0873 | W/m K |
| H2O | 0.0868 | W/m K |
| C2H4 | 0.1961 | W/m K |

Mixture thermal conductivity by Mason and Saxena (Reid, Prausnitz & Poling, pg 531)

| Γ | | | exponential terms | |
|---|---|---|---|---|
| Ar | 229.62 | W/m K^-1 | Ar | 1.519 |
| CO | 234.65 | W/m K^-1 | CO | 1.649 |
| H2O | 71.83 | W/m K^-1 | H2O | 0.553 |
| C2H4 | 208.80 | W/m K^-1 | C2H4 | 1.018 |

thermal conductivity calculation continued...

| $\lambda tri/\lambda trj$ i\ | Ar | CO | H2O | C2H4 |
|---|---|---|---|---|
| Ar | 1.0000 | 0.9415 | 0.8600 | 1.3567 |
| CO | 1.0621 | 1.0000 | 0.9134 | 1.4409 |
| H2O | 1.1628 | 1.0948 | 1.0000 | 1.5775 |
| C2H4 | 0.7371 | 0.6940 | 0.6339 | 1.0000 |

| Aij i\j | Ar | CO | H2O | C2H4 |
|---|---|---|---|---|
| Ar | 1.0000 | 0.9636 | 0.8956 | 1.1726 |
| CO | 1.0234 | 1.0000 | 0.9453 | 1.2104 |
| H2O | 1.0414 | 1.0348 | 1.0000 | 1.2451 |
| C2H4 | 0.8643 | 0.8400 | 0.7893 | 1.0000 |

| yjAij i\j | Ar | CO | H2O | C2H4 | sum |
|---|---|---|---|---|---|
| Ar | 0.1633 | 0.5375 | 0.1701 | 0.1043 | 0.9752 |
| CO | 0.1671 | 0.5578 | 0.1796 | 0.1077 | 1.0121 |
| H2O | 0.1700 | 0.5772 | 0.1900 | 0.1108 | 1.0480 |
| C2H4 | 0.1411 | 0.4686 | 0.1499 | 0.0890 | 0.8486 |

| | $yi\lambda i$ | $yi\lambda i/\Sigma(yjAij)$ |
|---|---|---|
| Ar | 0.0071 | 0.0073 |
| CO | 0.0487 | 0.0481 |
| H2O | 0.0165 | 0.0157 |
| C2H4 | 0.0174 | 0.0206 |
| | **$\lambda m$ =** | **0.0917 W/m K** |

Estimated thermal conducitvity of mixture

Estimated values

ρ = 1.02E-05 g/cm3

μ = 0.0530 cP

k = 0.0917 W/m K

Cp = 1.404 J/g K

Pr = Cp μ / k = 0.811307

Re = ρ v D / μ = 0.146533

Nu = 0.42*Pr^0.2 + 0.57*Pr^0.33*Re^0.5

1st term 0.402797

2nd term 0.203645

Nu = 0.606442

**h = Nu k/D = 218.9788 W/m^2 K**

StephanBoltzman constant

σ = 5.67E-08 W/m^2 K^4

Emmissivity of wire

ε = 0.95

Semi-infinite wire equilibrium temp (measured

Tinf. = 1325 K

**Gas Temperature**

Tg = Tinf. + (σ ε Tinf.^4 / h)

= **2083 K**

**Correction due to radiation**

**758 K**

Appendix F: ANOVA Tables for Measured Data

Yields in soot

| | | C60 | | C70 | | C60+C70 | |
|---|---|---|---|---|---|---|---|
| | df | SS | MS | SS | MS | SS | MS |
| P | 2 | 54.73 | 27.36 | 26.79 | 13.39 | 157.8 | 78.92 |
| v | 2 | 34.95 | 17.48 | 6.292 | 3.146 | 62.42 | 31.21 |
| $\phi$ | 2 | 141.1 | 70.55 | 154.8 | 77.4 | 583.4 | 291.7 |
| Pv | 4 | 45.29 | 11.32 | 40.21 | 10.05 | 160.8 | 40.19 |
| Pf | 4 | 35.66 | 8.916 | 17.95 | 4.486 | 101.7 | 25.42 |
| vf | 4 | 715.2 | 178.8 | 462.5 | 115.6 | 2304 | 576 |

Yields from carbon fed

| | | C60 | | C70 | | C60+C70 | |
|---|---|---|---|---|---|---|---|
| | df | SS | MS | SS | MS | SS | MS |
| P | 2 | 0.02 | 0.01 | 0.007 | 0.004 | 0.052 | 0.026 |
| v | 2 | 0.018 | 0.009 | 0.004 | 0.002 | 0.035 | 0.017 |
| $\phi$ | 2 | 0.007 | 0.003 | 3E-04 | 2E-04 | 0.01 | 0.005 |
| Pv | 4 | 0.029 | 0.007 | 0.012 | 0.003 | 0.077 | 0.019 |
| Pf | 4 | 0.013 | 0.003 | 0.004 | 9E-04 | 0.029 | 0.007 |
| vf | 4 | 0.056 | 0.014 | 0.021 | 0.005 | 0.13 | 0.033 |

Production rates

| | | C60 | | C70 | | C60+C70 | |
|---|---|---|---|---|---|---|---|
| | df | SS | MS | SS | MS | SS | MS |
| P | 2 | 0.403 | 0.201 | 0.221 | 0.11 | 1.219 | 0.61 |
| v | 2 | 0.33 | 0.165 | 0.128 | 0.064 | 0.864 | 0.432 |
| $\phi$ | 2 | 0.119 | 0.06 | 0.031 | 0.015 | 0.268 | 0.134 |
| Pv | 4 | 0.224 | 0.056 | 0.079 | 0.02 | 0.563 | 0.141 |
| Pf | 4 | 0.189 | 0.047 | 0.073 | 0.018 | 0.496 | 0.124 |
| vf | 4 | 0.696 | 0.174 | 0.227 | 0.057 | 1.661 | 0.415 |

## Appendix G: Regression Analysis Output

C60 yield in soot

| Regression Statistics | |
|---|---|
| Multiple R | 0.912 |
| R Square | 0.832 |
| Adjusted R Square | 0.781 |
| Standard Error | 1.549 |
| Observations | 31 |

ANOVA

| | df | SS | MS | F |
|---|---|---|---|---|
| Regression | 7 | 273.396 | 39.057 | 16.27653 |
| Residual | 23 | 55.190 | 2.400 | |
| Total | 30 | 328.586 | | |

| | Coefficients | Std. Error | t Stat | P-value |
|---|---|---|---|---|
| Intercept | 45.9434 | 103.2636 | 0.4449 | 0.6605 |
| P | 0.7926 | 0.7508 | 1.0557 | 0.3021 |
| v | 0.7195 | 0.5986 | 1.2019 | 0.2416 |
| f | -43.2042 | 85.6990 | -0.5041 | 0.6190 |
| vf | -0.4747 | 0.2638 | -1.7990 | 0.0852 |
| pv | 0.0227 | 0.0074 | 3.0660 | 0.0055 |
| pf | -0.6677 | 0.3719 | -1.7954 | 0.0857 |
| f^2 | 13.1700 | 18.6003 | 0.7081 | 0.4860 |

C70 yield in soot

| Regression Statistics | |
|---|---|
| Multiple R | 0.929 |
| R Square | 0.863 |
| Adjusted R Square | 0.822 |
| Standard Error | 1.192 |
| Observations | 31 |

ANOVA

| | df | SS | MS | F |
|---|---|---|---|---|
| Regression | 7 | 206.399 | 29.486 | 20.74719 |
| Residual | 23 | 32.687 | 1.421 | |
| Total | 30 | 239.086 | | |

| | Coefficients | Std Error | t Stat | P-value |
|---|---|---|---|---|
| Intercept | 187.2667 | 79.4705 | 2.3564 | 0.0273 |
| P | 0.6509 | 0.5778 | 1.1265 | 0.2716 |
| v | 0.1486 | 0.4607 | 0.3224 | 0.7500 |
| f | -149.9087 | 65.9530 | -2.2730 | 0.0327 |
| vf | -0.1879 | 0.2031 | -0.9253 | 0.3644 |
| pv | 0.0146 | 0.0057 | 2.5588 | 0.0176 |
| pf | -0.4875 | 0.2862 | -1.7035 | 0.1020 |
| f^2 | 32.3117 | 14.3146 | 2.2573 | 0.0338 |

C60+C70 yield in soot

| Regression Statistics | |
|---|---|
| Multiple R | 0.920 |
| R Square | 0.846 |
| Adjusted R Square | 0.799 |
| Standard Error | 2.700 |
| Observations | 31 |

ANOVA

| | df | SS | MS | F |
|---|---|---|---|---|
| Regression | 7 | 921.742 | 131.677 | 18.0667 |
| Residual | 23 | 167.633 | 7.288 | |
| Total | 30 | 1089.376 | | |

| | Coefficients | Std Error | t Stat | P-value |
|---|---|---|---|---|
| Intercept | 233.2101 | 179.9687 | 1.2958 | 0.2079 |
| P | 1.4435 | 1.3085 | 1.1032 | 0.2814 |
| v | 0.8680 | 1.0433 | 0.8320 | 0.4140 |
| f | -193.1129 | 149.3570 | -1.2930 | 0.2089 |
| vf | -0.6625 | 0.4598 | -1.4408 | 0.1631 |
| pv | 0.0373 | 0.0129 | 2.8891 | 0.0083 |
| pf | -1.1553 | 0.6481 | -1.7824 | 0.0879 |
| f^2 | 45.4817 | 32.4168 | 1.4030 | 0.1740 |

C60 yield from carbon fed

| Regression Statistics | |
|---|---|
| Multiple R | 0.757 |
| R Square | 0.574 |
| Adjusted R Square | 0.444 |
| Standard Error | 0.042 |
| Observations | 31 |

ANOVA

| | df | SS | MS | F |
|---|---|---|---|---|
| Regression | 7 | 0.056 | 0.008 | 4.42353 |
| Residual | 23 | 0.041 | 0.002 | |
| Total | 30 | 0.097 | | |

| | Coefficients | Std Error | t Stat | P-value |
|---|---|---|---|---|
| Intercept | -3.6745 | 2.8970 | -1.2684 | 0.2174 |
| P | -0.0085 | 0.0069 | -1.2353 | 0.2292 |
| v | -0.0048 | 0.0190 | -0.2505 | 0.8044 |
| f | 3.3281 | 2.3875 | 1.3939 | 0.1767 |
| vf | 0.0091 | 0.0072 | 1.2646 | 0.2187 |
| pv | 0.0003 | 0.0002 | 1.6822 | 0.1061 |
| v^2 | -0.0003 | 0.0002 | -1.5787 | 0.1281 |
| f^2 | -0.7821 | 0.5159 | -1.5162 | 0.1431 |

C70 yield from carbon fed

| *Regression Statistics* | |
|---|---|
| Multiple R | 0.619 |
| R Square | 0.383 |
| Adjusted R Square | 0.196 |
| Standard Error | 0.036 |
| Observations | 31 |

ANOVA

| | *df* | *SS* | *MS* | *F* |
|---|---|---|---|---|
| Regression | 7 | 0.018 | 0.003 | 2.042597 |
| Residual | 23 | 0.029 | 0.001 | |
| Total | 30 | 0.047 | | |

| | *Coefficients* | *Std Error* | *t Stat* | *P-value* |
|---|---|---|---|---|
| Intercept | -0.3439 | 2.4338 | -0.1413 | 0.8889 |
| P | -0.0043 | 0.0058 | -0.7396 | 0.4670 |
| v | -0.0080 | 0.0160 | -0.5028 | 0.6199 |
| f | 0.5438 | 2.0058 | 0.2711 | 0.7887 |
| vf | 0.0102 | 0.0060 | 1.6982 | 0.1030 |
| pv | 0.0002 | 0.0001 | 1.0721 | 0.2948 |
| v^2 | -0.0002 | 0.0001 | -1.7130 | 0.1002 |
| f^2 | -0.2021 | 0.4334 | -0.4663 | 0.6454 |

C60+C70 yield from carbon fed

| *Regression Statistics* | |
|---|---|
| Multiple R | 0.701 |
| R Square | 0.491 |
| Adjusted R Square | 0.336 |
| Standard Error | 0.077 |
| Observations | 31 |

ANOVA

| | *df* | *SS* | *MS* | *F* |
|---|---|---|---|---|
| Regression | 7 | 0.130 | 0.019 | 3.171756 |
| Residual | 23 | 0.135 | 0.006 | |
| Total | 30 | 0.265 | | |

| | *Coefficients* | *Std Error* | *t Stat* | *P-value* |
|---|---|---|---|---|
| Intercept | -4.0184 | 5.2367 | -0.7673 | 0.4507 |
| P | -0.0128 | 0.0125 | -1.0271 | 0.3151 |
| v | -0.0128 | 0.0344 | -0.3723 | 0.7131 |
| f | 3.8718 | 4.3157 | 0.8971 | 0.3789 |
| vf | 0.0193 | 0.0130 | 1.4889 | 0.1501 |
| pv | 0.0004 | 0.0003 | 1.4289 | 0.1665 |
| v^2 | -0.0005 | 0.0003 | -1.6695 | 0.1086 |
| f^2 | -0.9842 | 0.9325 | -1.0555 | 0.3022 |

C60 production rate

| Regression Statistics | |
|---|---|
| Multiple R | 0.902 |
| R Square | 0.813 |
| Adjusted R Square | 0.756 |
| Standard Error | 0.096 |
| Observations | 31 |

ANOVA

| | df | SS | MS | F |
|---|---|---|---|---|
| Regression | 7 | 0.932 | 0.133 | 14.30345 |
| Residual | 23 | 0.214 | 0.009 | |
| Total | 30 | 1.147 | | |

| | Coefficients | Std Error | t Stat | P-value |
|---|---|---|---|---|
| Intercept | -9.7668 | 6.5977 | -1.4803 | 0.1524 |
| P | -0.0288 | 0.0158 | -1.8256 | 0.0809 |
| v | -0.0322 | 0.0433 | -0.7432 | 0.4649 |
| f | 8.9050 | 5.4374 | 1.6377 | 0.1151 |
| vf | 0.0149 | 0.0163 | 0.9135 | 0.3705 |
| pv | 0.0011 | 0.0004 | 2.8953 | 0.0082 |
| f^2 | -1.9910 | 1.1748 | -1.6947 | 0.1036 |
| v^2 | -0.0003 | 0.0004 | -0.6684 | 0.5106 |

C70 production rate

| Regression Statistics | |
|---|---|
| Multiple R | 0.883 |
| R Square | 0.780 |
| Adjusted R Square | 0.713 |
| Standard Error | 0.072 |
| Observations | 31 |

ANOVA

| | df | SS | MS | F |
|---|---|---|---|---|
| Regression | 7 | 0.419 | 0.060 | 11.66498 |
| Residual | 23 | 0.118 | 0.005 | |
| Total | 30 | 0.537 | | |

| | Coefficients | Std Error | t Stat | P-value |
|---|---|---|---|---|
| Intercept | -2.3641 | 4.8953 | -0.4829 | 0.6337 |
| P | -0.0133 | 0.0117 | -1.1334 | 0.2687 |
| v | -0.0234 | 0.0321 | -0.7282 | 0.4738 |
| f | 2.4036 | 4.0344 | 0.5958 | 0.5571 |
| vf | 0.0176 | 0.0121 | 1.4492 | 0.1608 |
| pv | 0.0006 | 0.0003 | 2.2333 | 0.0355 |
| f^2 | -0.6374 | 0.8717 | -0.7312 | 0.4720 |
| v^2 | -0.0004 | 0.0003 | -1.2327 | 0.2301 |

C60+C70 production rate

| *Regression Statistics* | |
|---|---|
| Multiple R | 0.900 |
| R Square | 0.809 |
| Adjusted R Square | 0.751 |
| Standard Error | 0.162 |
| Observations | 31 |

ANOVA

| | *df* | *SS* | *MS* | *F* |
|---|---|---|---|---|
| Regression | 7 | 2.574 | 0.368 | 13.9596 |
| Residual | 23 | 0.606 | 0.026 | |
| Total | 30 | 3.180 | | |

| | *Coefficients* | *Std Error* | *t Stat* | *P-value* |
|---|---|---|---|---|
| Intercept | -12.1308 | 11.0967 | -1.0932 | 0.2856 |
| P | -0.0420 | 0.0265 | -1.5854 | 0.1265 |
| v | -0.0556 | 0.0728 | -0.7631 | 0.4532 |
| f | 11.3086 | 9.1451 | 1.2366 | 0.2287 |
| vf | 0.0325 | 0.0275 | 1.1825 | 0.2491 |
| pv | 0.0017 | 0.0006 | 2.7067 | 0.0126 |
| f^2 | -2.6284 | 1.9759 | -1.3302 | 0.1965 |
| v^2 | -0.0006 | 0.0007 | -0.9412 | 0.3564 |